Master's degree in
Environmental and Land Engineering

Integrated Assessment of PFAS Characterization, Regulatory Compliance and GAC Adsorption Competition in Leachate and Groundwater:

GAIA Cerro Tanaro Landfill Case Study

Candidate:
Parsa KHAYAT KAHNOI

Supervisor:
Prof. Rajandrea SETHI

Politecnico di Torino
March 20, 2026

I hereby declare that the contents and organisation of this dissertation constitute my own original work and does not compromise in any way the rights of third parties, including those relating to the security of personal data.

Parsa Khayat Kahnoi Turin, March 20, 2026

Summary

Per- and polyfluoroalkyl substances (PFASs) are synthetic fluorinated compounds that persist in the environment and have been linked to adverse health effects. Recent European regulations classify PFOS, PFOA and PFHxS as persistent organic pollutants and limit their presence in products and wastes, while Piedmont's regional law sets low discharge limits for PFAS in surface waters. Landfills have been identified as major secondary reservoirs of PFAS because disposed consumer products and industrial wastes release these chemicals into leachate. This thesis investigates PFAS contamination at the GAIA non-hazardous waste landfill (Cerro Tanaro, Italy) and evaluates granular activated carbon (GAC) adsorption for PFAS removal from leachate with high total organic carbon (TOC).

Mixed leachate from tanks C1-C3 and groundwater from upstream (PZ3ter) and downstream (PZ38) piezometers were analyzed. Leachate exhibited extremely high TOC (~2000 mg L^{-1}) and contained multiple PFAS at µg L^{-1} levels. In C1-C3 leachate, PFBS (12.5 µg L^{-1}), PFHxA (10.0 µg L^{-1}), PFPeA (4.8 µg L^{-1}), PFBA (4.4 µg L^{-1}), PFOA (1.85 µg L^{-1}) and PFOS (0.27 µg L^{-1}) were predominant, together with emerging C6O4 (21.8 µg L^{-1}).

Groundwater concentrations were three orders of magnitude lower: upstream samples contained only PFPeA, PFHxA, PFHpA and PFOA (2.1-2.9 ng L^{-1}), with PFOS below detection, while downstream samples showed PFOA (2.9 ng L^{-1}), PFOS (1.20 ng L^{-1}) and C6O4 (3.0 ng L^{-1}). All values remained below regional thresholds, confirming significant attenuation from leachate to aquifer.

Preliminary TOC adsorption tests demonstrated that even at high GAC doses, TOC removal did not exceed 30%, and residual TOC remained 40 mg L^{-1}, indicating strong matrix persistence. Consequently, dilution was adopted to reduce competitive background prior to PFAS adsorption experiments. Batch adsorption tests (0-10 g L^{-1} GAC, 70-141 h) were performed with PFBA, PFBS, PFOA and PFOS spike (100 µg L^{-1} each).

Freundlich modeling revealed clear competitive effects of dissolved organic matter. Compared with single-solute standards, K_f values decreased by up to one order of magnitude in leachate matrices. For PFBA, K_f declined from 0.44 (standard) to 1.3×10^{-2} (raw leachate) and 6×10^{-3} (oxidized leachate). PFBS showed K_f values of 4.6×10^{-3}-7.6×10^{-3} in raw leachate and 4.0×10^{-3}-4.8×10^{-3} in oxidized leachate. PFOA exhibited stronger adsorption (K_f up to 4.3×10^{-3} in competitive systems), while PFOS rapidly entered a near-depletion regime at low doses,

preventing robust global Freundlich fitting. Overall adsorption strength followed the hierarchy PFOS > PFOA > PFBS > PFBA, confirming chain-length and functional-group effects (sulfonate > carboxylate).

Experiments with two additional GAC materials (Organosorb 10-AA and Organosorb 10-AM) assessed the influence of granular activated carbon characteristics on adsorption performance; results showed that Organosorb 10-AA achieved the highest PFAS removal under competitive leachate conditions, indicating that effective pore accessibility and pore size distribution governed performance, and that a higher BET surface area alone did not translate into superior adsorption efficiency in complex matrices.

This study provides a comprehensive assessment of PFAS occurrence, characterization and competitive adsorption behavior at a major Piedmont landfill. The results highlight the critical role of dissolved organic matter in suppressing PFAS adsorption, confirm molecular structure-dependent adsorption hierarchies, and emphasize the need for optimized adsorbent selection to meet emerging European and regional water-quality standards.

Acknowledgment

I would like to express my sincere gratitude to my academic supervisor for the guidance, scientific rigor, and continuous support provided throughout the development of this thesis. Their expertise and constructive feedback were essential to the quality and direction of this research.

I am deeply thankful to GAIA S.p.A., particularly the Monitoring Department, and to Eng. Roberta Lanfranco and Dr. Cecilia Binello for their availability, technical support, and for granting access to operational and environmental monitoring data. Their collaboration significantly strengthened the applied relevance of this work.

I also wish to acknowledge the CWC Laboratory at Politecnico di Torino for providing a stimulating research environment. Special thanks to Marco Coha, Francesca Nunzio, and Carlo Bianco for their valuable support, technical assistance, and insightful discussions during the experimental activities.

Dedication

First and foremost, I dedicate this work to my beloved wife, Samin.

Your support has been the foundation beneath every step of this journey. You carried hope when I felt tired, and you stood beside me with patience, kindness, and unwavering belief. This achievement is as much yours as it is mine, because your encouragement and love made it possible.

I dedicate this work to my family in Iran. Even across distance, your presence has always been with me. Your trust in my efforts and the values you taught me have shaped who I am. You gave me the strength to continue when challenges arose. Whatever I accomplish carries your imprint, no matter how far away I may be.

Finally, I dedicate this thesis to the people of my country. To those who, despite hardship and suffering, chose courage over silence. To those who stood with dignity in the face of oppression. Your resilience, your determination, and your fight for freedom have deeply inspired me. In moments of difficulty, I remembered your strength, and it reminded me that perseverance has meaning. May this work honor, in its own small way, your courage and your hope for a better future.

Contents

List of Figures

List of Tables

Chapter 1

Introduction

1.1 PFAS general information

Per- and polyfluoroalkyl substances (PFAS) are a family of fluorinated organic compounds of anthropogenic origin. Due to their unique chemical properties, widespread production, environmental distribution, long-term persistence, bioaccumulative potential, and associated risks for human health, PFAS have been classified as persistent organic. Concentrations of PFAS in surface and groundwater range in value along the ng L^{-1}-µg L^{-1} scale. The review reports that PFAS are widespread despite being phased out, they have been detected in different continents irrespective of the level of industrial development. Their occurrence far from the potential sources suggests that long-range atmospheric transport is an important pathway of PFAS distribution. Recently, several studies have investigated the health impacts of PFAS exposure - they have been detected in biota, drinking water, food, air, and human serum (Kurwadkar et al., 2022).

Table 1. Abbreviations and chemical structures of PFASs including their related mass-labelled surrogate (Xiujuan Wang et al., 2025; Yutao Chen et al., 2023)

Type	Group	Abbreviation	Formula	Chemical Structure
Perfluoroalkyl Acids (PFAAs)	Perfluoroalkyl carboxylic acids (PFCAs)	PFBA (C_4, n=3[a])	$C_4HF_7O_2$	
		PFPeA (C_5, n=4)	$C_5HF_9O_2$	
		PFHxA (C_6, n=5)	$C_6HF_{11}O_2$	
		PFHpA (C_7, n=6)	$C_7HF_{13}O_2$	
		PFOA (C_8, n=7)	$C_8HF_{15}O_2$	
		PFNA (C_9, n=8)	$C_9HF_{17}O_2$	

		PFDA (C_{10}, n=9)	$C_{10}HF_{19}O_2$	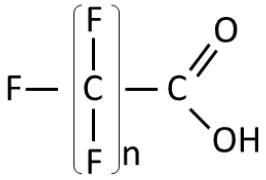
		PFUnA (C_{11}, n=10)	$C_{11}HF_{21}O_2$	
		PFDoA (C_{12}, n=11)	$C_{12}HF_{23}O_2$	
		PFTrDA (C_{13}, n=12)	$C_{13}HF_{25}O_2$	
		PFTeDA (C_{14}, n=13)	$C_{14}HF_{27}O_2$	
	Perfluoroalkyl sulfonic acids (PFSAs)	PFBS (C_4, n=4)	$C_4HF_9O_3S$	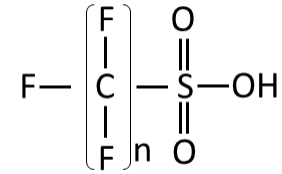
		PFPeS (C_5, n=5)	$C_5HF_{11}O_3S$	
		PFHxS (C_6, n=6)	$C_6HF_{13}O_3S$	
		PFHpS (C_7, n=7)	$C_7HF_{15}O_3S$	
		PFOS (C_8, n=8)	$C_8HF_{17}O_3S$	
		PFNS (C_9, n=9)	$C_9HF_{19}O_3S$	
		PFDS (C_{10}, n=10)	$C_{10}HF_{21}O_3S$	
PFAA Precursors	Fluorotelomer carboxylic acids (FTCAs)	5:3 FTCA (n=5)	$C_8H_5F_{11}O_2$	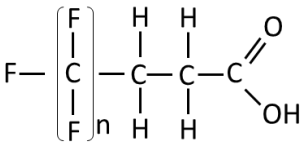
		7:3 FTCA (n=7)	$C_{10}H_5F_{15}O_2$	
	Perfluorooctane sulfonamides (FOSAs)	PFOSAA (n=8, R_1, R_2=H)	$C_8H_2F_{17}NO_2S$	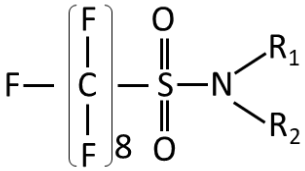
		NMeFOSAA (n=8, R_1= CH_2COOH, R_2=CH_3)	$C_{11}H_6F_{17}NO_4$	
		NEtFOSAA (n=8, R_1= CH_2COOH, R_2=CH_2CH_3)	$C_{12}H_8F_{17}NO_4S$	
	Fluorotelomer sulfonic acids (FTSAs)	4:2 FTS (n=4)	$C_6H_4F_9NaO_3S$	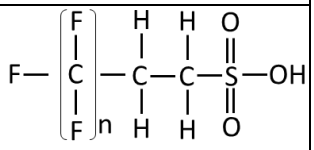
		6:2 FTS (n=6)	$C_8H_4F_{13}NaO_3S$	
		8:2 FTS (n=8)	$C_{10}H_4F_{17}NaO_3S$	

1.2 Introducing case study and study period

1.2.1 Corporate Framework and Governance Structure

The present research was conducted in collaboration with G.A.I.A. S.p.A. (Gestione Ambientale Integrata dell'Astigiano), the integrated environmental management company serving the Province of Asti, Piedmont, Italy. GAIA represents a public–private institutional model of waste governance, operating as the owner and manager of the principal waste treatment and disposal facilities within the province.

The company is jointly owned by 114 municipalities of the Asti area and the industrial partner IREN Ambiente. The current shareholding structure reflects this hybrid governance model: 24% Municipality of Asti, 16% municipalities with fewer than 2,000 inhabitants, 15% municipalities with more than 2,000 inhabitants,

and 45% IREN Ambiente. This structure positions GAIA as both a public service operator and a technically advanced environmental management entity.

GAIA is responsible for the treatment, recovery, and final disposal of municipal waste generated across the province, as well as for waste streams originating from other Italian territories associated with IREN Ambiente. Its integrated operational model encompasses material recovery, biological treatment, energy recovery, and landfill disposal, ensuring vertical control of the waste management chain.

1.2.2 Facility Network and Operational Scope

GAIA's infrastructure system includes:

1- The registered corporate office in Asti.

2- A waste treatment center located in the industrial area of Asti, comprising:

- A plant dedicated to material recovery from separately collected waste.
- A mechanical-biological treatment (MBT) facility for unsorted municipal waste.

3- A composting, anaerobic digestion, and biomethane production plant in San Damiano d'Asti, dedicated to organic waste valorization.

4- The non-hazardous waste landfill located in the municipality of Cerro Tanaro.

5- Twelve eco-stations distributed strategically across the province.

6- Environmental monitoring responsibilities for the exhausted Vallemanina landfill in Asti.

This integrated facility system reflects a transition from linear disposal-oriented waste management toward circular resource recovery and controlled final disposal.

1.2.3 Certifications, Regulatory Compliance, and Environmental Governance

GAIA operates under a structured Integrated Management System aligned with international standards. The company holds the following certifications:

- ISO 9001 (Quality Management)
- ISO 14001 (Environmental Management)
- ISO 45001 (Occupational Health and Safety)
- ISO 50001 (Energy Management)
- EMAS Registration (Eco-Management and Audit Scheme)

Additionally, GAIA has adopted an Organizational Management and Control Model pursuant to Legislative Decree 231/01, including a Supervisory Body. This

framework reinforces regulatory compliance, transparency, and environmental accountability.

Such institutional and regulatory robustness is particularly relevant in the context of emerging contaminants such as PFAS, which require advanced monitoring and adaptive management approaches.

1.3 The Cerro Tanaro Landfill: Site Characteristics, Operations, and Expansions

1.3.1 Site Description and Disposal Capacity

The GAIA non-hazardous waste landfill is in Cerro Tanaro (Province of Asti) and began operations in 2003. It serves as the final disposal facility for non-recoverable pretreated municipal waste and residues from material recovery processes.

The landfill's total authorized disposal volume is currently 2,549,000 m³, distributed as follows:

- Tanks A and B (721,000 m³), nearly exhausted.
- Tanks C1/C2/C3 (707,000 m³), currently operational.
- Tanks C4-D-E (1,121,000 m³), authorized under Integrated Environmental Authorization (D.D. No. 279 of January 30, 2025), with construction ongoing.

These expansions reflect the strategic importance of the site for regional waste management planning and emphasize the need for continuous environmental impact assessment.

Figure 1: Cerro Tanaro landfill Sentinel-2 Highlight Optimized Natural Color image (29/11/2025)

Figure 2: Cerro Tanaro Landfill Google satellite image

Figure 3: Cerro Tanaro Landfill landscape

1.3.2 Operational Configuration and Environmental Protection Systems

The landfill operates primarily with baled waste (approximately 70% of total input), while loose waste (approximately 30%) is used for structural shaping. Organic fractions undergo microbial degradation, producing biogas composed mainly of methane and carbon dioxide.

The biogas is captured through a network of vertical extraction wells connected via HDPE piping and conveyed to energy recovery units. When recovery is not feasible, high-temperature flares ensure controlled combustion.

Environmental protection measures include:

- Multi-layer soil and subsoil impermeable barriers.
- Leachate drainage and collection systems.
- Controlled water management infrastructure.
- Continuous groundwater monitoring.

Operations are governed by the current Integrated Environmental Authorization (AIA D.D. No. 279/2025), which includes a Surveillance and Control Plan.

1.3.3 Monitoring Network and Hydrogeological Control

The site is equipped with an extensive groundwater monitoring network comprising historical piezometers (installed between 2002 and 2015) and six additional piezometers drilled in 2022 to improve hydrogeological characterization.

Routine monitoring includes monthly water level measurements and chemical analyses of groundwater and leachate. Specific attention is given to upstream and downstream control wells to assess potential contaminant migration.

1.3.4 PFAS Monitoring Framework and Research Collaboration

Under Section 3.1 of the AIA, annual analyses include determination of PFAS in both leachate and selected piezometers (PZ38 upstream and PZ3ter downstream). Monitoring follows Regulation (EU) 2019/1021 (POPs) and subsequent amendments, including compounds such as PFBA, PFBS, PFOA, PFOS, GenX, and other long-chain PFCAs and PFSAs.

Currently, PFAS analyses are conducted primarily for research purposes, reflecting growing regulatory and scientific attention to these persistent contaminants.

1.4 Hydrogeological and geological context

The hydrogeological setting around the GAIA's Cerro Tanaro landfill is complex. A geological investigation conducted in November 2024 analyzed fluctuations in water levels and their relation to rainfall. The report noted that piezometric levels showed positive increments across several wells following the end of the dry season: increases of 0-20 cm were recorded at wells on the western side and at PZ23 near the planned basin D; increments of 0-40 cm were observed at PZ17, PZ18, PZ16bis, PZ14bis, PZ3ter, PZ32, PZ4 and PZ2; 0-70 cm increases at PZ33 and PZ7; and more pronounced rises of 0.1-1.4 m at PZ21 and PZ8.

Notably, PZ21 and PZ8 exhibited the largest excursions, exceeding the values assumed in the original design (1.14 m); these variations occurred despite relatively low precipitation between July and October 2024. To interpret these fluctuations, ARPA requested an analysis of historical piezometric data, including correlations with rainfall, an explanation of water-table behavior, a verification of the maximum positive excursions and clarification regarding missing measurements at PZ22.

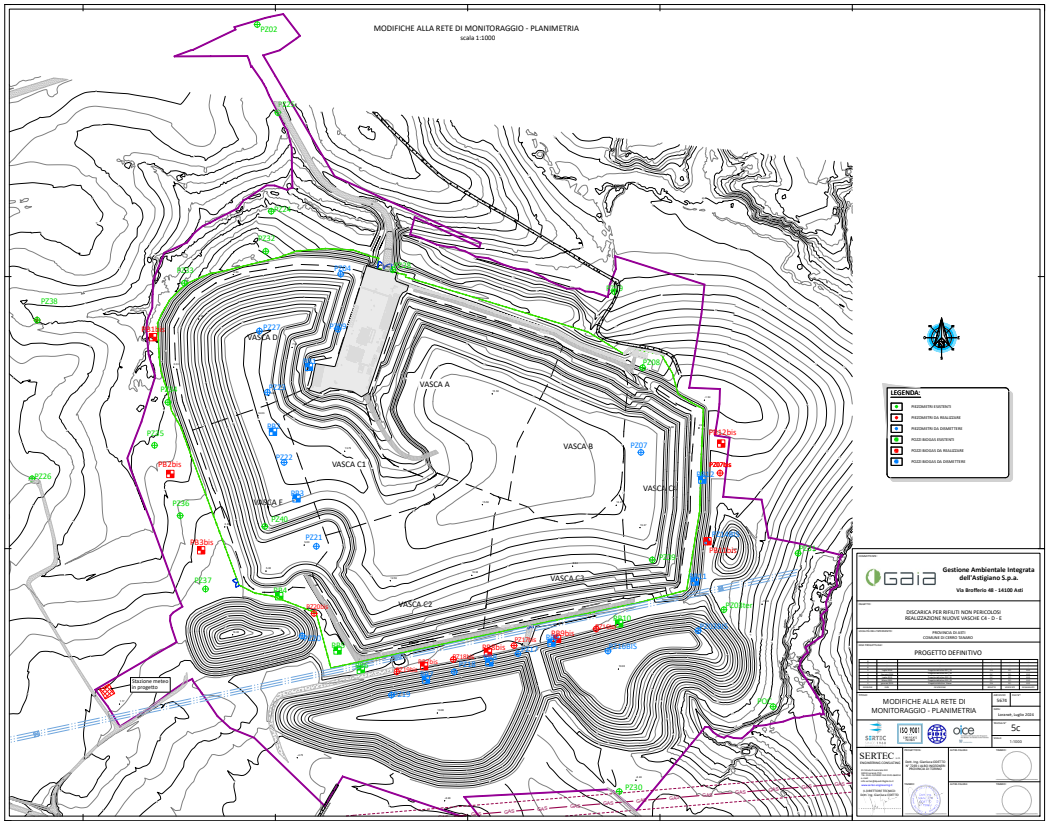

Figure 4: Landfill overall plan and geometry

The geological report emphasizes that water levels in the piezometers stabilize at the interface between permeable and impermeable layers and are influenced by complex processes. Sudden rainfall events may cause infiltration from above, leading to formation of suspended phreatic zones and mobilization of fine particles that can clog measuring devices. The report advises interpreting water-level data by considering trends and coherence across multiple wells rather than focusing on isolated anomalies. Importantly, it notes that even if the piezometric level at PZ21 were to rise by 20 cm, the freeboard would remain 6.5 m, while the design of PZ8 already accounts for a 2.45 m increment. This information supports the conclusion that the landfill's geological barriers provide sufficient safety margins against groundwater intrusion.

The hydrogeological context thus reveals spatial variability: some wells show modest seasonal fluctuations, whereas others (PZ21, PZ8) exhibit larger excursions. The investigation underscores the need for ongoing monitoring and for careful interpretation of piezometric data in relation to rainfall, drainage design and geological heterogeneity. These observations directly inform the thesis by

highlighting potential pathways for leachate-groundwater interaction and by defining the baseline conditions that adsorption experiments must respect.

1.5 Piedmont Regional PFAS monitoring program

1.5.1 Expansion of PFAS surveillance

The Piedmont environmental agency (ARPA Piemonte) has developed one of Italy's most comprehensive PFAS monitoring networks. Since 2010 ARPA has analyzed PFAS in surface waters, initially focusing on PFOA and PFOS, and progressively expanding to six compounds (PFBA, PFBS, PFHxA, PFOA, PFOS, PFPeA). By 2025 the monitoring network comprised **about 350 surface-water stations**, **360 superficial aquifer stations**, **190 deep-aquifer stations** and **10 spring stations**, together with point-specific surveillance near industrial discharges. The surface-water stations monitor 3×10^5 km of rivers and channels, while the groundwater stations cover the major aquifers in the region. In addition, ARPA started controlling PFAS discharges from wastewater treatment plants, landfills and industrial sites in 2019, anticipating regulatory changes introduced by the Piedmont Regional Law 25/2021. A network of 528 groundwater monitoring wells and 124 surface-water stations is also highlighted in ARPA's 2025 PFAS observatory slides, reflecting the agency's intense surveillance effort.

1.5.2 Surface-water and groundwater findings

ARPA's data reveal that PFOS is by far the most frequently detected PFAS. In the 2022-2023 monitoring campaign, PFOS was found in 551 of 741 surface-water samples (2022) and 445 of 703 samples (2023), whereas other PFAS were detected far less often. The report attributes this discrepancy to the lower LOQ for PFOS; most monitoring stations recorded only PFOS, while multiple PFAS detections occurred in a few subregions (Alessandrino, Novarese, Biellese and parts of the Turin metropolitan area). Some surface-water stations exceeded the PFOS environmental standard. In groundwater, ARPA monitors PFBS, PFHxA, PFOA, PFOS and PFPeA in both shallow and deep aquifers. Table 1.6 of the report summarises measures and detections across groundwater bodies (GWBs) from 2020 to 2023; certain GWBs (P1 and S3a) show repeated detections of PFOS and other PFAS, while many GWBs have none.

1.5.3 Leachate and sewage-sludge investigations

ARPA extended its monitoring to PFAS in landfill leachate and wastewater-treatment sludge. In 2024 the agency sampled 20 leachate streams from 19 landfills (municipal and special waste). Leachate is classified as non-hazardous waste (EER 190703) yet often contains elevated PFAS because waste decomposition products and disposed consumer items leach fluorinated compounds. Facilities treat leachate before discharge: consortia biological plants with integrated authorization, chemical-physical treatment plants and plants without AIA that accept leachate as liquid waste. ARPA's results show that PFOA is present in all leachate samples except those from mono-dedicated landfills, with concentrations generally higher than PFOS; special-waste landfills exhibited the highest concentrations. Minimum and maximum PFAS levels for closed municipal-waste landfills ranged from 0.7 µg L^{-1} to 30 µg L^{-1}, for active municipal-waste landfills 6.8 µg L^{-1} to 45 µg L^{-1}, and for special-waste landfills 17 µg L^{-1} to 382.8 µg L^{-1}. The study concluded that PFAS are ubiquitous in leachate and that long-chain molecules were often absent, possibly due to sorption onto waste or degradation. Around 77 % of leachate generated in Piedmont is treated within the region, with annual production exceeding 300,000 tons.

A separate survey analyzed 21 sewage-sludge samples from 19 wastewater-treatment plants. PFOS concentrations were generally higher than PFOA, suggesting that sludges can act as sinks for sulfonates. However, PFAS levels did not correlate directly with the volume of sludge produced; some plants with high input volumes (e.g. Torino) had relatively low PFAS concentrations, while smaller plants exhibited higher concentrations (229.9-256.3 µg kg^{-1} dry weight). These findings imply that sludge PFAS burdens depend more on waste composition and treatment processes than on throughput.

1.5.4 Regulatory developments

In response to the rising awareness of PFAS, Piedmont enacted Regional Law 25/2021 ("Legge annuale di riordino") establishing emission limits for PFAS discharges to surface waters. Article 74 of the law prohibits the discharge of PFAS-containing effluents to soil or superficial subsoil and mandates that effluents discharged into sewer networks comply with technical norms and limit values adopted by competent authorities. Annex A of the law sets concentration limits for key PFAS in wastewater discharges; for example, PFOS limits are 0.02 µg L^{-1} during the first 36 months after the law's entry into force and 0.00065 µg L^{-1}

thereafter, while the limit for PFOA is 0.30 μg L^{-1} initially and 0.10 μg L^{-1} subsequently. These limits are more stringent than the EU Drinking Water Directive thresholds (0.5 μg L^{-1} total PFAS and 0.1 μg L^{-1} for the sum of 20 PFAS, effective January 2026), underscoring the region's proactive stance. ARPA regulatory timeline indicates: PFOS use was restricted in 2006, PFOA in 2020, and the regional law introduced discharge limits for 16 PFAS. These regulatory drivers justify GAIA's monitoring program and the present thesis, which aims to assess PFAS behavior in leachate and groundwater under real-world conditions.

1.5.5 Hydrogeological interpretation and potential PFAS migration

Although GAIA's 2024 report did not detect PFAS, the hydrogeological information it provides is critical for understanding potential PFAS pathways. The positive increments in piezometric levels at PZ21 and PZ8 (0.1-1.4 m) and the infiltration phenomena described in the geological report highlight the possibility of lateral and vertical water movement around the landfill. The presence of suspended phreatic zones and fine-particle mobilization could enhance the transport of dissolved PFAS if these compounds were present in leachate or waste. Conversely, the large freeboard values (≥6.5 m at PZ21) and the design of impermeable liners and drainage systems provide substantial protection. The pump-and-purge sampling design ensures that groundwater samples are representative of aquifer conditions and not biased by stagnant water or well contamination. Finally, these procedures create a robust framework for evaluating PFAS behavior once they are included in the monitoring program.

1.5.6 Lessons from Leachate and sludge analyses

ARPA's regional Leachate study offers important insights for GAIA. The detection of PFOA in nearly all leachates and the wide range of PFAS concentrations, particularly the high values in special-waste landfills (up to 382.8 μg L^{-1}), indicate that landfill leachate can be a significant source of PFAS.

At GAIA, waste composition includes municipal pretreated residues and industrial residues, which may contain PFAS. Given that the leachate produced by Piedmont's landfills is mostly treated within the region and that PFAS removal efficiencies vary by process, the levels of PFAS in treated effluent and residual sludge may influence downstream water bodies. Sewage-sludge data reveal that PFOS can accumulate in sludge at levels up to 256 μg kg^{-1} dry weight, suggesting that disposal of sludge on land could also contribute to PFAS dissemination. These

findings justify the thesis objectives of quantifying PFAS and precursors in leachate and groundwater and investigating adsorption processes.

Chapter 2

Literature Review, Research questions objectives

2.1 Review of Existing Literature

2.1.1 Characteristics and Environmental Occurrence of PFAS in Landfill Systems

PFAS are a diverse class of chemicals with a common aliphatic carbon backbone in which hydrogen atoms are fully (per fluorinated) or partially (poly-fluorinated) replaced by fluorine. They possess high polarity, and strong, chemically inert carbon- fluorine (CF) bonds, which give them unique chemical attributes, including extremely high thermal and chemical stability. (Rahman et al., 2014; Fernandez et al., 2016)

PFAS have been found in soil and water at or near waste sites, such as landfills; disposal and hazardous waste sites, where aqueous-film-forming foams are used to extinguish flammable liquid-based fires, manufacturing or chemical production facilities that produce or utilize PFAS, food packaging, household products that are stain and water repellent, cleaning products, non-stick cookware, paints, sealants, personal care products and biosolids (Schumacher et al., 2024).

Landfills are major repositories of PFAS; in a study of landfills, median results show that PFAS levels in municipal solid-waste leachate were the highest (10000 ng L^{-1}), construction and demolition debris leachate were intermediate (6200 ng L^{-1}) and municipal solid-waste incinerator ash leachate were the lowest (1300 ng L^{-1}). PFAS levels in gas condensate (7000 ng L^{-1}) were like municipal solid-waste leachate. PFAS in stormwater and groundwater were low (medians were less than 500 ng L^{-1}). Dominant subgroups included perfluorocarboxylic acids and perfluoroalkyl acid precursors in all leachates (Chen et al., 2023).

2.1.2 Molecular Controls on PFAS Adsorption

The adsorption behavior of per- and polyfluoroalkyl substances (PFAS) onto activated carbon is fundamentally governed by molecular structure. A seminal study demonstrated that sorption of perfluorinated surfactants to sediments increases systematically with perfluoroalkyl chain length (Higgins & Luthy, 2006).

This relationship has since been consistently observed in activated carbon systems and is widely interpreted as a consequence of enhanced hydrophobic interactions and van der Waals forces for longer-chain compounds (Yu et al., 2009; Appleman et al., 2014).

Chain-length dependence is one of the most robust findings in PFAS adsorption research. Long-chain PFAS such as PFOA and PFOS exhibit significantly stronger adsorption affinity than short-chain homologues such as PFBA or PFBS (Yu et al., 2009; McCleaf et al., 2017). This behavior is attributed to increased hydrophobic surface area, reduced aqueous solvation, and stronger interaction with microporous carbon domains (Higgins & Luthy, 2006).

Functional group chemistry also plays a critical role. Sulfonate PFAS generally exhibit stronger adsorption than carboxylates of equivalent chain length (Higgins & Luthy, 2006). Experimental isotherm studies confirm that PFOS typically adsorbs more strongly than PFOA under comparable conditions (Yu et al., 2009). This distinction is attributed to differences in hydration energy and electrostatic interaction potential.

These molecular determinants provide the theoretical basis for evaluating PFBA, PFBS, PFOA, and PFOS within a comparative adsorption framework, particularly under competitive leachate conditions.

2.1.3 Activated Carbon Structure and Micropore Accessibility

Activated carbon adsorption performance depends not only on molecular properties but also on pore structure characteristics. Adsorption capacity has been shown to vary significantly between activated carbons despite similar nominal surface areas, emphasizing the importance of micropore distribution and accessibility (Yu et al., 2009).

Full-scale treatment systems were evaluated, and it was reported that GAC performance is strongly influenced by carbon properties and operational conditions. The work highlighted that BET surface area alone does not reliably predict PFAS removal efficiency (Appleman et al., 2014).

Micropore confinement effects enhance adsorption by increasing contact surface area and stabilizing hydrophobic interactions (Higgins & Luthy, 2006). However, accessibility of these micropores can be reduced under competitive organic loading conditions, particularly in matrices containing natural organic matter.

Granular activated carbon (GAC) is also widely used to remove PFAS from water. In sorption experiments, the sorption capacity was chain-length dependent with the following order: PFOS > PFOA > PFBS > PFBA. GAC exhibited high maximum Langmuir sorption capacity for both PFOS (123.5 μmol g^{-1}) and PFOA (86.2 μmol g^{-1}), which were 43 % and 39.6 % greater than biochar. The sorption of PFASs increased with the decrease in pH, and the competitive sorption of PFASs occurred during the sorption process, resulting in decreased PFAS removal efficiencies (Zhang et al., 2021).

Using colloidal activated carbon, the adsorption affinity of PFAS was in the order PFOS > 6:2 FTS > PFHxS > PFOA > PFBS > PFPeA > PFBA. This result indicates that hydrophobic interaction was the predominant adsorption mechanism, and hydrophilic compounds such as PFBA and PFPeA will break through CAC barriers first. Co-contaminants also matter: the presence of 0.5-4.8 mg L^{-1} benzene or 0.5-8 mg L^{-1} trichloroethylene diminished PFOS adsorption but had no effect or even slightly enhanced PFOA adsorption (Hakimabadi et al., 2023).

Therefore, evaluation of GAC materials requires consideration of effective pore accessibility rather than solely nominal porosity metrics.

2.1.4 Dissolved Organic Matter (DOM) Competition

Dissolved organic matter influences adsorption: low-molecular-weight DOM increases the number of effective adsorption sites and promotes PFAS diffusion, thereby enhancing adsorption; larger DOM molecules (>10 kDa) mainly form an adsorption layer on the sand surface, capturing PFAS via hydrophobic interactions; under the influence of 5-10 kDa DOM, PFASs exhibit the lowest adsorption capacity (Hui et al., 2026).

The suppressive influence of dissolved organic matter (DOM) on PFAS adsorption has been demonstrated in multiple studies. Reduced PFAS removal efficiencies were observed in full-scale systems when background organic matter was present (Appleman et al., 2014).

Earlier breakthrough of PFAS in column systems under conditions of organic competition was reported (McCleaf et al., 2017).

DOM competes directly for adsorption sites and may physically block micropores, thereby reducing effective capacity (Appleman et al., 2014). This effect is particularly pronounced for short-chain PFAS, which exhibit weaker intrinsic hydrophobic interactions (McCleaf et al., 2017).

Most DOM competition studies have focused on drinking water systems with relatively moderate TOC concentrations. In contrast, landfill leachate systems may exhibit TOC concentrations in the range of 10^2-10^3 mg L^{-1} (Kjeldsen et al., 2002). The magnitude of competitive suppression under such conditions remains comparatively underexplored.

However, little research has examined Italian landfills specifically or evaluated competitive adsorption among multiple PFAS in real leachate matrices with high total organic carbon. (Röhler et al., 2023).

This represents a critical gap addressed by the present thesis.

2.1.5 Freundlich Modeling and Interpretation Limits

Freundlich isotherm modeling has been widely applied to PFAS adsorption systems to describe heterogeneous surface interactions (Yu et al., 2009). The Freundlich capacity constant (K_f) and intensity parameter ($1/n$) are commonly used to compare adsorption performance between carbons.

However, adsorption modeling under competitive conditions introduces interpretive limitations. Apparent Freundlich constants may reflect competitive suppression rather than intrinsic adsorption affinity (Appleman et al., 2014). Furthermore, near-depletion conditions for strongly adsorbing compounds such as PFOS can compress equilibrium concentrations into narrow ranges, limiting regression robustness (McCleaf et al., 2017).

These modeling constraints underscore the need for careful interpretation of Freundlich parameters, particularly in high-DOM matrices.

2.1.6 Short-Chain and Emerging PFAS

Short-chain PFAS have emerged as a significant treatment challenge due to their increased mobility and reduced adsorption affinity (Rahman et al., 2014). Shorter-chain PFAS exhibit earlier breakthrough in GAC systems compared with long-chain compounds (McCleaf et al., 2017).

Given that landfill leachate often contains substantial fractions of short-chain and replacement PFAS, adsorption systems must be evaluated under conditions that reflect this contaminant distribution.

2.2 Identification of Research Gaps

Despite extensive PFAS adsorption research, several limitations persist:

-Most adsorption studies focus on clean or low-TOC waters rather than high-TOC landfill leachate matrices.

-Limited integration exists between hydrochemical source characterization and adsorption experimentation.

-Comparative multi-GAC evaluations under identical competitive landfill matrices remain scarce.

-Freundlich modeling limits under near-depletion multi-solute systems are insufficiently emphasized.

-Few studies quantify solvent-derived carbon contributions in laboratory PFAS spiking experiments.

By integrating environmental characterization, competitive adsorption experimentation, solvent mass-balance verification, and multi-GAC evaluation under quantified TOC conditions, the present thesis addresses these interrelated gaps and advances PFAS adsorption understanding under GAIA Spa Cerro Tanaro landfill realistic leachate conditions.

2.3 Research questions and hypotheses

Based on the identified gap, the central research questions are:

1- What are the temporal and spatial distributions of PFAS in mixed leachate (C1 + C2 + C3) and upstream versus downstream groundwater at the Cerro Tanaro landfill over the period 2025-January 2026?

2- How does competitive adsorption among PFBA, PFBS, PFOA and PFOS vary between original and oxidized leachate matrices with high organic carbon, and how do different GAC materials and dissolved organic matter influence adsorption isotherms?

The underlying hypotheses are that short-chain PFAS will dominate in groundwater due to higher mobility, that precursor oxidation will reveal substantially higher PFAS concentrations, and that competitive adsorption will reduce removal efficiencies, especially in the presence of high dissolved organic carbon.

2.4 Objectives

To answer these questions, the thesis sets five objectives that logically derive from the literature:

1- Characterize the Cerro Tanaro landfill's leachate and groundwater by measuring PFAS, pH, conductivity, ion composition and dissolved organic carbona and other characterizations building on reports that landfill leachate has high PFAS levels and unique chemistry.

2- Quantify spatial and temporal PFAS distributions in mixed leachate and in upstream and downstream wells, addressing the need for site-specific monitoring and considering seasonal changes.

3- Conduct batch adsorption experiments to build adsorption isotherms for PFBA, PFBS, PFOA and PFOS on different GAC concentrations in original versus oxidized leachate, using total organic carbon analysis to track matrix competition and high-performance liquid chromatography-mass spectrometry (HPLC/MS) to quantify residual PFAS. This follows findings that adsorption capacity depends on PFAS chain length and adsorption competition in complex matrices for which isotherms can be modelled by Langmuir and/or Freundlich equations.

5- Compare adsorption performance among GAC materials to evaluate how pore structure and surface chemistry influence PFAS removal.

2.5 Methodological overview

2.5.1 Site and sampling

Mixed leachate samples were collected from the C1, C2 and C3 tanks of the Cerro Tanaro non-hazardous waste landfill (GAIA), which began operations in 2003. Upstream and downstream groundwater samples were taken from piezometer wells by pump and purge operation to capture spatial trends across the landfill boundary. Samplings were carried out repeatedly during the last year and in January to account for temporal variations.

2.5.2 Physicochemical characterization

The leachate and groundwater samples were analyzed for full characterization purposes including PFAS, pH, electrical conductivity, dissolved organic carbon etc. Total organic carbon (TOC) concentrations were determined using a TOC analyzer to quantify the organic load in each matrix. PFAS concentrations were measured by high-performance liquid chromatography coupled to tandem mass spectrometry

(HPLC-MS/MS). These analyses were performed externally by accredited laboratories.

2.5.3 Batch adsorption experiments

Competitive adsorption among PFBA, PFBS, PFOA and PFOS with an innovative approach was evaluated through batch isotherm tests. Adsorption experiments were conducted at the Politecnico di Torino's Clean Water Center (CWC), an interdepartmental center that addresses technological challenges related to water safety and supply; its goals are the design and advancement of innovative water treatment systems to purify and reclaim contaminated water streams efficiently. The CWC hosts various membrane separation setups, including nanofiltration, reverse osmosis, forward osmosis and ultrafiltration systems, and is acquiring analytical instruments such as HPLC-MS for water analysis. Batch tests were performed using different granular activated carbon (GAC) materials with varying pore structures and surface chemistries. Isotherms were generated by measuring equilibrium concentrations via HPLC-MS/MS Equipped with Q-TOF mass spectrometer. and by monitoring TOC removal to assess competition between PFAS and dissolved organic matter. Freundlich models were fitted to the equilibrium data to quantify maximum capacities and adsorption affinities.

Chapter 3

Regulations and Methodology

3.1 Environmental context and regulatory framework

European Regulation of Persistent Organic Pollutants:

In the environmental and regulatory context, the key European legislative instrument is Regulation (EU) 2019/1021 on persistent organic pollutants (POPs), which recasts and consolidates earlier POP rules.

According to Article 1, the Regulation's objective, invoking the precautionary principle, is to protect human health and the environment from POPs by prohibiting or phasing out their manufacture and use, minimizing releases to eliminate them where feasible, and establishing provisions for managing waste containing POPs. It implements obligations under the Stockholm Convention and the UN Protocol on POPs and allows Member States to apply stricter measures.

Article 3- Control of manufacturing, placing on the market and use:

Article 3 prohibits the manufacturing, placing on the market and use of substances listed in Annex I (Part A) and restricts those in Annex II. For Annex I substances - which include certain per- and polyfluoroalkyl substances (PFAS) - the regulation bans their production and marketing, whether as pure substances, in mixtures or within articles, subject to limited exemptions set out in Article 4. Member States and the Commission must consider POP criteria when assessing substances and take measures to prevent the introduction of new POPs. Waste containing substances listed in Annex IV is regulated separately under Article 7, but Article 3 ensures that new PFAS (e.g., PFOS, PFOA, PFHxS) are effectively phased out of commerce.

Annex I - Substances subject to prohibitions:

Annex I sets out the substances for which manufacture, placing on the market and use are prohibited (subject to exemptions). The annex includes:

Perfluorooctane sulfonic acid (PFOS) and its salts and PFOS-related compounds. For PFOS or its salts present in substances, mixtures or articles, concentrations must not exceed 0.025 mg kg^{-1} (0.0000025 % by weight). The sum of PFOS-related compounds must not exceed 1 mg kg^{-1} (0.0001 % by weight). Use of PFOS-containing articles placed on the market before 25 August 2010 is permitted, but placing new PFOS on the market is banned.

Perfluorooctanoic acid (PFOA), its salts and PFOA-related compounds. PFOA or its salts may only be present as an unintentional trace contaminant up to 0.025 mg kg^{-1} in substances, mixtures or articles. PFOA-related compounds are limited to 1 mg kg^{-1}, with a higher temporary limit of 20 mg kg^{-1} allowed for transported isolated intermediates used to produce fluorochemicals with C-chains ≤6 carbons. Special provisions permit concentrations up to 1 mg kg^{-1} in PTFE micro powders produced by irradiation or thermal degradation until 18 August 2023. For firefighting foams already installed, PFOA and its salts may be present up to 1 mg kg^{-1}, and individual PFOA-related compounds up to 10 mg kg^{-1} until 3 August 2028; fluorine-free foams cleaned using best techniques may contain up to 10 mg kg^{-1} combined PFAS. Exemptions allow use of PFOA in specific sectors (photolithography, photographic coatings, protective textiles for workers, medical devices) until July 2023-2025. Use of firefighting foam containing PFOA is banned after 3 December 2025, with strict containment requirements and prohibition on training or uncontrolled testing.

Perfluorohexane sulfonic acid (PFHxS), its salts and PFHxS-related compounds. PFHxS or its salts must not exceed 0.025 mg kg^{-1} in substances, mixtures or articles, and the sum of PFHxS-related compounds must not exceed 1 mg kg^{-1}. A temporary exemption allows PFHxS (and its salts and related compounds) in concentrated firefighting foam mixtures at up to 0.1 mg kg^{-1} (0.00001 %) until 28 August 2026, after which stricter limits will apply.

Article 7 - Waste management

Article 7 sets out detailed rules for managing waste that contains or is contaminated by POPs. Producers and holders of waste must avoid contamination with substances listed in Annex IV (the annex that enumerates POPs and sets concentration limits). Waste containing POPs must be disposed of or recovered without undue delay in a manner that destroys or irreversibly transforms the POP content, so that the remaining waste and releases no longer exhibit POP characteristics. Isolation of POPs from waste is permitted only if the isolated substances are subsequently destroyed by an approved method. Crucially,

recycling, reclamation or reuse operations that would recover the POP itself are prohibited; waste must not be processed in a way that returns these substances to the market. An exception (Article 7(4)) allows waste containing POPs below the concentration limits specified in Annex IV to be disposed of or recovered according to other EU waste legislation. Member States may authorize alternative operations for certain wastes if decontamination is unfeasible, if destruction is not environmentally preferable, and if they notify the Commission and other Member States. Finally, Article 7 requires Member States to ensure control and traceability of waste containing POPs, as stipulated by the Waste Framework Directive. In the context of the Cerro Tanaro landfill, these provisions mean GAIA must prevent PFAS contamination of waste streams, ensure that any PFAS-bearing waste is treated by destruction or irreversible transformation (e.g., high-temperature incineration), and maintain records demonstrating compliance.

Annex IV - Concentration limits for POPs in waste (relevant PFAS)

Annex IV lists the POPs subject to the waste-management rules of Article 7 and specifies concentration limits above which waste must be destroyed or irreversibly transformed. The annex identifies several PFAS:

Perfluorooctane sulfonic acid (PFOS) and its derivatives have a concentration limit of 50 mg kg^{-1}.

Perfluorooctanoic acid (PFOA), its salts and PFOA-related compounds are limited to 1 mg kg^{-1} for PFOA and its salts, and 40 mg kg^{-1} for the sum of PFOA-related compounds.

Perfluorohexane sulfonic acid (PFHxS), its salts and PFHxS-related compounds have the same limits as PFOA: 1 mg kg^{-1} for the acid and salts and 40 mg kg^{-1} for related compounds.

The Regulation requires the European Commission to review these concentration limits by 30 December 2027 and, where feasible, propose lower values. These waste thresholds are critical for landfill operations:

If PFAS concentrations in solid wastes (e.g., industrial sludges or PFAS-contaminated media) exceed these limits, the waste cannot be stored in a non-hazardous landfill like Cerro Tanaro but must be treated by methods that destroy or transform the PFAS (incineration, physio-chemical treatment or other Annex V operations).

Table 2. Summary of PFAS limitations in Regulation (EU) 2019/1021 (articles 3 & 7, annexes I & IV)

PFAS family	Manufacturing/placing-on-market restrictions (Article 3 & Annex I)	Waste management concentration limits (Article 7 & Annex IV)
Perfluorooctane sulfonic acid (PFOS) & salts	Manufacturing, placing on the market and use of PFOS and its salts are prohibited except for narrow exemptions. In new substances, mixtures or articles, PFOS and its salts may only be present as **unintentional trace contaminants** up to **0.025 mg kg^{-1}** (0.0000025 % by weight). The sum of PFOS-related compounds must not exceed **1 mg kg^{-1}** (0.0001 % by weight). Articles already in use before **25 Aug 2010** may continue to be used.	Waste containing PFOS and its derivatives must be disposed of or recovered so that the PFOS content is destroyed or irreversibly transformed (no recycling/reuse). Wast e with PFOS below **50 mg kg^{-1}** may be otherwise disposed or recovered in accordance with EU waste law.
Perfluorooctanoi c acid (PFOA), its salts & related compounds	Manufacture, placing on the market and use are banned except for limited time-bound derogations. PFOA or its salts may only be present at **≤ 0.025 mg kg^{-1}** in substances/mixtures/articles; any individual PFOA-related compound (or combination of compounds) must be **≤ 1 mg kg^{-1}**. A higher limit of **20 mg kg^{-1}** applies to PFOA-related compounds in transported isolated intermediates used to produce short-chain fluorochemicals. Special temporary provisions allow concentrations up to **1 mg kg^{-1}** PFOA (and **10 mg kg^{-1}** PFOA-related compounds) in PTFE micro powders until 18 Aug 2023 and in Class B firefighting foams until	Waste containing PFOA must be treated so that the PFOA is destroyed or irreversibly transformed. If PFOA or its salts are present above **1 mg kg^{-1}** or PFOA-related compounds above **40 mg kg^{-1}**, the waste must undergo destruction; below these levels it may be disposed or recovered in accordance with EU legislation.

	3 Aug 2028. Certain uses (photolithography, photographic coatings, protective textiles, medical devices) are allowed until 2023-2025.	
Perfluorohexane sulfonic acid (PFHxS), its salts & related compounds	Manufacturing, placing on the market and use are banned with narrow exemptions. PFHxS or its salts may be present only as unintentional contaminants up to **0.025 mg kg⁻¹** in substances/mixtures/articles. Th e sum of PFHxS-related compounds must not exceed **1 mg kg⁻¹**. A temporary exemption allows up to **0.1 mg kg⁻¹** PFHxS (and related compounds) in concentrated firefighting foam mixtures until **28 Aug 2026**.	Waste containing PFHxS must be treated so that PFHxS is destroyed or irreversibly transformed. Waste with PFHxS or its salts above **1 mg kg⁻¹** or PFHxS-related compounds above **40 mg kg⁻¹** must undergo destruction; below these levels the waste may be disposed or recovered.

Overview of the Piedmont regional law:

The "Legge regionale 19 ottobre 2021, n. 25" is an annual reorganization law ("legge annuale di riordino") passed by the Piedmont Regional Council. It amends multiple sectoral laws (tourism, culture, territory, environment) and introduces new provisions. Within this broad legislative package, Article 74 addresses environmental protection by setting emission limits for perfluoroalkyl substances (PFAS) in wastewater discharges into surface waters, and Annex A lists the specific limit values and implementation timelines.

Article 74 - Discharge of PFAS:

Article 74 states that, throughout the regional territory, emission limits for PFAS discharges to surface waters are established as indicated in Annex A, according to the timelines specified there. More stringent limits set by the competent authority during the Integrated Environmental Authorization (AIA) process take precedence. The article prohibits the discharge of PFAS-containing effluents onto soil or into superficial subsoil layers, except for storm overflow devices serving sewer networks.

Industrial wastewater discharges containing PFAS that enter sewer systems must comply with technical standards, regulatory prescriptions and limit values adopted by the local governing body and competent operators so that the emission limits in surface waters are respected.

Annex A - Emission limits for PFAS:

Annex A lists the maximum allowable PFAS concentrations in discharges to surface waters (Valori-limite di emissione, VLE), with distinct limits during an initial transition period (first 36 months after the law comes into force) and stricter limits thereafter. Key values relevant to the case study are summarised below:

PFOS (perfluorooctane sulfonic acid): 0.02 μg L^{-1} for the first 36 months; 0.00065 μg L^{-1} thereafter.

PFOA (perfluorooctanoic acid): 0.30 μg L^{-1} for the first 36 months; 0.10 μg L^{-1} thereafter.

Short-chain PFCAs: PFBA (7.0 μg L^{-1}), PFPeA (3.0 μg L^{-1}), PFHxA (1.0 μg L^{-1}).

Short-chain PFSAs: PFBS (3.0 μg L^{-1}), PFHxS (1.0 μg L^{-1}).

Long-chain PFCAs (PFHpA, PFNA, PFDeA, PFUnA, PFDoA): 1.0 μg L^{-1} each.

Emerging PFAS: cC6O4 limits decrease from 7.0 μg L^{-1} (months 13-24) to 3.5 μg L^{-1} (months 25-36) and to 0.5 μg L^{-1} thereafter; ADV limits decrease from 2.0 μg L^{-1} (months 13-24) to 0.5 μg L^{-1} thereafter.

Other PFAS: For compounds with carbon chains of 3-6, the limit is 3 μg L^{-1}; for chains of 7 or more, the limit is 1 μg L^{-1}.

Table 3. Emission limits for PFAS discharges into surface waters in Piedmont (Italy)

PFAS (substance/group)	**Emission limit in the first 36 months (μg L^{-1})**	**Emission limit after 36 months (μg L^{-1})**
PFOS - perfluorooctane sulfonic acid and its salts	0.02	0.00065
PFOA - perfluorooctanoic acid	0.30	0.10
PFBA - perfluorobutanoic acid	7.0	7.0
PFPeA - perfluoropentanoic acid	3.0	3.0
PFHxA - perfluorohexanoic acid	1.0	1.0
PFBS - perfluorobutanesulfonic acid	3.0	3.0

PFHpA - perfluoroheptanoic acid	1.0	1.0
PFHxS - perfluorohexanesulfonic acid	1.0	1.0
PFNA - perfluorononanoic acid	1.0	1.0
PFDeA - perfluorodecanoic acid	1.0	1.0
PFUnA - perfluoroundecanoic acid	1.0	1.0
PFDoA - perfluorododecanoic acid	1.0	1.0
cC6O4 - perfluoro {acetic acid, 2-[(5-methoxy-1,3-dioxolan-4-yl) oxy]}, ammonium salt	7.0 (months 13-24); 3.5 (months 25-36)	0.5
ADV - 1-Propene, 1,1,2,3,3,3-hexafluoro- telomer with chlorotrifluoroethene (oxidized, reduced, hydrolyzed)	2.0 (months 13-24)	0.5
Other PFAS (C_3-C_6 carbon chains, including new-generation)	3.0 per compound	-
Other PFAS (C_7+ carbon chains, including new generation)	1.0 per compound	-

ARPA Analytical sensitivity and environmental quality standards:

The ARPA 2025 report lists method detection limits (limits of quantification, LOQs) and environmental quality standards for the six PFAS monitored in surface and groundwater. The laboratory LOQs are 0.01 µg L^{-1} for PFBA, PFBS, PFHxA, PFOA and PFPeA, whereas for PFOS the LOQ is 0.0002 µg L^{-1}.

The corresponding environmental quality standards for surface waters are 7 µg L^{-1} (PFBA), 3 µg L^{-1} (PFBS), 1 µg L^{-1} (PFHxA), 0.1 µg L^{-1} (PFOA), 0.00065 µg L^{-1} (PFOS) and 3 µg L^{-1} (PFPeA); for PFOS there is also a short-term maximum admissible concentration of 36 µg L^{-1}.

These extremely low thresholds for PFOS reflect its high toxicity and bioaccumulation potential. Groundwater standards are similar but adjust for the aquifer context; the Italian "valore soglia" for PFOS is 0.03 µg L^{-1}, for PFOA 0.5 µg L^{-1}, for PFHxA 1 µg L^{-1}, and for PFBS and PFPeA 3 µg L^{-1}.

Table 4. ARPA Analytical environmental quality standards

PFAS compound	**Limit of quantification (LOQ) µg L^{-1}**	**Surface water standard µg L^{-1}**	**Short-term max µg L^{-1}**	**Groundwater threshold µg L^{-1}**
PFBA	0.01	7	-	-
PFBS	0.01	3	-	3
PFHxA	0.01	1	-	1

PFOA	0.01	0.1	-	0.5
PFOS	0.0002	0.00065	36	0.03
PFPeA	0.01	3	-	3

3.2 Sampling strategy

3.2.1 Leachate and groundwater collection

Leachate and groundwater samples were collected from the GAIA non-hazardous waste landfill for chemical characterization and adsorption tests. Leachate sampling focused on the effluent from basins C1, C2 and C3, which best represents the mixture that is stored and treated onsite. Sampling was carried out via the existing leachate extraction system, ensuring that the influent to the treatment plant was captured.

Groundwater monitoring included upgradient (background) and downgradient (impacted) piezometers; purge volumes were calculated to exchange at least three well volumes, and samples were collected using a pump-and-purge method to ensure representative formation water. Samples were stored in polypropylene bottles (avoiding fluoropolymer materials) and transported at 4 °C to laboratory.

3.2.2 Physicochemical characterization

Upon reception, samples were split for different analyses. Total organic carbon (TOC) was measured using a TOC analyzer. Suspended solids and colloids in leachate were noted to contribute to turbidity and complicate analyses. To preserve PFAS integrity, no filtration was performed before analysis, despite the high turbidity. These measurements established baseline conditions for the batch experiments and informed the dilution factors used in later tests.

The pump-and-purge approach for groundwater sampling, while necessary to obtain representative samples, required careful flow control to avoid well collapse and needed large purge volumes, which limited the frequency of sampling.

3.3 Groundwater monitoring

Monitoring of the upstream and downstream piezometers enabled evaluation of PFAS migration from the landfill. Field measurements included pH, conductivity, temperature and redox potential. Samples were analyzed for major

ions, TOC and target PFAS. The pump-and-purge method was chosen to remove stagnant water and ensure the collection of formation water; purge volumes were adjusted based on well depth and diameter. The monitoring results were used as a baseline to compare with leachate concentrations and to assess the potential for contaminant plumes.

3.4 Methodological and experimental approach

3.4.1 Context and problem statement

Leachate collected at the GAIA landfill exhibit extremely high concentrations of dissolved organic matter. In the raw leachate, total organic carbon (TOC) was measured around 2 000 mg L^{-1}. Such high organic loads can:

1- Interfere with high-performance liquid chromatography-mass spectrometry (HPLC-MS/MS) quantification of per- and polyfluoroalkyl substances (PFAS)

2-Compete for adsorption sites on granular activated carbon (GAC). The methodological challenge, therefore, was to design batch adsorption competition tests capable of quantifying PFAS and TOC removal while reducing TOC to a manageable level without filtration (which could induce PFAS losses).

A systematic series of experiments, including three initial scenarios (A-C), two redesigned scenarios (D-E) and a final low-dose redesign, were undertaken to address these challenges.

3.4.2 Overall experimental design and initial scenarios

To explore how oxidation and dilution influence TOC adsorption, three initial scenarios were defined:

Scenario A: Raw Leachate + GAC. Untreated leachate was contacted with GAC at a range of dosages. This scenario represents the most realistic matrix but carries a risk that TOC remains too high for PFAS analysis and increases competition for adsorption sites.

Scenario B: Oxidized leachate + GAC. Leachate was oxidized with hydrogen peroxide (H_2O_2) to transform organic matter and potentially reduce

fouling. Oxidation may however generate by-products and colloids that influence adsorption and analysis.

Scenario C: Oxidized + diluted leachate + GAC. Oxidized leachate was further diluted with deionized water to reach a lower TOC range. This combined approach reduces representativeness but facilitates experimentation.

In all initial scenarios, batch reactors were 30 mL glass vials containing 10 mL deionized water for GAC conditioning and 20 mL of leachate-based matrix, giving a total liquid volume of 30 mL (0.03 L).

GAC doses were 0, 10, 20, 40, 60, 80 and 100 g L^{-1} and required mass of GAC per vial was calculated as:

$$m_{GAC}\,(g) = C_{GAC}(gL^{-1}) \times V_{vial}(0.03L)$$

Yielding 0.30 g at 10 gL^{-1} and 3.00 g at 100 g L^{-1}.

Table 5. First GAC dosing

GAC concentration (g/L)	Vial volume (L)	GAC mass per vial (g)
0	0.03	0.00
10	0.03	0.30
20	0.03	0.60
40	0.03	1.20
60	0.03	1.80
80	0.03	2.40
100	0.03	3.00

Two contact times were used, approximately 48 h (timepoint 1) and 72/120 h (timepoint 2), to assess kinetic effects and the achievement of the system's equilibrium state. For each matrix type, 14 vials (7 doses × 2 timepoints) were prepared.

3.4.3 GAC conditioning protocol

To maximize reproducibility and available adsorption surface area, the GAC was conditioned before contact:

Washing: GAC was rinsed repeatedly with deionized water until the supernatant was visibly clear, removing fines and soluble impurities.

Drying: Washed GAC was oven-dried at 60 °C overnight to standardize its moisture content without thermal degradation.

Vacuum wetting: For each vial, the appropriate mass of dried GAC was dosed, and 10 mL deionized water was added. Vials were placed under vacuum for at least 1 h to remove entrained air and ensure complete pore wetting.

Matrix addition: After conditioning, 20 mL of the contaminant solution (raw leachate, oxidized leachate, or oxidized + diluted leachate) was added to each vial to reach the final volume (30 mL).

All reactors were placed under rotational agitation throughout the test duration to ensure better contact between GAC and the adsorbates.

3.4.4 Oxidation procedure and reasoning

The oxidation step aimed to alter the molecular weight distribution of natural organic matter (NOM) and reduce fouling. Hydrogen peroxide (H_2O_2) was used as the oxidant.

The procedure involved adding 30 mL of H_2O_2 to 300 mL of raw leachate every 2 h, repeated three times (total 90 mL H_2O_2). This staged addition minimizes localized high oxidant concentrations and promotes homogeneous oxidation. After the third addition, the mixture was left to react, and the final oxidized leachate volume was 390 mL. The oxidized leachate (referred to hereafter as "Ox") served as the matrix for Scenarios B and C.

3.4.5 Preliminary TOC screening and necessity for methodology redesign

TOC reductions achieved in the initial scenarios were modest. In the oxidized + diluted matrix (Scenario C), the best case, 100 g L^{-1} GAC after ~66 h, reduced TOC to ≈ 41 mg L^{-1}.

Moreover, TOC occasionally increased with GAC dose, attributed to carbon fines and leachable organic compounds released from the adsorbent. Because filtration was avoided, these fines were oxidized in the TOC analyzer, inflating measured values.

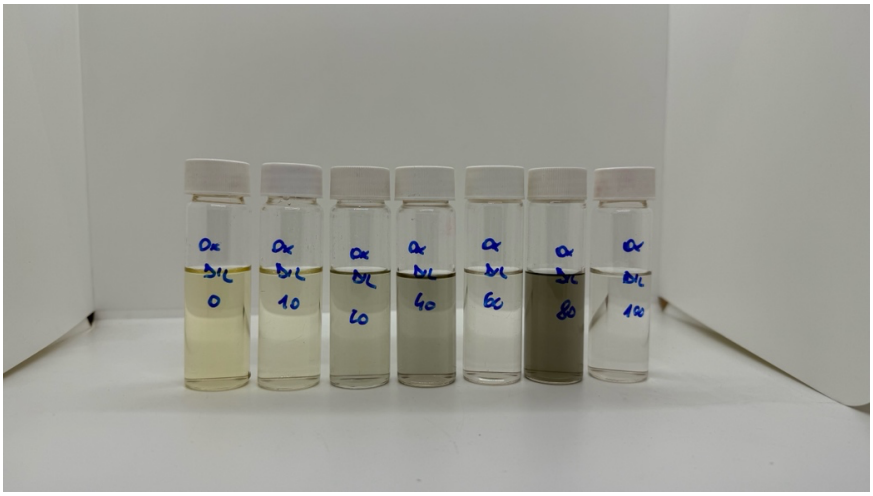

Figure 5. Diluted and oxidized leachate samples after 48 h contact at increasing GAC doses (0-100 g L^{-1}) during the preliminary TOC removal test, showing moderate clarification at intermediate doses and visible carbon suspension at higher concentrations.

These findings led to a redesign of the experimental plan. A mass-balance check suggested that diluting raw leachate (≈2 000 mg L^{-1} TOC) by a factor of 1:50 would yield ~40 mg L^{-1}, similar to the best oxidized + diluted scenario (Scenario C). Therefore, oxidation was not essential for TOC reduction; dilution alone could achieve comparable results while preserving a more realistic matrix.

Additionally, because high GAC doses were impractical (due to extensive PFAS removal and TOC artefacts), the GAC dose range was extended toward lower concentrations.

3.4.6 Revised experimental design: Scenarios D and E

The revised plan introduced two new scenarios: Scenario D (raw leachate diluted 1:50) and Scenario E (oxidized leachate diluted 1:40). Working solutions were prepared as follows:

Scenario D (1:50 dilution): 20 mL raw leachate + 980 mL deionized water: 1 L diluted raw leachate.

Scenario E (1:40 dilution): 25 mL oxidized leachate + 975 mL deionized water: 1 L diluted oxidized leachate.

Table 6. Redesigned dilutions for new scenarios

Matrix	Target dilution	Total volume (mL)	Leachate/oxidized stock volume (mL)	DIW volume (mL)
Diluted raw leachate	1:50	1000	20.0	980.0
Oxidized + Diluted leachate	1:40	1000	25.0	975.0

3.4.7 PFAS spiking and GAC dosage expansion

In raw leachate, PFAS concentrations are typically in the ng L^{-1} (ppt-ppb) range, whereas TOC is in the mg L^{-1} (ppm) range. To construct adsorption isotherms and ensure measurable concentration changes, PFAS were therefore spiked into the matrices.

Preparation of the mixed PFAS working stock (spike solution)

A mixed PFAS working stock was prepared from four native PFAS standards (PFBA, PFBS, PFOA and PFOS) supplied at 1 g L^{-1} in methanol. To obtain a multi-analyte solution, 250 µL of each individual standard were combined (total standard volume = 1.00 mL, methanolic) and diluted to a final volume of 10.0 mL with deionized water (DIW). This produced a mixed stock containing 25 mg L^{-1} of each analyte (i.e., 100 mg L^{-1} total PFAS) and 10% (v/v) methanol (1 mL MeOH in 10 mL total).

Spiking of sample vials

The mixed PFAS stock was added to the batch reactors to reach a target concentration of 100 µg L^{-1} per analyte (400 µg L^{-1} total). For each 30 mL vial, the required spike volume was calculated using the dilution equation $C1 \times V1 = C2 \times V2$ with $C1$= 25 mg L^{-1} per analyte (= 25,000 µg L^{-1}), $C2$= 100 µg L^{-1} total, and $V2$ = 30 mL:

$$V1 = \frac{(100 \mu g L^{-1} \times 30\ ml)}{25000\ \mu g L^{-1}} = 0.12\ mL$$

Thus 120 µL of stock solution was added to each vial.

The GAC dosage series was also expanded to 0, 1, 5, 10, 20, 40, 60, 80 and 100 g L^{-1}. For each concentration, two vials were prepared to permit two contact times (≈48 h and ≈70 h). Calculated GAC masses (for 0.03 L vials) ranged from 0.03 g (1 g L^{-1}) to 3.00 g (100 g L^{-1}).

Table 7. Expanded GAC dosage

Target GAC concentration (g/L)	Vial volume (L)	GAC mass per vial (g)
0	0.03	0.00
1	0.03	0.03
5	0.03	0.15
10	0.03	0.30
20	0.03	0.60
40	0.03	1.20
60	0.03	1.80
80	0.03	2.40
100	0.03	3.00

After spiking and GAC dosage expansion, the vials were agitated on a mechanical agitator at ambient temperature. Two sets of contact times (48 h and 70 h) were used. At the end of contact, aliquots were withdrawn (without filtration) for TOC analysis and HPLC-MS/MS quantification of PFAS. The use of unfiltered aliquots means that suspended carbon particles and leached organics can be included in the TOC measurement which is an important consideration in interpreting results.

The same conditioning procedures for GAC were followed as in the initial scenarios. However, the spiking level ensured that equilibrium concentrations remained within the calibration range even at high GAC doses. The comparison of TOC and PFAS removal between diluted raw and diluted oxidized matrices would reveal whether oxidation alters competition for adsorption sites.

3.4.8 Further redesign: low-dose GAC and larger reactors

The first revised experiments revealed that high GAC doses still drove PFAS concentrations below detection specifically for PFBS, PFOA, PFOS and produced non-monotonic TOC behavior due to particulate carbon.

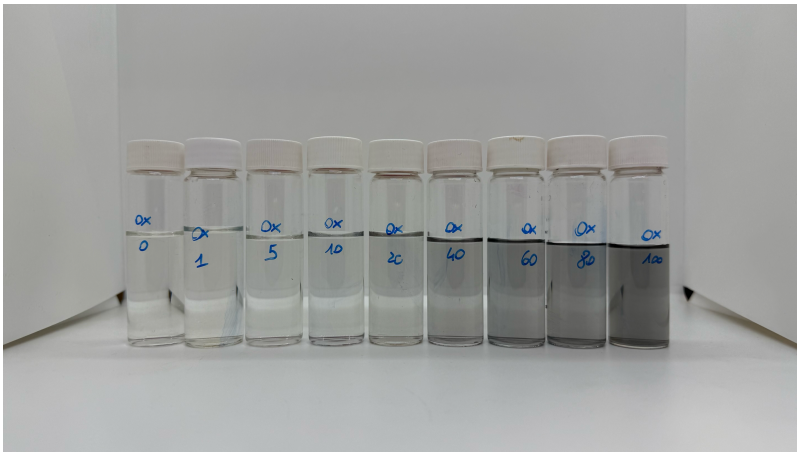

Figure 6. Oxidized leachate samples after 48 h contact with increasing GAC doses (0-100 g L^{-1}), showing progressive darkening at higher doses.

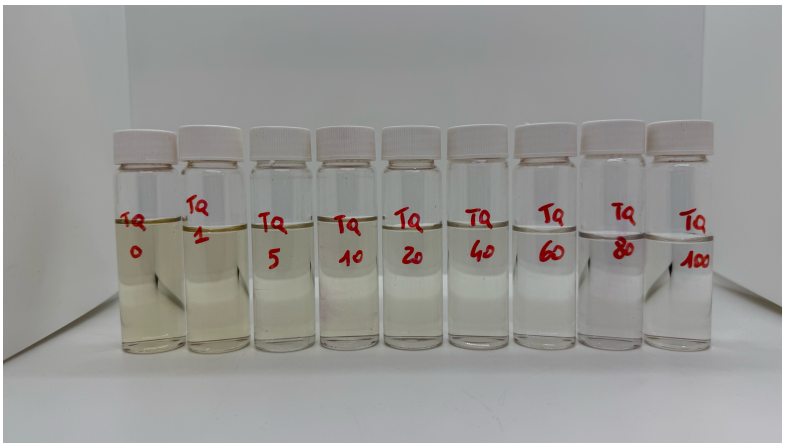

Figure 7. Raw leachate samples after 48 h contact with increasing GAC doses (0-100 g L^{-1}), illustrating higher initial turbidity and gradual clarification at elevated GAC concentrations.

Therefore, a second redesign adopted lower GAC concentrations and larger reactors to improve analytical resolution and minimize sampling disturbance.

3.4.9 Final experiment design

The new GAC dose series was 0, 0.5, 1, 1.5, 2, 3, 5 and 10 g L^{-1}. This range focuses on low to moderate doses where PFAS removal remains partial and within analytical quantification limits. Batch experiments were conducted using both diluted raw leachate and diluted oxidized leachate in order to compare competitive

adsorption behavior under different organic matrix compositions. The mass of GAC per reactor was recalculated accordingly for the larger working volumes.

Larger reactors and adjusted volumes

Reactor size was increased from 30 mL vials to 100 mL bottles. The bottles contained 66 mL of diluted matrix and 33 mL deionized water (2:1 ratio of matrix: DIW), maintaining the same dilution as in Scenarios D and E. For a 0.1 L solution, the GAC mass (m_{GAC}) for a target concentration C is:

$$m_{GAC}\,(g) = C_{GAC}(gL^{-1}) \times V_{bottle}(0.1L)$$

Thus, at 0.5 g L^{-1} the bottle contained 0.05 g (50 mg) GAC, while at 10 g L^{-1} it contained 1.00 g.

Table 8. Low GAC dosage in each bottle

GAC concentration (g/L)	Bottle volume (L)	GAC mass (g)	GAC mass (mg)
0	0.10	0.000	0
0.5	0.10	0.050	50
1	0.10	0.100	100
1.5	0.10	0.150	150
2	0.10	0.200	200
3	0.10	0.300	300
5	0.10	0.500	500
10	0.10	1.000	1000

The larger volume provided sufficient sample for duplicate PFAS injections and TOC analyses and reduced the impact of aliquot removal on the liquid-solid ratio. Two contact times were used: an intermediate time (70 h) was omitted for TOC analysis to avoid removing large aliquots from the bottles; instead, only the long-contact time (141 h) was sampled for TOC analysis but for PFAS analysis both contact times were sampled and analyzed by HPLC/MS-MS.

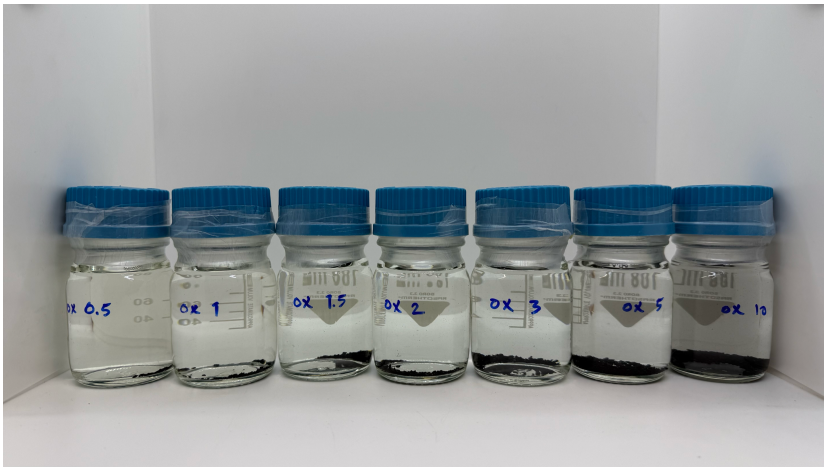

Figure 8. Oxidized leachate samples after 141 h contact time in the final experimental design, showing progressive darkening at higher GAC doses (0.5-10 g L^{-1})

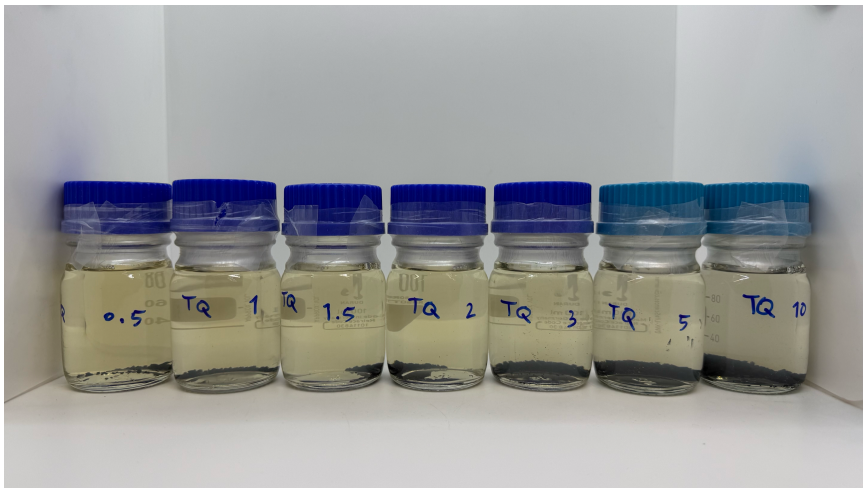

Figure 9. Raw leachate samples after 141 h contact time in the final experimental design, showing persistent color and visible carbon sedimentation at increasing GAC concentrations (0.5–10 g L^{-1})

3.4.10 Experiment on different GAC material properties

To complete the adsorption study, a final set of batch tests is being carried out using the same protocol as the 100 mL bottle experiments described earlier. These tests use only raw landfill leachate (no oxidized matrix) spiked with 100 µg L^{-1} of each PFAS (PFBA, PFBS, PFOA and PFOS). The granular activated carbon (GAC) dose series remains 0, 0.5, 1.0, 1.5, 2.0, 3.0, 5.0 and 10.0 g L^{-1}, and one

contact time of 72hr is evaluated. Unlike previous tests that used a single adsorbent, two other commercial GAC products are used.

The experiment used the same spiking and sampling as described earlier. By comparing PFAS and TOC removal in raw leachate at the same GAC doses for the two adsorbents, the study will quantify how adsorbent properties (surface area, particle size and iodine number) influence competitive adsorption in a high-organic-carbon and complex matrix. Results will be analyzed using the mass-balance equation and Freundlich isotherm fitting, with attention to shifts in adsorption capacity K_f and intensity ($\frac{1}{n}$) due to differences in adsorbent microstructure and pore distribution.

Table 9. Physicochemical Properties of Granular Activated Carbons

Property	**Carbopur 1240**	**Organosorb 10-AA**	**Organosorb 10-AM**
Carbon Type	Granular activated (coal)	Agglomerated GAC (coal blend)	Agglomerated GAC (coal blend)
Iodine Number (min.)	950 mg/g	900 mg/g	1100 mg/g
Particle Size	12×40 $mesh$ ($0.425 - 1.70$ mm)	$0.425 - 1.70$ mm	$0.60 - 2.36$ mm
Particle Size (min)	93% (> 0.425 mm)	90% (> 0.425 mm)	90% ($< 2.36, > 0.60$ mm)
Apparent Density	490 ± 10 kg/m^3	430 kg/m^3	470 kg/m^3
BET Surface Area	1009 m^2/g	940 m^2/g	1150 m^2/g
Hardness (min.)	95%	93%	93%
Ash Content (max.)	15%	-	-
pH (water)	9.4	-	-

3.4.11 Data analysis and modelling

Removal efficiency (R) quantifies the proportion of a contaminant removed from solution during an adsorption test. It is expressed as a percentage and calculated from the initial concentration (C_0) and the equilibrium concentration after contact with the adsorbent (C_e):

$$R = \frac{C_0 - C_e}{C_0} \times 100$$

For total organic carbon (TOC) removal, C_0 and C_e are the initial and final TOC concentrations in solution (mg L^{-1}). For PFAS removal, they represent the initial and equilibrium concentrations of the specific PFAS (in µg L^{-1}).

This ratio reflects the fraction of contaminant mass eliminated from the solution relative to the starting mass. A higher percentage means a greater proportion of the contaminant has been removed. Removal efficiency is particularly useful when comparing:

While removal efficiency indicates how much of the contaminant is removed relative to its initial concentration, it does not reflect how much contaminant is taken up per unit mass of adsorbent.

For each PFAS and TOC, the amount adsorbed per unit mass of GAC was determined by mass balance:

$$q_e = \frac{(C_0 - C_e) \times V}{m_{GAC}}$$

where C_0 is the initial concentration (µg L^{-1}), C_e is the equilibrium concentration, V is the solution volume (L) and m_{GAC} is the mass of GAC (g).

Adsorption isotherms were fitted using the Freundlich model,

$$q_e = K_f \times C_e^{\frac{1}{n}}$$

And linearized by plotting:

$$Log\ q_e = Log\ K_f \times \frac{1}{n}\ Log\ C_e$$

The Freundlich capacity coefficient K_f and the heterogeneity parameter $\frac{1}{n}$ were derived from the intercept and slope respectively. Values of $n > 1$ $(0 < 1/n < 1)$ indicate favourable, nonlinear adsorption typical of heterogeneous sorbents.

Separate isotherms were constructed in deionized water (single-solute baseline) and in the diluted matrices (competitive systems). Comparison of K_f and n across matrices allows assessment of how residual TOC and oxidation alter adsorption capacity and intensity.

Finally, these methodological and experimental developments resulted in a robust experimental protocol suitable for constructing PFAS adsorption isotherms in complex landfill leachate matrices. The trials and redesigns underscore the need for flexible experimental design when dealing with complex matrices and highlight the interplay between adsorbent dosage, contact time, dilution, oxidation and analytical constraints.

Chapter 4

Characterization Results and Discussion

4.1 Characterization of incoming waste streams (W1-W12) and implications for leachate quality

To contextualize the variability observed in mixed leachate (C1+C2+C3) and to anticipate matrix-driven limitations during GAC adsorption tests, twelve representative incoming waste streams (W1-W12) were characterized through bulk parameters (pH, density, dry residue/moisture, ash, TOC) and eluate properties (pH, conductivity, DOC), together with targeted PFAS screening in the solid phase (PFOS). Overall, the dataset highlights that leachate "matrix strength" is controlled primarily by dissolved organics and salts, rather than by the PFAS loading measured in the solid wastes. Only W1 and W5 showed quantifiable PFOS (both 0.036 mg/kg), while all other wastes were below detection limits.

Range and heterogeneity of key properties:

Table 10. Waste stream characteristics

Waste	pH (s)	Density (g/mL)	Dry 105 (%)	Moist (%)	Ash600 (%)	TOC (%)	pH (el)	Cond (µS/cm)	DOC (mg/L)	PFOS (mg/kg)
W1	7.02	0.48	77.5	22.5	10.6	37	7.6	1330	613	0.036
W2	7.28	0.56	65.2	34.8	10.5	28	8.3	1960	125	<0.0044
W3	9.7	0.43	56.2	43.8	15.4	28	9.1	4340	1440	<0.0047
W4	8.21	0.37	81.1	18.9	10.6	45	8.6	852	488	<0.0094
W5	7.18	0.32	54.6	45.4	4.86	33	6.32	5670	2480	0.036
W6	5.67	0.172	96	4	19.5	47	6.32	2160	683	<0.0093
W7	6.89	0.4	74.2	25.8	15.1	33	7.1	1800	259	<0.0045
W8	7.19	0.45	77	23	27.4	29	7.6	2840	832	<0.0043
W9	7.4	0.32	94.9	5.1	7.78	55	7.86	967	512	<0.0045

W10	7.18	0.159	94	6	10.4	63	7.74	343	161	<0.0042
W11	8.21	0.37	81.1	18.9	10.6	45	8.63	852	488	<0.0094
W12	6.74	0.42	58.7	41.3	22.6	23	7.32	1990	465	<0.0044

Across W1-W12, moisture spans between 4-45%, TOC 23-63%, DOC 161-2480 mg/L, and Conductivity 343-5670 µS/cm, confirming that the landfill receives materials capable of generating leachates ranging from relatively "mild" to "extremely complex". This heterogeneity is consistent with the field evidence that GAIA leachate is characterized by very high organic content (TOC on the order of 2,000 mg/L), which motivated the staged experimental strategy (oxidation/dilution and low-dose GAC) to enable robust PFAS analysis and competitive adsorption testing.

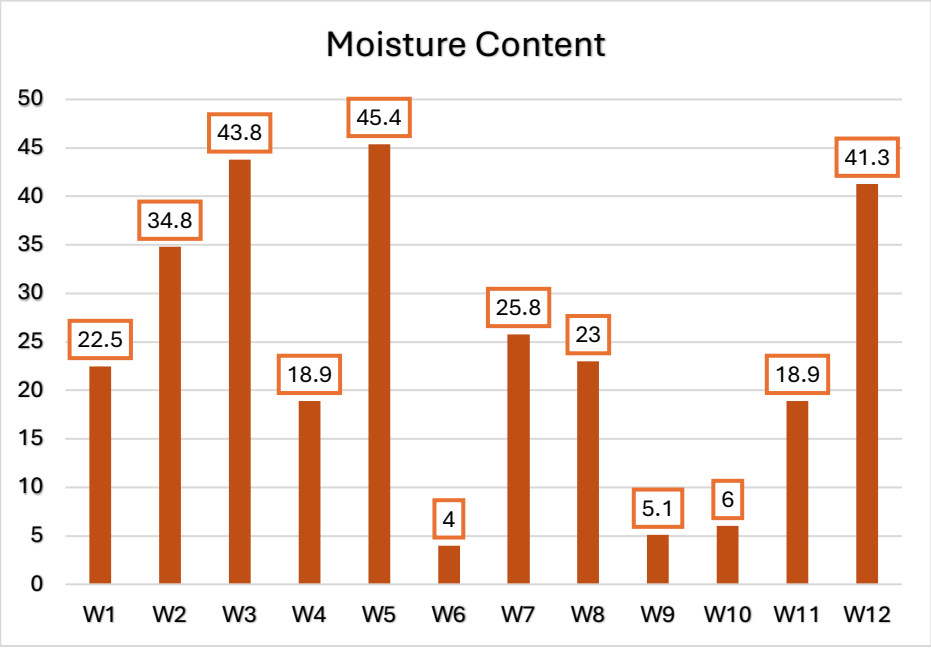

Figure 10. Moisture content (%) of different waste streams (W1-W12), showing substantial variability among samples, with highest values observed in W5 and W3 (>40%) and lowest values in W6, W9, and W10 (<10%).

Two patterns in the waste dataset are particularly relevant for PFAS adsorption:

1- DOC and conductivity tend to increase together in the incoming wastes, suggesting that high DOM conditions often coincide with higher ionic strength,

although some streams (e.g., W2, W7) show elevated conductivity with relatively low DOC, indicating salt-driven conductivity independent of DOM.

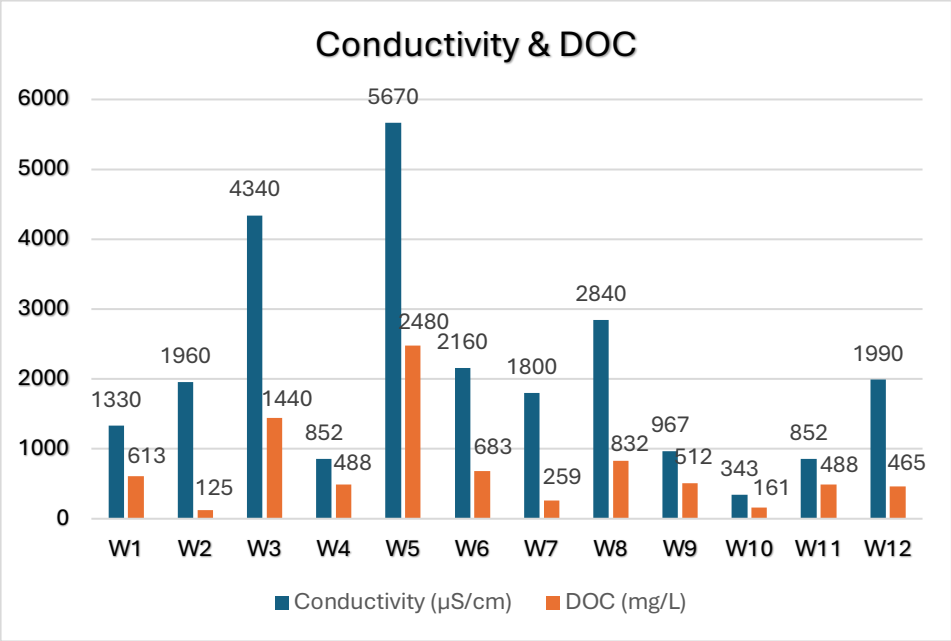

Figure 11. Electrical conductivity (µS cm^{-1}) and dissolved organic carbon (DOC, mg L^{-1}) of waste streams W1-W12, highlighting marked variability among samples and a general correspondence between higher conductivity and elevated DOC levels in selected streams.

2- TOC is not a good predictor of DOC, meaning that a waste can be carbon-rich but still release limited dissolved organics (i.e., carbon largely insoluble/refractory).

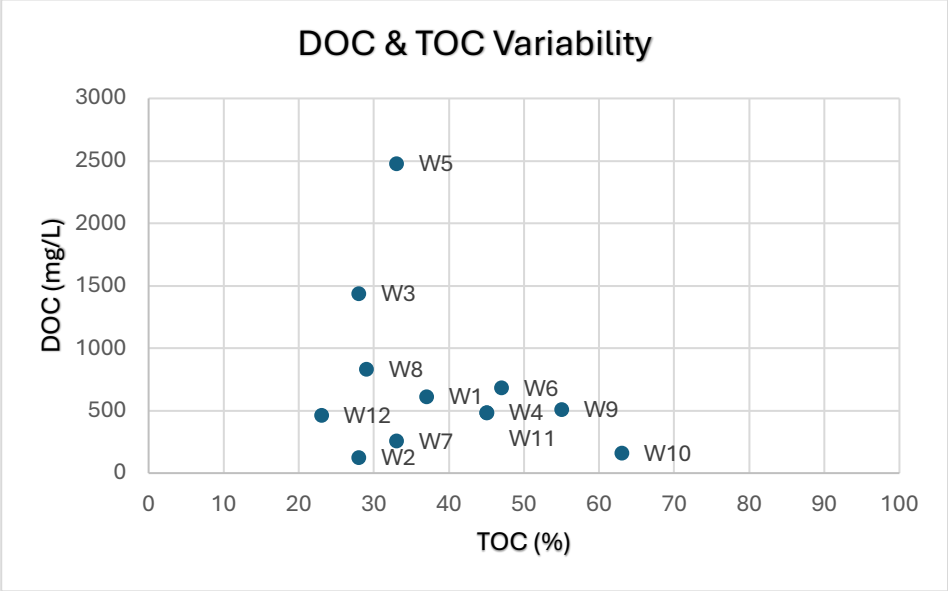

Figure 12. DOC (mg L^{-1}) versus TOC (%) for waste streams W1-W12, showing marked variability and non-linear correlation between total and dissolved organic fractions.

Matrix-driven "worst-case" and "best-case" leachate scenarios:

From an adsorption standpoint, the waste streams can be grouped into operationally meaningful classes:

1- Worst-case matrices (high DOC + high conductivity): W3, W5, W8

W5 shows the most critical combination: DOC 2480 mg/L and conductivity 5670 µS/cm, together with measurable PFOS (0.036 mg/kg) and detectable PFOA salts. This stream therefore represents the most challenging condition: high PFAS relevance and maximal competitive inhibition (pore blocking + site competition + ionic effects).

W3 exhibits very high DOC (1440 mg/L) and high conductivity (4340 µS/cm), coupled with alkaline eluate pH (9), a condition that can further reduce electrostatic attraction of anionic PFAS to carbon surfaces and exacerbate competition.

W8 (compost off-spec) also yields a high-strength eluate (DOC 832 mg/L; conductivity 2840 µS/cm), indicating substantial dissolved organics likely capable of rapid pore fouling and competitive uptake.

Implication could be that even if PFAS concentrations are low in the solids, these wastes can generate leachates where PFAS removal is limited by the matrix, aligning with the need to interpret Freundlich parameters as “effective” (matrix-dependent) rather than intrinsic sorbent properties.

2- Intermediate matrices (moderate DOC and/or high salts): W1, W4/W11, W6, W7, W9, W12

W1 has moderate DOC (613 mg/L) and measurable PFOS (0.036 mg/kg), representing a realistic but not extreme competition scenario.

W4 and W11 are essentially replicates (DOC 488 mg/L; Conductivity 852 µS/cm), providing internal confirmation that similar waste composition yields consistent eluate strength and therefore comparable adsorption constraints.

W7 is notable for relatively low DOC (259 mg/L) but very high sulfate, suggesting that ionic strength (rather than DOM) may dominate adsorption suppression for some streams.

W12 combines high moisture with moderate DOC (465 mg/L) and relatively high conductivity (1990 µS/cm), indicating balanced organic and ionic competition.

Implication could be that these wastes likely generate leachates where PFAS adsorption remains feasible but with measurable reductions in capacity and slower kinetics, especially for shorter-chain PFAS that are already less strongly adsorbed.

3- Best-case matrices (low DOC + low conductivity): W10 (and partly W2)

W10 shows the lowest DOC (161 mg/L) and conductivity (343 µS/cm), despite having very high TOC in the bulk solid. This indicates that most carbon is not readily dissolved and therefore contributes less to competitive adsorption.

W2 has very low DOC (125 mg/L) but higher Conductivity (1960 µS/cm), suggesting that adsorption limitations, if any, may be more attributable to ionic effects than DOM competition.

Implication could be that these streams represent conditions where GAC should exhibit the highest apparent affinity and capacity for PFAS, providing a useful contrast against W3/W5/W8-type matrices.

Relevance for interpreting leachate and adsorption outcomes:

The waste-stream dataset supports a key interpretative framework for the subsequent adsorption results:

1- PFAS mass loading in solids is not the dominant driver in this set (most PFOS are <LOQ.

2- DOC and conductivity are the dominant controls on adsorption performance, consistent with the broader observation that GAIA leachate contains very high organic carbon and multiple PFAS at µg/L levels.

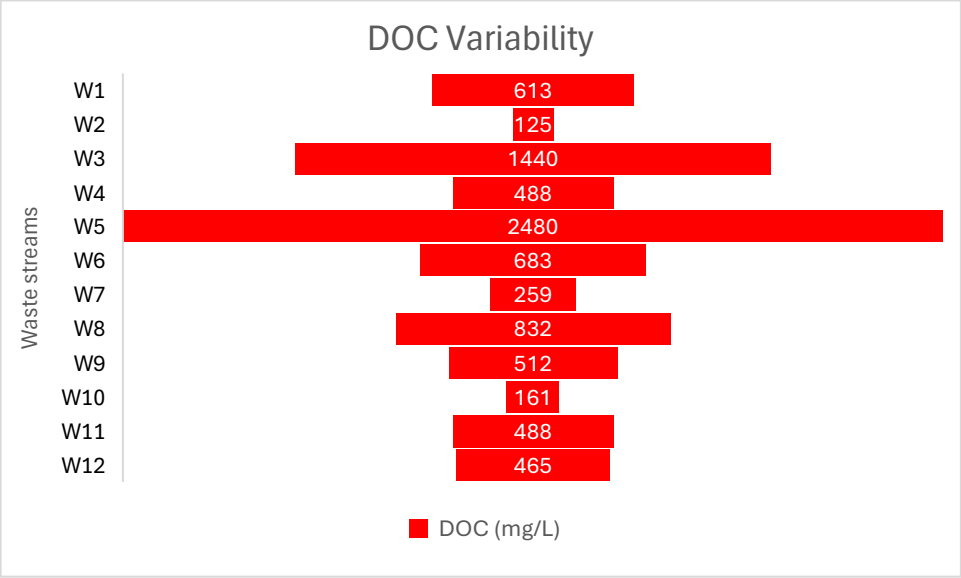

Figure 13. DOC (mg L^{-1}) variability among waste streams (W1-W12), emphasizing its influence on adsorption system behavior.

Therefore, differences observed between adsorption scenarios (raw vs oxidized vs diluted matrices; different GAC types) should be interpreted primarily as matrix effects (competitive adsorption and pore blocking) rather than as changes in PFAS availability alone.

4.2 Landfill Leachate and Groundwater Characterization

4.2.1 Monthly and cumulative leachate production:

Monthly monitoring datas show how rainfall influences the quantity of leachate collected. Rainfall (in mm) and the mass of leachate collected (in tons) were recorded alongside the number of rainy days. Table 2 lists these data and provides cumulative values.

The environmental significance of this table is twofold. First, it quantifies the water balance at the landfill: rainfall infiltration through the waste mass produces leachate, which must be collected and treated to protect groundwater and surface waters. Second, it provides evidence for regulatory compliance with the European Union Landfill Directive and its Italian implementation, which require operators to minimize infiltration and monitor leachate volumes.

Table 11. Monthly and cumulative leachate production data (Half-Yearly report on operations and environmental monitoring, GAIA)

Month	Monthly rainfall (mm)	Cumulative rainfall (mm)	Rainy days (no.)	Max daily rainfall (mm)	Monthly leachate (t)	Cumulative leachate (t)
Jan	42.6	42.6	19	30.4	257.5	257.5
Feb	129.2	171.8	16	58.2	400.5	658.0
Mar	206.6	378.4	16	30.8	1202.9	1860.9
Apr	61.4	439.8	12	23.4	2171.6	4032.5
May	117.8	557.6	18	22.8	2557.5	6590.0
Jun	42.8	600.4	14	10.8	2208.2	8798.2
Jul	56.2	656.6	7	24.6	2148.2	10946.3
Aug	23.4	680.0	8	14.4	1744.3	12690.7
Sep	110.4	790.4	17	41.6	1208.8	13899.5
Oct	182.6	973.0	26	34.6	1225.8	15125.2
Nov	6.2	979.2	19	1.2	1389.6	16514.9
Dec	17.0	996.2	17	6.8	1220.2	17735.1

Analysis of rainfall-leachate relationships:

R_i denote the rainfall (mm) in month i and L_i corresponding mass of leachate produced (ton). The overall infiltration coefficient I_T for the year is defined as the ratio of total leachate to total rainfall:

$$I_T = \frac{\sum_{i=1}^{12} L_i}{\sum_{i=1}^{12} R_i}$$

For 2024, the total rainfall was $\sum_i R_i = 996.2\ mm$ and the total leachate was $\sum_i L_i = 17735.1\ ton$. Substituting these values gives:

$$I_T = \frac{17735.1\ ton}{996.2\ mm} \approx 17.8\ t.mm^{-1}$$

Assuming the density of leachate is close to that of water (1 t ≈ 1 m³), I_T can be interpreted as the approximate volume of leachate generated per millimeter of rainfall. The value of ~18 t mm⁻¹ indicates that, on average, each millimeter of rainfall results in about 18 tons (or cubic meters) of leachate collected and it includes not only direct infiltration of rainfall but also percolation of water accumulated in previous months, and liquid produced by waste decomposition and leachate recirculation.

Relation to PFAS monitoring:

Because leachate transports per- and polyfluoroalkyl substances (PFAS) from waste to the environment, understanding its generation is essential for assessing PFAS risks. The recast EU Drinking Water Directive sets a maximum allowable concentration of 0.5 µg L⁻¹ for total PFAS and 0.1 µg L⁻¹ for the sum of 20 specific PFAS. High leachate volumes can dilute PFAS concentrations, whereas low rainfall but persistent leachate may concentrate them. Continuous PFAS monitoring in leachate and downstream groundwater is therefore necessary, especially when infiltration ratios are high.

4.2.2 Leachate (C1+C2+C3) characterizations

The leachate from tanks C1+C2+C3 showed the typical signature of a mature landfill leachate: neutral-slightly alkaline pH, high ionic strength, and high organic and nitrogen load.

Table 12. Leachate Characterization (C1+C2+C3)

Parameter	Apr 2025	Jan 2026
pH	7.64	7.97

Electrical conductivity (µS/cm)	23600	19900
TOC (mg/L)	**1080**	**1330**
COD (mg/L)	7660	4500
BOD5 (mg/L)	1000	1600
NH4 (mg/L)	2660	1640
TKN (mg/L)	2070	1470
Total nitrogen (mg/L)	2070	1470
TSS (mg/L)	85	167
Chloride (mg/L)	**23.8**	**2960**
Sulfate (mg/L)	**0.236**	**186**

In April 2025, the leachate exhibited pH 7.64 ± 0.17 and a very high conductivity (23,600 µS cm^{-1}), confirming strong mineralization. The organic fraction was substantial (TOC 1,080 mg L^{-1}, COD 7,660 mg L^{-1}, BOD_5 1,000 mg L^{-1}) and nitrogen was dominated by reduced forms (NH_4^+-N 2,660 mg L^{-1}, TKN 2,070 mg L^{-1}), consistent with an anaerobic, highly loaded matrix.

In January 2026, pH remained in the same range (7.97 ± 0.17) while conductivity was still high (19,900 ± 2,000 µS cm^{-1}). The organic load remained elevated (TOC 1,330 ± 400 mg L^{-1}, COD 4,500 ± 1,100 mg L^{-1}, BOD_5 1,600 ± 560 mg L^{-1}) and nitrogen was again largely ammoniacal (NH_4^+-N 1,640 ± 330 mg L^{-1}, TKN 1,470 ± 370 mg L^{-1}).

A key temporal change was observed in the inorganic composition: chloride increased from 23.8 ± 3.6 mg L^{-1} (April 2025) to 2,960 ± 440 mg L^{-1} (January 2026), and sulfate increased from 0.236 mg L^{-1} to 186 ± 28 mg L^{-1}.

This shift indicates a substantial evolution of ionic composition between campaigns. Such changes can plausibly reflect operational and hydrologic variability (e.g., changes in leachate recirculation, dilution balance, seasonal water input, or shifts in contributing waste streams). Importantly, these variations imply that the adsorption tests must be interpreted in the context of a strongly variable competitive matrix, where ionic strength and dissolved constituents may modulate PFAS uptake and apparent adsorption capacity.

Leachate (C1+C2+C3) PFAS characterization:

PFAS were detected in leachate at µg L^{-1} concentrations, with a profile dominated by short-chain compounds and a strong contribution from the emerging replacement PFAS, C6O4.

Table 13. PFASs in Leachate (C1+C2+C3)

Analyte	Apr 2025 (µg/L)	Jan 2026 (µg/L)
6:2 FTA	<5*	2.7±1.1
ADONA	<0.28	<0.016
C6O4	18.5±7.4	21.8±8.7
GenX	<0.29	<0.014
PFBA	4.7±1.9	4.4±1.8
PFBS	11.5±4.6	12.5±5
PFDA	<0.18	<0.014
PFDoA	<0.23	<0.017
PFDoDS	<0.26	<0.017
PFDS	<0.19	<0.014
PFHpA	1.46±0.58	0.83±0.33
PFHpS	<0.19	<0.014
PFHxA	9±3.6	10±4
PFHxS	<0.26	0.122±0.049
PFNA	<0.21	<0.015
PFNS	<0.18	<0.011
PFOA	1.39±0.56	1.85±0.74
PFOS	<0.21	0.27±0.11
PFPeA	7±2.8	4.8±1.9
PFPeS	<0.21	<0.0085
PFTeDA	<0.46	<0.017
PFTrDA	<0.28	<0.013
PFTrDS	<0.19	<0.013
PFUnA	<0.32	<0.015
PFUnDS	<0.33	<0.019

In April 2025, the most abundant compounds were C6O4 (18.5 µg L^{-1}) and PFBS (11.5 µg L^{-1}), followed by PFHxA (9.0 µg L^{-1}), PFPeA (7.0 µg L^{-1}) and PFBA (4.7 µg L^{-1}); longer-chain species occurred at lower levels (PFOA 1.39 µg L^{-1}, PFHpA 1.46 µg L^{-1}). The sum of detected PFAS was approximately 53.6 µg L^{-1}.

In January 2026, the PFAS pattern remained broadly consistent but with some additions: C6O4 increased to 21.8 µg L^{-1}, and PFBS (12.5 µg L^{-1}) and PFHxA (10.0 µg L^{-1}) remained dominant.

Additional detections included 6:2 FTA (2.7 µg L^{-1}) and low but measurable levels of sulfonates and longer chains (PFOS 0.27 µg L^{-1}, PFHxS 0.122 µg L^{-1},

PFDeA 0.166 µg L^{-1}). The sum of detected PFAS increased slightly to approximately 59.4 µg L^{-1}.

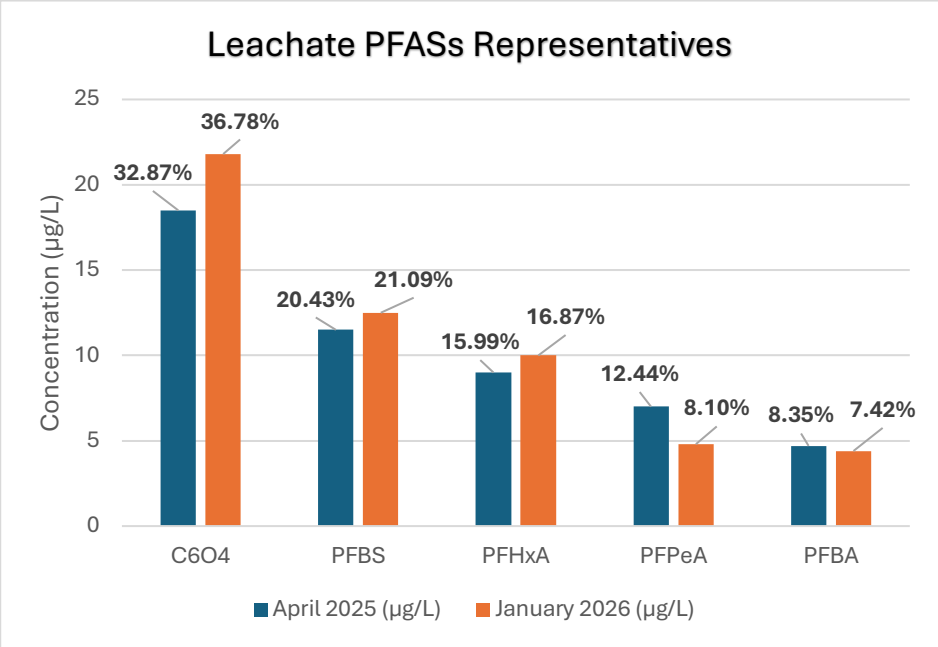

Figure 14. Detected concentrations (µg L^{-1}) and relative abundance (%) of PFAS representatives in leachate for April 2025 and January 2026.

Discussion about leachate PFAS characterization:

Across both campaigns, the leachate profile is clearly weighted toward short-chain PFAS (C4-C6), with PFBS (C4 sulfonate), PFBA (C4 carboxylate), PFPeA (C5 carboxylate) and PFHxA (C6 carboxylate) constituting a substantial fraction of the total signal. In contrast, longer-chain PFCA/PFSA are present only at low concentrations (e.g., PFHpA (C7) and PFOA (C8) at 1-2 µg L^{-1}, and PFOS (C8 sulfonate), PFHxS (C6 sulfonate) and PFDeA (C10) detectable mainly in January 2026 at sub-µg L^{-1} levels).

This indicates that, while legacy long-chain compounds persist, the leachate burden is increasingly driven by more mobile, lower-sorption short-chain homologues, which are also typically more challenging for conventional treatment trains due to weaker hydrophobic and pore-filling interactions on sorbents. Notably, C6O4 remains among the most concentrated analytes in both datasets (18-22 µg L^{-1}), supporting its use as a site-relevant marker of "replacement PFAS" alongside short-chain sulfonates (PFBS) and carboxylates (PFHxA/PFBA).

The detection of 6:2 FTA in January 2026 further suggests the potential contribution of precursor-related inputs, consistent with temporal variability in waste composition or leachate generation dynamics.

Overall, the combined presence of (i) dominant short-chain PFAS, (ii) a high replacement PFAS signal (C6O4), and (iii) low but detectable legacy long-chain PFAS provides a robust basis to discuss both mobility-driven environmental behavior and differential treatability in subsequent adsorption experiments.

4.2.3 Groundwater characterization (Upstream PZ38 and Downstream PZ3TER)

Groundwater general characterization:

Groundwater presented moderate mineralization compared to leachate, with conductivity around 0.8-1.1 mS cm^{-1}, and oxidability in the low mg O_2 L^{-1} range.

Table 14. Groundwater characterization (upstream & downstream)

Parameter	Apr 2025 PZ38 upstream	Apr 2025 PZ3TER downstream	Jan 2026 PZ38 upstream	Jan 2026 PZ3TER downstream
pH	6.95	7.03	7.35	7.49
Conductivity (µS/cm)	1120	802	1090	1010
TOC (mg/L)	1.35	6.3	-	-
Oxidability (mg O2/L)	3.70	3.84	2.53	3.86
NH4 (mg/L)	0.109	0.0525	0.143	0.0674
Nitrates (mg/L)	20.0	12.0	34.0	38.0
Nitrites (µg/L)	12.7	19.5	7.16	30.9
Sulfates (mg/L)	51.0	45.2	55.9	61.3
Chlorides (mg/L)	60.0	19.0	73	48.0

In April 2025, upstream PZ38 showed Conductivity 1120 µS cm^{-1} and TOC 1.35 mg L^{-1}, while downstream PZ3TER had Conductivity 802 µS cm^{-1} and TOC 6.3 mg L^{-1}. Major ions were in the tens of mg L^{-1} range (e.g., nitrates 12-20 mg L^{-1}; sulfates 45-51 mg L^{-1}; chlorides 19-60 mg L^{-1}), consistent with a typical shallow aquifer chemistry.

In January 2026, pH remained near neutral (7.35 upstream; 7.49 downstream) and conductivity remained comparable (1,090 µS cm^{-1} upstream; 1,010 µS cm^{-1} downstream). Nitrates increased to 34-38 mg L^{-1}, and sulfate and chloride remained in the same order of magnitude as April 2025 (sulfates 56-61 mg L^{-1}; chlorides 48-73 mg L^{-1}), while nitrites were detectable at low concentrations (µg L^{-1} range).

Groundwater PFAS occurrence and spatial/temporal comparison:

Groundwater PFAS were detected at ng L^{-1} levels, i.e., ~10^3-10^4 times lower than leachate (µg L^{-1}), consistent with strong attenuation between the leachate source and the aquifer.

Table 15. PFASs in groundwater, April 2025 (Upstream & Downstream)

Analyte	Apr 2025 PZ38 (ng/L) Upstream	Apr 2025 PZ3TER (ng/L) Downstream
6:2 FTA	<5	<5
ADONA	<0.28	<0.28
C6O4	9.7±3.9	8±3.2
PFBA	<0.21	10±4
PFBS	2.6±1.1	<0.22
PFDA	<0.18	<0.18
PFDeA	<0.18	<0.18
PFDoA	<0.23	<0.23
PFDoDS	<0.26	<0.26
PFDS	<0.19	<0.19
PFHpS	<0.19	<0.19
PFHxA	4.7±1.9	6.9±2.7
PFHxS	<0.26	<0.26
PFNA	0.953	<0.2
PFNS	<0.18	<0.18
PFOA	4±1.6	4.2±1.7
PFOS	1.43±0.57	<0.2
PFPeA	6.9±2.7	8.8±3.5
PFHpA	1.28	3.2
PFPeS	<0.21	<0.21
PFTeDA	<0.46	<0.46
PFTrDA	<0.28	<0.28
PFTrDS	<0.19	<0.19
PFUnDS	<0.33	<0.33

In April 2025, upstream PZ38 included C6O4 (9.7 ng L^{-1}), PFPeA (6.9 ng L^{-1}), PFHxA (4.7 ng L^{-1}), PFOA (4.0 ng L^{-1}), PFBS (2.6 ng L^{-1}) and PFOS (1.43 ng L^{-1}), with a detected sum of approximately 30.3 ng L^{-1}.

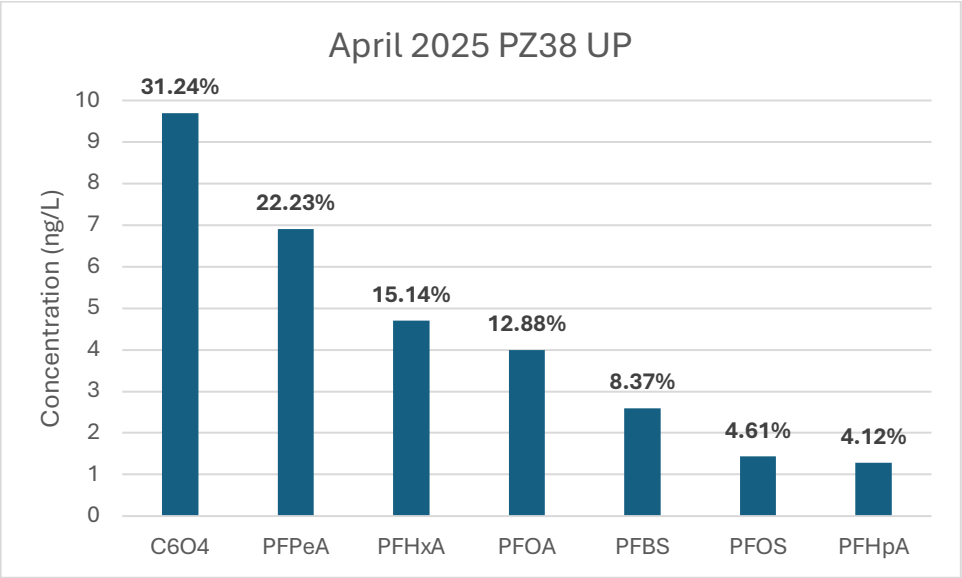

Figure 15. Concentrations (ng L^{-1}) and relative distribution (%) of selected marker PFAS in upstream piezometer PZ38 (April 2025), with C6O4 representing the dominant compound.

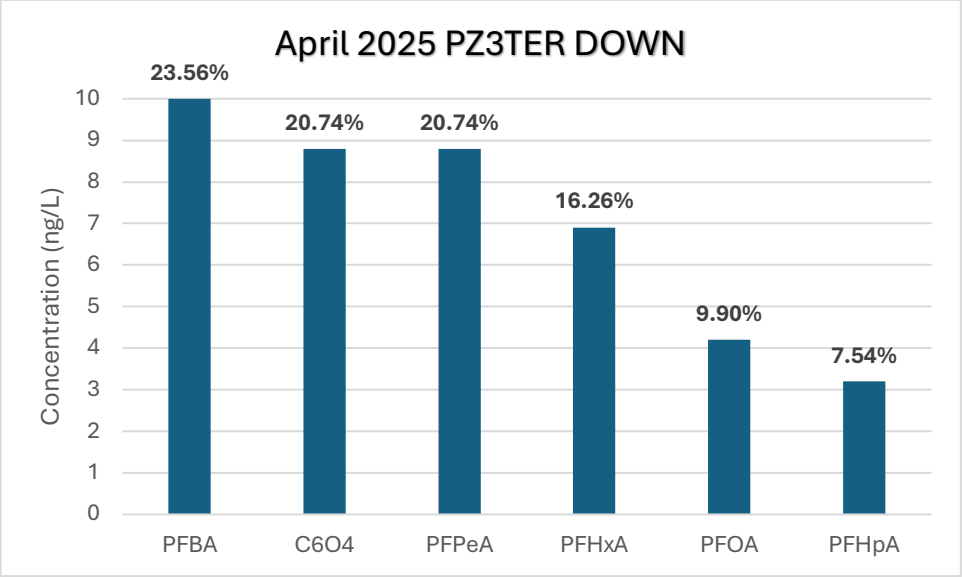

Figure 16. Concentrations (ng L^{-1}) and relative distribution (%) of selected marker PFAS in downstream piezometer PZ3TER (April 2025), showing a broader distribution with PFBA as the most abundant species.

Downstream PZ3TER included PFBA (10.0 ng L^{-1}), C6O4 (8.0 ng L^{-1}), PFPeA (8.8 ng L^{-1}), PFHxA (6.9 ng L^{-1}) and PFOA (4.2 ng L^{-1}), with a detected sum of approximately 37.9 ng L^{-1}.

Table 16. PFASs in Groundwater, January 2026 (Upstream & Downstream)

Analyte	Jan 2026 PZ38 (ng/L) Upstream	Jan 2026 PZ3TER (ng/L) Downstream
6:2 FTA	<0.36	<0.36
ADONA	<0.16	<0.16
C6O4	3.0±1.2	1.80±0.72
PFBA	<0.23	<0.23
PFBS	<0.2	<0.2
PFDA	<0.14	<0.14
PFDeA	<0.14	<0.14
PFDoA	<0.12	<0.12
PFDoDS	<0.17	<0.17
PFDS	<0.14	<0.14
PFHpA	0.663	1.60±0.64
PFHpS	<0.14	<0.14
PFHxA	2.00±0.79	2.9±1.2
PFHxS	<0.17	1.20±0.50
PFNA	<0.15	<0.15
PFNS	<0.11	<0.11
PFOA	2.9±1.2	2.9±1.2
PFOS	1.20±0.50	<0.14
PFPeA	2.8±1.1	2.10±0.84
PFPeS	<0.085	0.585±0.23
PFTeDA	<0.34	<0.34
PFTrDA	<0.2	<0.2
PFTrDS	<0.13	<0.13
PFUnDS	<0.19	<0.19

In January 2026, detected sums decreased in both wells to ~12-13 ng L^{-1}, with upstream PZ38 dominated by C6O4 (3.0 ng L^{-1}), PFOA (2.9 ng L^{-1}) and PFPeA (2.8 ng L^{-1}), and downstream PZ3TER including PFHxA (2.9 ng L^{-1}), PFOA (2.9

ng L^{-1}), C6O4 (1.8 ng L^{-1}), and additional sulfonates (PFHxS 1.2 ng L^{-1}, PFPeS 0.585 ng L^{-1}).

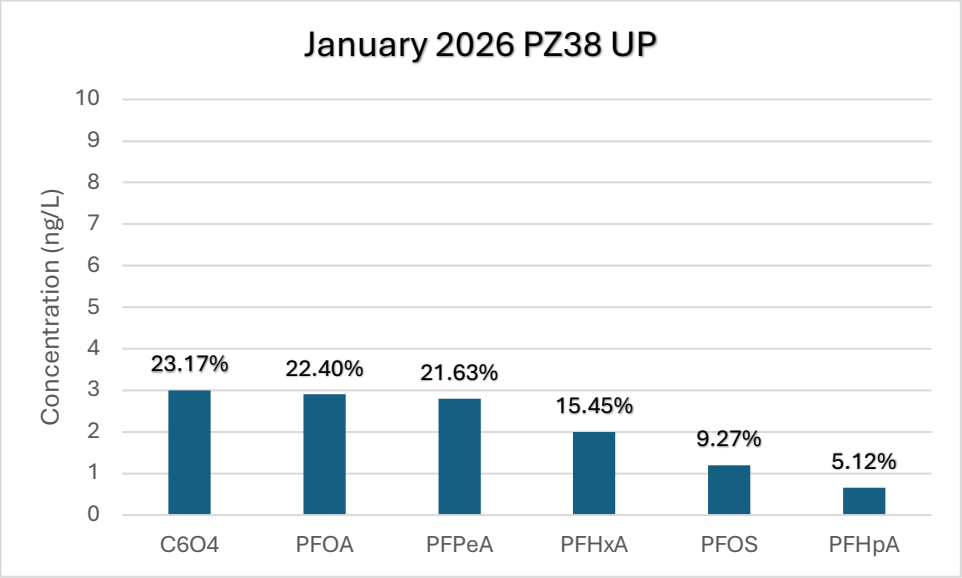

Figure 17. Marker PFASs Concentrations and Ratio in PZ38 (January 2026)

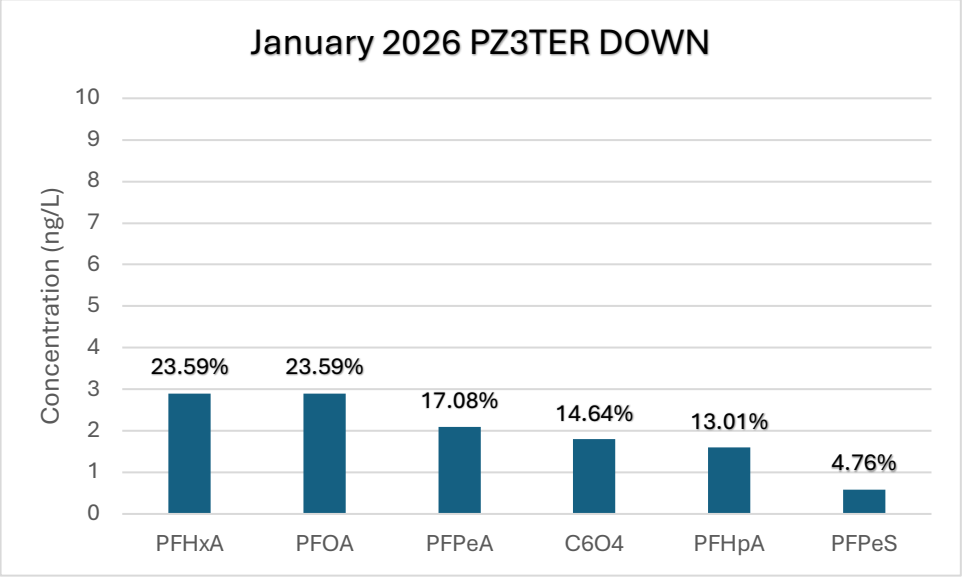

Figure 18. Marker PFASs Concentrations and Ratio in PZ3TER (January 2026)

Discussion about groundwater PFAS occurrence and spatial/temporal comparison:

1- Temporal interpretation

Two fundamental findings are: 1- groundwater PFAS concentrations remain orders of magnitude lower than leachate, consistent with attenuation along the pathway; and 2- the groundwater signature is dominated by short-chain PFAS and C6O4, supporting their role as conservative mobility markers at the site.

Importantly, the temporal decrease from April 2025 to January 2026 is coherent with the site's leachate-generation regime in 2024 which was discussed in chapter 2: January corresponds to a low-production month (257.5 t), whereas April lies in a high-throughput phase (2,171.6 t), an 8.4× increase in leachate mass production. Under higher leachate throughput (April-like conditions), greater drainage and internal mixing can enhance PFAS mobilization and exported mass flux, while lower-throughput conditions (January-like) reduce loading and make groundwater concentrations more dominated by dilution/dispersion.

This pattern is reflected in the measurements.

In April 2025, detected ΣPFAS were higher in both wells (PZ38 upstream 30.3 ng L^{-1}; PZ3TER downstream 37.9 ng L^{-1}), with a clear contribution from mobile short chains and C6O4 (e.g., C6O4 9.7 ng L^{-1} in PZ38 and 8.0 ng L^{-1} in PZ3TER; PFHxA 4.7-6.9 ng L^{-1}; PFOA 4.0-4.2 ng L^{-1}), and PFOS detectable upstream (1.43 ng L^{-1}).

In January 2026, ΣPFAS decreased to ~12-13 ng L^{-1} (PZ38 12.6 ng L^{-1}; PZ3TER 13.1 ng L^{-1}), accompanied by lower marker concentrations (e.g., C6O4 3.0 ng L^{-1} upstream and 1.8 ng L^{-1} downstream; PFHxA 2.0-2.9 ng L^{-1}; PFOA 2.9 ng L^{-1} in both wells), while PFOS remained detectable upstream (1.20 ng L^{-1}).

Overall, the April-to-January reduction in groundwater PFAS is therefore consistent with the shift from high to low leachate production (and associated mass export potential), whereas the persistence of C6O4 and short-chain PFAS across both campaigns aligns with their comparatively higher mobility and weaker attenuation.

2- Spatial interpretation

A clear upstream-downstream gradient is evident in April 2025: ΣPFAS increased from 30.3 ng L^{-1} (PZ38, upstream) to 7.9 ng L^{-1} (PZ3TER, downstream),

i.e., +7.6 ng L^{-1} corresponding to a 25% higher detected burden downstream (37.9/30.3 = 1.25).

This downstream enrichment is supported by compound-level differences: PFBA was detected only downstream (10.0 ng L^{-1}), representing 24% of the downstream detected sum, while upstream was comparatively characterized by C6O4 (9.7 ng L^{-1}), 32% of its detected sum.

For compounds detected in both wells, concentrations were broadly comparable (e.g., PFOA ~4.0-4.2 ng L^{-1}), suggesting that the spatial contrast in April is driven mainly by the appearance/accumulation of the most mobile short-chain PFCA downstream rather than uniform increases across all analytes.

In January 2026, the spatial contrast largely disappears: ΣPFAS is 12.6 ng L^{-1} upstream vs 13.1 ng L^{-1} downstream, a difference of only 0.5 ng L^{-1} (4%). Marker compounds show similarly small gradients: PFOA is identical in both wells (2.9 ng L^{-1}), while C6O4 is slightly higher upstream (3.0 vs 1.8 ng L^{-1}), indicating that under low-loading conditions the downstream enhancement seen in April is not systematic and that concentrations are more strongly controlled by dilution/dispersion and transient hydraulic conditions.

Overall, the spatial pattern is therefore conditional: a downstream increase is evident during the higher-loading April campaign (ΣPFAS +25%), but it collapses during the lower-loading January campaign (4%), consistent with a flow-path signal that becomes detectable primarily when system forcing (leachate generation/mass export) is higher.

Chapter 5

GAC Adsorption Batch Test, Results and Discussion

5.1 TOC screening results

5.1.1 TOC Adsorption Isotherms

This section presents and interprets the TOC screening tests performed to quantify how total organic carbon from leachate interacts with granular activated carbon (GAC) under three matrices: Raw Leachate (RAW), Oxidized Leachate (OX), and Oxidized + Diluted leachate (OX+DIL). The objective of this results section is to (i) describe how equilibrium TOC (C_{eq}) changes with increasing GAC dose, and (ii) compare the apparent adsorption behavior of TOC using log-log Freundlich fits. Because TOC is a heterogeneous mixture and each scenario was evaluated at its maximum available contact time (RAW 120 h; OX 94 h; OX+DIL 66 h), the fitted Freundlich parameters are interpreted as comparative screening descriptors rather than intrinsic equilibrium constants.

The Freundlich relationship was fitted in log-log form as:

$$Log\ S = Log\ K_f + \frac{1}{n}\ Log\ C_{eq}$$

where C_{eq} is expressed in g/L, and S is the sorbed amount in g/g (TOC mass adsorbed per mass of GAC).

5.1.2 Concentration trend (C_{eq} vs GAC dose) for TOC screening

Raw leachate started at TOC 230.9 mg/L (0 g/L GAC). Increasing GAC dose reduced TOC progressively to approximately 120.7 mg/L (40 g/L) and 100 mg/L

(80-100 g/L). Overall, the curve shows a clear reduction with dose, with diminishing improvements at high dose.

Oxidized leachate started at TOC 160.8 mg/L. With increasing GAC dose, TOC decreased from 129.9 mg/L (10 g/L) to 76.9 mg/L (40 g/L) and ultimately to 61.18 mg/L (100 g/L). The largest reductions occur up to 40 g/L, then the curve flattens (diminishing returns), indicating that a fraction of oxidized TOC remains weakly removable under these conditions.

Oxidized Diluted Leachate started at TOC 154.3 mg/L and decreased strongly with GAC dose to 81.22 mg/L (10 g/L), 61.01 mg/L (40 g/L), and 41.45 mg/L (100 g/L). This scenario reaches the lowest residual TOC among all matrices, indicating the most effective reduction of TOC within the tested window.

Table 17. TOC (C_{eq} vs GAC dose) for Scenarios A, B and C

	TOC		
	Raw Leachate (120 h)	OX Samples (94 h)	OX+DIL Samples (66 h)
Conc GAC (g/L)	**Conc C_{eq} (ppm)**	**Conc C_{eq} (ppm)**	**Conc C_{eq} (ppm)**
0	230.9	160.8	154.3
10	145.8	129.9	81.22
20	138.2	102.90	65.84
40	120.7	76.91	61.01
60	109.4	77.03	48.95
80	100.4	69.29	66.09
100	103	61.18	41.45

5.1.3 Log-Log Freundlich Isotherm results for TOC screening

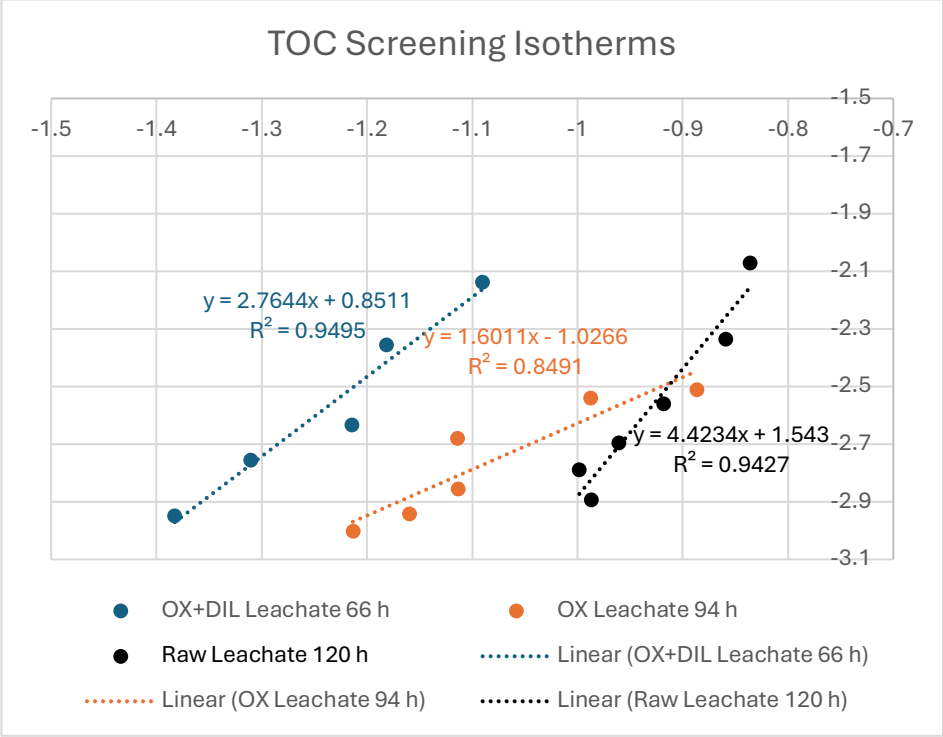

Figure 19. Freundlich (Log-Log) TOC adsorption isotherms for Carbopur 1240 GAC (0-100 g L^{-1}) under Oxidized + diluted, Oxidized, and Raw leachate conditions, showing matrix-dependent differences in adsorption behavior.

Scenario A - Raw Leachate

$$Log\ S = 4.4234\ Log\ C_{eq} + 1.543 \qquad R^2 = 0.943$$

Slope 1/n = 4.4234 indicates strong concentration sensitivity across the tested range. A larger slope indicates that S increases more rapidly with C_{eq} on a logarithmic scale.

Intercept $Log\ K_f = 1.543$ indicates that higher apparent uptake level at the reference point $C_{eq} = 1\ \frac{g}{L}$ (used as a comparative descriptor).

Raw Leachate shows a consistent power-law behavior (high R^2), indicating that TOC uptake can be described by a single log-log relationship across the tested doses. The high slope reflects strong sensitivity of TOC-GAC interactions in the raw matrix, consistent with a complex DOM mixture where uptake changes sharply with the equilibrium concentration within the tested window.

Scenario B - Oxidized Leachate

$Log\ S = 1.6011\ Log\ C_{eq} + 1.0266 \qquad R^2 = 0.849$

Slope 1/n = 1.6011indicates lower concentration sensitivity than RAW and OX+DIL (less steep log-log response).

Intercept $Log\ K_f = -1.0266$ shows lowest apparent uptake level at $C_{eq} = 1\ \frac{g}{L}$ among the three fits.

Lower R^2: suggests that oxidized TOC behaves less like a single Freundlich-type solute across the whole dose range (greater mixture heterogeneity relative to a single power-law).

Oxidized leachate achieves substantially lower residual TOC than RAW at comparable doses, but the weaker linearity in log-log space indicates a less uniform adsorption behavior, consistent with oxidation producing a more compositionally diverse DOM pool in which different fractions may adsorb with different effective behaviors.

Scenario C - Oxidized Diluted Leachate

$Log\ S = 2.7644\ Log\ C_{eq} + 0.8512 \qquad R^2 = 0.950$

Slope 1/n = 2.7644: strong concentration sensitivity (more than oxidized; less than Raw leachate).

Intercept $Log\ K_f = 0.8512$ intermediate apparent uptake level at $C_{eq} = 1\ \frac{g}{L}$.

Highest R^2: indicates the most consistent single power-law behavior across the fitted range among the three matrices.

Oxidized Diluted Leachate combines strong TOC reduction (lowest C_{eq} at high dose) with the most internally consistent Freundlich screening fit, supporting the reasoning for its use as a controlled matrix for subsequent adsorption experiments where TOC concentration must be reduced.

5.2 From TOC screening to PFAS-TOC adsorption competition batch tests

The TOC screening phase was required to make the subsequent PFAS adsorption competition assessment scientifically interpretable. In raw leachate, TOC occurs at g/L levels (10^3 mg/L), whereas target PFAS occur at µg/L levels (10^{-3} mg/L); this 10^6-fold difference means that, without TOC reduction, the adsorption response of GAC would be dominated by TOC uptake and fouling, masking PFAS-specific trends.

Therefore, the purpose of the screening step was not to achieve complete organic-carbon removal, but to identify a practical lower TOC window that still preserves leachate matrix characteristics while allowing measurable PFAS adsorption and enabling meaningful comparison of competitive effects (PFAS-TOC) across experimental conditions.

A simple mass-balance reasoning provided a key decision point: if raw leachate TOC is approximately 2000 mg/L, a 1:50 dilution yields approximately 40 mg/L, which matches the best TOC level observed during TOC screening. This implies that a dilution-only approach can reproduce the "lowest TOC window" identified in the screening phase without requiring oxidation, thus maintaining a more representative leachate chemistry (including native dissolved constituents that may influence PFAS adsorption). In parallel, oxidation tests performed previously indicated that an oxidized leachate stock with TOC around 1357 mg/L could reach the same target window using a 1:40 dilution, providing a second matrix with comparable TOC magnitude but altered TOC character.

5.3 PFAS-TOC adsorption competition results (Scenario D & E)

The study proceeded with two revised scenarios at comparable TOC magnitude: GAC adsorption batch test on Raw Leachate (Scenario D), and GAC adsorption batch test on Oxidized Leachate (Scenario E).

In both cases, a controlled PFAS mixture was spiked to enable quantifiable adsorption trends and to support direct comparison across PFAS classes (short-chain vs long-chain; carboxylates vs sulfonates) under similar organic-carbon background. The sections that follow present:

1- Verification of TOC levels, Isotherms and adsorption-capacity outcomes achieved in the PFAS-spiked systems for both Scenarios.

2-The resulting PFASs Isotherms and adsorption-capacity outcomes, with emphasis on matrix-dependent competition effects between Scenarios D and E.

5.3.1 TOC adsorption results and competition behavior (Scenario D and E)

Table 18. Raw and Oxidized Leachate Batch test results for TOC (48 h)

TOC		
48 h		
Conc GAC (g/L)	Conc C_{eq} ppm	
	Raw Leachate	Oxidized Leachate
0	190.4	162.5
1	189.8	203.1
5	173.6	178.2
10	164.9	148.4
20	158.2	135.5
40	152.3	126.7
60	148.9	125.9
80	147.7	120.8
100	132.1	117.4

Raw leachate exhibits a moderate TOC removal with dose, with clear diminishing returns at higher doses. highlighted values indicate anomalies (TOC values higher than the control)

Oxidized leachate at 10-100 g/L, TOC decreases strongly but at the lowest doses (1 and 5 g/L), TOC is higher than the 0 g/L control (203.1 and 178.2 mg/L). Since this happens only at the lowest loadings and is not sustained at higher doses (where TOC decreases as expected), it should be treated as an isolated deviation that does not affect the overall dose-response trend.

In the PFAS-spiked oxidized matrix, equilibrium TOC values were generally lower than in the raw matrix at the same GAC doses, particularly in the medium-high dose range.

Relative to Scenario D, Scenario E operates at a lower equilibrium TOC background across key GAC doses, implying a weaker solution-phase competitor pool at 48 h. This is important because PFAS adsorption in Scenario E is expected to be less suppressed by dissolved organic competition.

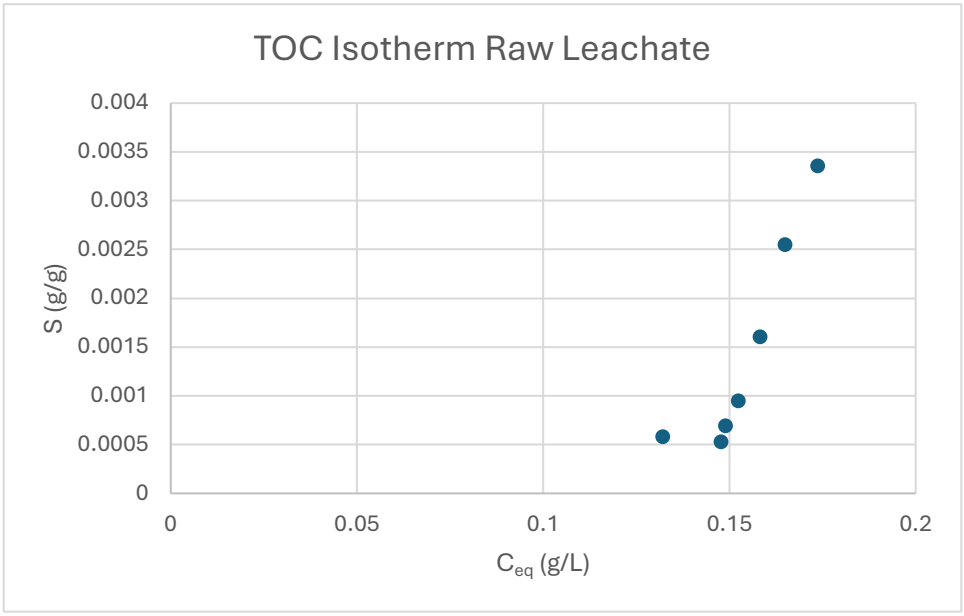

Figure 20. TOC adsorption isotherm ($S - C_{eq}$) for raw leachate under Scenario D using Carbopur 1240 GAC, illustrating increasing TOC uptake with decreasing equilibrium concentration.

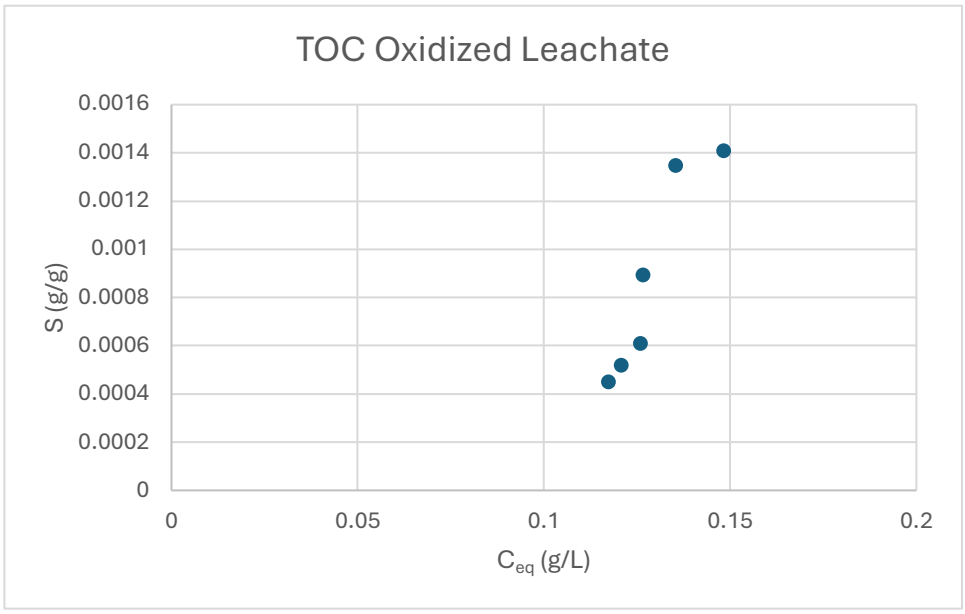

Figure 21. TOC adsorption isotherm ($S - C_{eq}$) for oxidized leachate under Scenario E using Carbopur 1240 GAC, showing lower sorption capacity compared to raw leachate

Log-Log Freundlich Isotherm results (Scenario D and E)

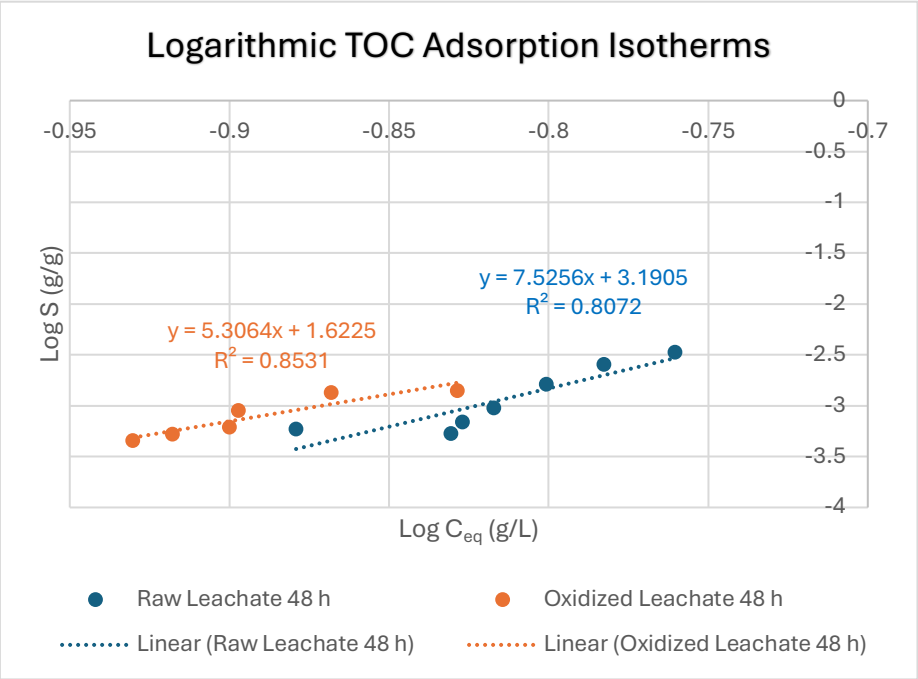

Figure 22. Log-log (Freundlich) TOC adsorption isotherms for Raw and Oxidized leachate (48 h), highlighting stronger adsorption intensity in raw leachate based on the higher slope of the linearized fit.

Scenario D - Raw Leachate

$$Log\ S = 7.5256\ Log\ C_{eq} + 3.1905 \qquad R^2 = 0.8072$$

Slope 1/n = 7.5256

Intercept $Log\ K_f$ = 3.1905

Scenario E - Oxidized Leachate

For Scenario E, the fitted relationship was:

$Log\ S = 5.3064\ Log\ C_{eq} + 1.6225$ $R^2 = 0.8531$

Slope 1/n = 5.3064

Intercept $Log\ K_f$ = 1.6225

Compared with Scenario D, Scenario E shows a lower slope on the log-log plot, meaning $Log\ S$ increases less steeply with $Log\ C_{eq}$ over the measured range. This indicates a different concentration-dependence of TOC partitioning to GAC under oxidized conditions. The slightly higher R^2 suggests that the oxidized matrix behaves more consistently as a single power-law descriptor across the fitted points, which is useful when coupling TOC competition descriptors with PFAS adsorption parameters.

The intercept again controls the vertical position of the fitted line within the adopted model and is used as a comparative descriptor rather than a standalone "capacity constant."

5.3.2 PFAS adsorption results under competitive conditions (Scenarios D and E)

PFAS adsorption outcomes was obtained under the revised competitive matrices (Scenario D and E), where the primary goal was to quantify PFAS uptake on GAC in the presence of a moderated organic background. In these systems, TOC remains higher than PFAS (10^2 mg/L vs 10^{-1} mg/L total PFAS), so PFAS adsorption must be interpreted as a competition problem: PFAS-TOC competition **for** adsorption sites and pore access, together with potential TOC-driven fouling effects.

However, under the initial dose series applied in Scenarios D and E, only PFBA remained within the quantifiable range, while PFBS, PFOA, and PFOS fell below detection/quantification limits. This outcome is consistent with the expected selectivity of GAC for PFAS: sulfonates and longer-chain PFAS (PFOS, PFOA, and often PFBS relative to PFBA) exhibit higher adsorption affinity and can be driven to near-complete depletion at high adsorbent loadings, preventing construction of isotherms from measurable equilibrium concentrations.

PFBA, as a short-chain carboxylate with comparatively weaker adsorption, remains measurable under stronger competition and/or higher GAC doses, making

it a practical indicator compound for the first-pass assessment of competitive adsorption behavior. The following results therefore focus on PFBA, while the subsequent experimental redesign (lower GAC doses and increased batch volume in 100 mL bottles) was implemented to recover measurable equilibrium ranges for the other PFAS (methodological details reported in Chapter 3).

PFBA concentrations reported as small negative values at high GAC dosages are not physically meaningful and indicate that the instrumental response fell below the quantification range (baseline and correction noise). Accordingly, negative PFBA values were treated as below the limit of quantification (<LOQ) in tables and figures and excluded from regression analyses.

PFBA isotherms under competitive matrices

Table 19. PFBA batch test results (scenarios D and E)

	Raw Leachate	**Oxidized Leachate**
GAC Conc g/L	**PFBA Conc (ppb)**	**PFBA Conc (ppb)**
0	72.9544	67.6311
1	21.8009	23.9077
5	2.2861	2.5186
10	0.4136	1.4692
20	0.1436	0.1574
40	0.0394	0.0252
60	$< LOQ$	$< LOQ$
80	$< LOQ$	$< LOQ$
100	$< LOQ$	$< LOQ$

In Raw Leachate matrix a significant depletion trend was observed, with PFBA decreasing from 72.95 µg/L at 0 g/L to 21.80 µg/L (1 g/L), 2.29 µg/L (5 g/L), 0.41 µg/L (10 g/L), 0.14 µg/L (20 g/L), and 0.04 µg/L (40 g/L), followed by <LOQ at 60 g/L. The rapid approach toward LOQ confirms that the originally applied GAC range was sufficiently high to drive PFBA near-complete removal and to fully deplete the more strongly sorbing PFAS (PFBS, PFOA, PFOS), explaining their non-detectability under these conditions.

For Oxidized Leachate matrix PFBA decreased sharply with increasing GAC concentration, from 67.6 µg/L at 0 g/L to 23.9 µg/L (1 g/L), 2.5 µg/L (5 g/L), 1.5 µg/L (10 g/L), 0.157 µg/L (20 g/L), and 0.0252 µg/L (40 g/L). At 60, 80 and 100 g/L points were <LOQ. This pattern indicates that, even under a TOC-rich

competitive background, PFBA (short-chain PFCA) approached the quantification limit at moderate-to-high GAC dosages, compressing the equilibrium concentration range available for isotherm construction.

The quantifiable range of PFBA was matrix-dependent but consistently restricted to the low-to-intermediate GAC doses. In Oxidized Leachate, PFBA remained quantifiable up to 40 g/L (0.0252 µg/L), becoming <LOQ at 60-80-100 g/L. In diluted raw leachate, PFBA remained quantifiable up to 40 g/L (0.04 µg/L) and became <LOQ at 60 g/L, with higher doses unavailable. Therefore, the informative range for competition analysis was primarily the 1-20 g/L range (and secondarily up to 40 g/L), where PFBA equilibrium concentrations were consistently measurable and matrix effects could be resolved.

PFBA Standard isotherm reference and matrix suppression

A PFBA standard isotherm (clean-matrix reference) was used to isolate intrinsic PFBA-GAC interactions from matrix-driven competition. This reference is essential because, at high GAC dosages, all matrices tend toward near-zero equilibrium concentrations, masking competitive effects; competition is therefore diagnosed most clearly within the measurable low-dose window.

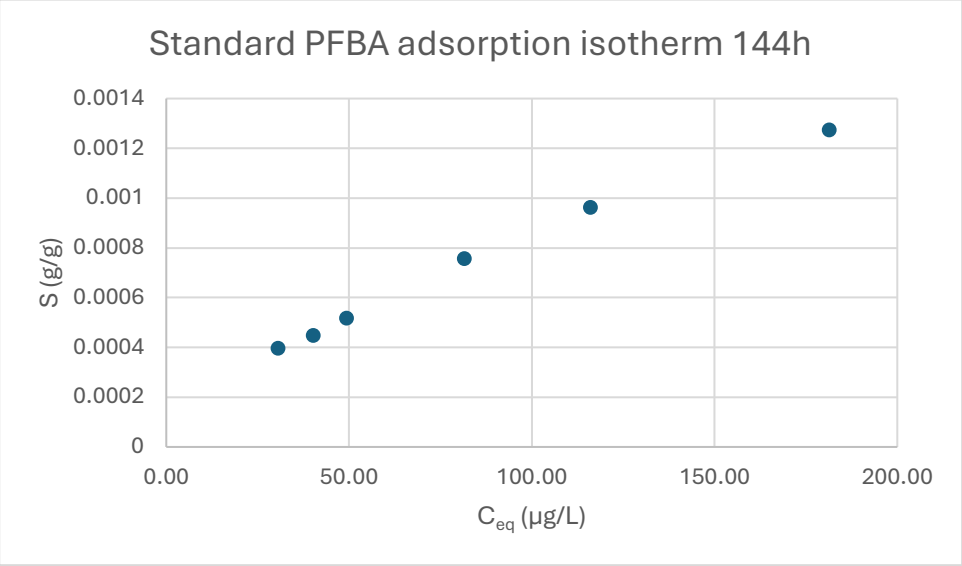

Figure 23. Standard PFBA adsorption isotherm at 144 h contact time using Carbopur 1240 GAC, illustrating the Freundlich-type increase in sorbed amount (S) with equilibrium concentration (C_{eq}) under single-solute conditions.

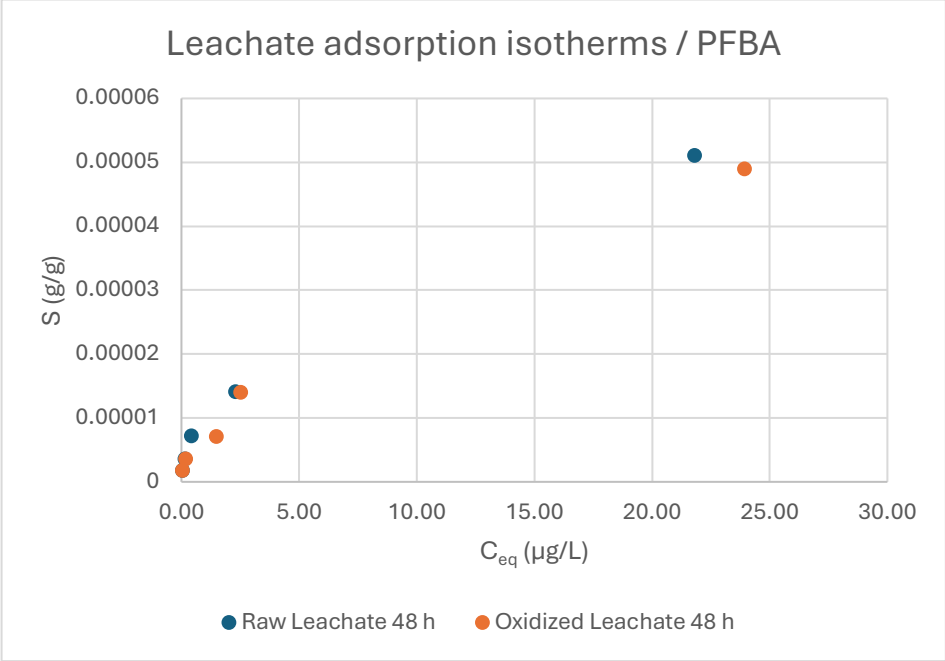

Figure 24. PFBA adsorption isotherms in raw and oxidized leachate (48 h) using Carbopur 1240 GAC, highlighting reduced sorption capacity compared to the standard system due to matrix competition effects.

Both plots show a monotonic increase of S with C_{eq}, consistent with equilibrium adsorption behavior expected by Freundlich Isotherms. The leachate matrices populate a much narrower low-C_{eq} window and show strong clustering near the lower end of measurable concentrations, which is consistent with matrix adsorption conditions and indicates limited resolution of competition effects within the plotted range; raw and oxidized leachate responses are broadly similar for PFBA under these conditions.

Evaluation of the TOC and PFBA nonlinear Freundlich Isotherms indicates that PFBA adsorption occurred while TOC was concurrently adsorbed onto GAC, qualitatively speaking. The TOC isotherms show substantial sorbed organic loadings within the same low-to-moderate GAC dose domain in which PFBA equilibrium concentrations decrease sharply, confirming that PFBA uptake in Scenarios D and E took place under an active competitive organic background rather than under DIW conditions.

Despite this competition, PFBA approached low equilibrium concentrations already at 5-10 g/L GAC, indicating that the applied adsorbent loading provided sufficient accessible capacity for PFBA uptake within the investigated range. Consequently, the selected dose range rapidly entered a near-depletion regime for PFBA, compressing the measurable

equilibrium range and limiting the resolution of matrix-dependent differences at higher GAC dosages.

This compression of the PFBA equilibrium window, together with non-detects for the more strongly sorbing PFASs (PFBS, PFOA, PFOA), motivated the subsequent shift to lower GAC dosages and larger reactor volumes to preserve measurable C_{eq} values for multi-PFAS competition analysis.

Log-Log Freundlich Isotherm for PFBA (Scenario D and E)

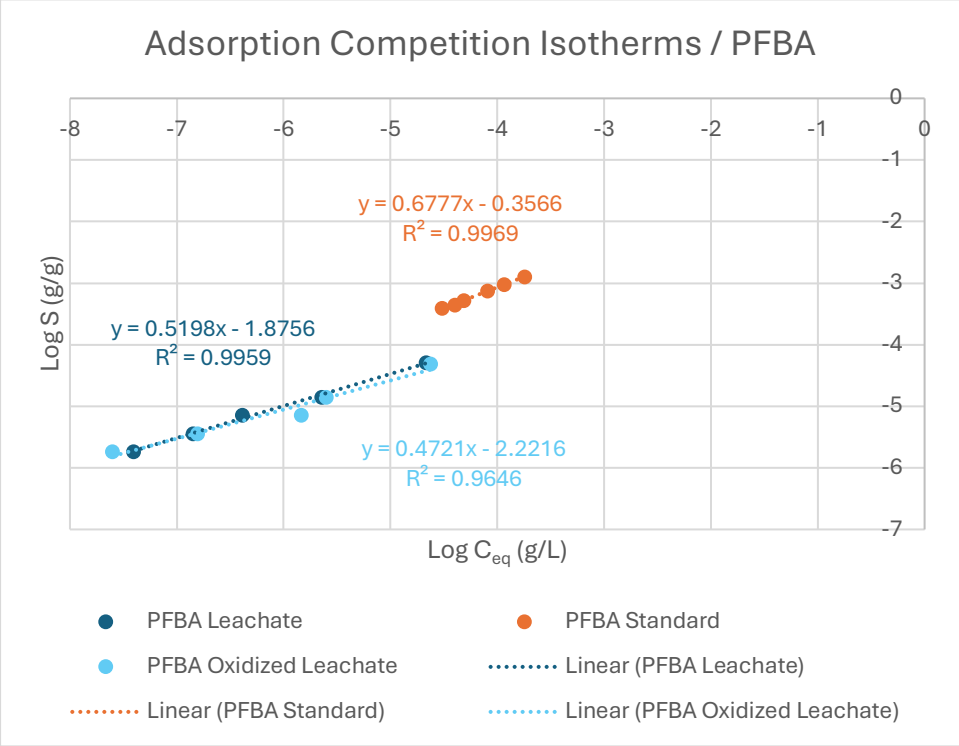

Figure 25. Freundlich log-log PFBA adsorption isotherms (Carbopur 1240 GAC) for standard and leachate matrices, highlighting significant decreases in adsorption capacity (K_f) under competitive conditions

Freundlich relationships were evaluated:

PFBA Standard:

$Log\ S = 0.6777\ Log\ C_{eq} - 0.3566 \qquad R^2 = 0.9969$

$K_f = 0.44\ , n\ =\ 1.48$

PFBA in Raw Leachate (Scenario D):

$Log\ S = 0.5198\ Log\ C_{eq} - 1.8756 \qquad R^2 = 0.9959$

$K_f = 0.013\ , n\ =\ 1.92$

PFBA in Oxidized Leachate (Scenario E):

$Log\ S = 0.4721\ Log\ C_{eq} - 2.2216 \qquad R^2 = 0.9646$

$K_f = 0.006\ , n\ =\ 2.12$

The pronounced reduction in K_f from the Standard matrix to Leachate matrices reflects a strong downward shift in apparent capacity under competition. Quantitatively, the apparent K_f decreased from 0.44 (Standard) to 0.013 (Raw Leachate; 34× lower) and 0.006 (Oxidized Leachate; 73× lower).

In parallel, the lower slopes (1/n) in Leachate matrices relative to the Standard indicate reduced apparent adsorption intensity across the measured equilibrium range, consistent with a diminished availability of high-energy adsorption environments under matrix competition.

Experimental redesign for final PFAS adsorption competition analysis

The PFBA dataset demonstrates that the initial GAC dose series rapidly drove PFBA toward the quantification limit and fully depleted PFBS, PFOA and PFOS. Since isotherm identification requires measurable non-zero equilibrium concentrations across multiple points, the initially applied GAC dose range limited interpretability for the strongly sorbing PFAS. This outcome provides the experimental justification for the subsequent redesign (lower GAC dosages and increased reactor volume), which aims to preserve measurable equilibrium concentrations for all PFAS, improve resolution in the low-dose competition range, and enable robust comparison of adsorption selectivity (short-chain vs long-chain; carboxylates vs sulfonates) in comparison with Scenarios D and E.

5.4 Observation of TOC baseline shift after PFAS spiking and mechanistic verification

During the transition from TOC-only screening (Scenarios A-C) to PFAS competition tests (revised Scenarios D-E), an unexpected but systematic shift was observed: TOC levels in the diluted matrices increased from the expected “tens of mg/L” range to the “hundreds

of mg/L" range, even though the leachate source, dilution factors, oxidation conditions, and GAC conditioning procedures were unchanged. This increase was also evident in 0 g/L GAC control samples, indicating that it could not be attributed solely to carbon fines or adsorbent-related artifacts.

Replicate preparations using cleaner vials, re-dilution of the same leachate stock, use of fresh GAC and improved conditioning procedures reproduced the same elevated TOC levels. Conversely, repeating the same matrix preparation without PFAS spiking returned TOC values to the expected range (tens of mg/L), consistent with the original screening results. Together, these observations identified the PFAS spiking step as the element responsible for the baseline increase in measured TOC.

A simple order-of-magnitude argument confirms that the increase cannot originate from the PFAS molecules themselves. The total PFAS spike concentration was 400 µg/L (0.4 mg/L) (100 µg/L each of PFBA, PFBS, PFOA, PFOS), whereas measured TOC after spiking was typically ~10^2 mg/L. Even if PFAS mass were fully counted as organic carbon (which is not the case), 0.4 mg/L cannot explain an increase on the order of 10^2 mg/L. Therefore, the only plausible explanation was that TOC was increased by co-introduced organic carbon associated with the spike solution, rather than by PFAS carbon.

5.4.1 Quantitative explanation: Methanol contribution from PFAS spike preparation

Due to the fact that the mixed PFAS working stock used for spiking was prepared from four native PFAS standards supplied at 1 g/L in methanol, 250 µL of each standard were combined (total methanolic standard volume 1.00 mL) and diluted to 10.0 mL with DIW. The working pfas spike was then added to both 30 mL vials (this experiment with scenario D and E) and 100 mL bottles (Final experiment) 120 ppb and 400 ppb respectively, resulting the same final methanol fraction in both systems:

$$MeOH_{final} = 0.4\% \times 10\% = 0.04\% \text{ (v/v)}$$

This methanol fraction is sufficient to shift TOC into the observed range. For example, in a 30 mL vial spiked with 120 ppb of working stock, the methanol volume added is 12 µL. Using methanol density $\rho = 0.791\ g\ mL^{-1}$ and carbon mass fraction in methanol $= 12/32 = 0.375$, the organic carbon added by methanol is:

Methanol mass = $0.012\ mL \times 0.791 = 9.49 \times 10^{-3}\ g$

Carbon mass = $9.49 \times 10^{-3}\ g \times 0.375 = 3.56 \times 10^{-3}\ g\ C = 3.56\ mg\ C$

Dividing by the final vial volume (0.03012 L) gives:

$$TOC_{from\ MeOH} = \frac{3.56\ mg\ C}{0.03012\ L} = 118\ mg\ C\ L^{-1}$$

Because the same 0.4% v/v stock addition was used in the 100 mL bottles (Final Experiment), the calculated methanol-derived TOC contribution is essentially identical (118 mg C/L). When added to the expected background TOC of the diluted leachate (40 mg/L), the combined TOC falls in the same order of magnitude as observed in the PFAS-spiked batch systems (i.e., 10^2 mg/L). This provides a mechanistically consistent explanation for the systematic upward shift in TOC observed only when PFAS spiking is performed.

Verification Control

To verify this hypothesis experimentally, control solutions were prepared and analyzed for TOC:

1- DIW + Methanol at the same final methanol fraction as in the spiked reactors (0.04% v/v)

2- DIW + PFAS working stock added at the same volumetric fraction as used in the reactors (0.4% v/v), thereby reproducing the same methanol content.

The measured TOC values were:
DIW + MeOH: 140 mg/L
DIW + PFAS working stock: 146 mg/L

These results closely match the theoretical methanol-derived TOC contribution (118 mg/L), considering analytical variability and minor dilution effects. Importantly, the difference between the two control samples (6 mg/L) is negligible relative to the total TOC level, confirming that the dominant TOC contribution originates from the methanol solvent rather than from the PFAS themselves.

Furthermore, the measured TOC values (140-146 mg/L) align with the elevated TOC concentrations previously observed in PFAS-spiked leachate systems, once combined with the background leachate TOC (40 mg/L).

Consequently, all adsorption results must be interpreted as PFAS uptake occurring under competitive conditions defined by Leachate TOC and a quantified, solvent-derived TOC background that was consistently introduced across all spiked systems.

5.5 Final PFAS-TOC adsorption competition experiment

This final batch system was conceived to quantify competitive adsorption on GAC, i.e., simultaneous uptake of TOC and spiked PFAS. Under these conditions TOC is treated as the dominant competitor that controls site availability and pore access for PFAS.

5.5.1 TOC batch adsorption test Results

A further element relevant to TOC is that the PFAS spike introduced a reproducible amount of solvent-derived organic carbon (Methanol); this contribution affects the absolute TOC baseline but, because the same spike fraction was applied across all doses and both matrices, it is expected to be approximately dose-independent within each series. Consequently, the TOC results are interpreted primarily in terms of : 1- how much TOC remains in solution at equilibrium (C_{eq}, solution-phase competition); 2- how much TOC loads onto the adsorbent (S, occupancy/fouling proxy).

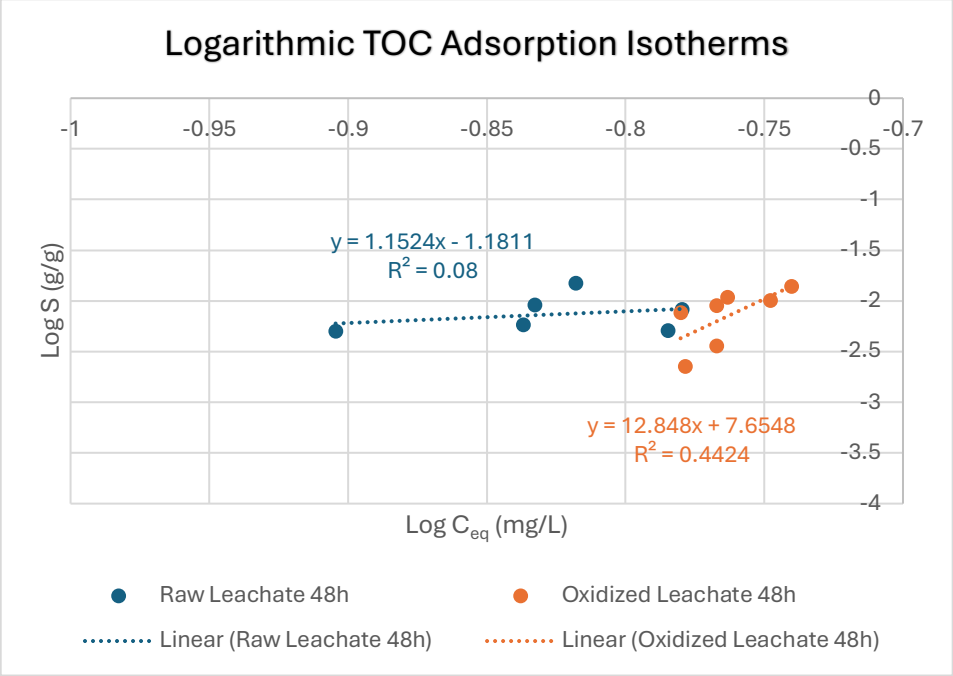

Figure 26. Log-Log TOC adsorption isotherms (Carbopur 1240 GAC, 48 h) for Raw and Oxidized leachate, showing limited Freundlich linearity and strong matrix-dependent adsorption variability.

Raw Leachate: TOC adsorption regime and competition behavior

The equilibrium TOC values show an overall decrease with increasing GAC dose over 0-10 g/L, while remaining in the 10^2 mg/L range throughout. This pattern indicates a low dose adsorption regime in which GAC removes part of the TOC pool, but a substantial dissolved fraction persists, maintaining strong solution-phase competition for PFAS across all doses. Minor non-monotonic steps at the lowest doses do not alter this regime interpretation because the equilibrium range is relatively narrow and TOC represents a heterogeneous mixture rather than a single solute.

Table 20. Raw Leachate batch test results for TOC (141 h)

Raw Leachate	
141h	
GAC	**TOC**
Conc GAC (g/L)	**Conc C_{eq} ppm**
0	174.3
0.5	177.2
1	166.1
1.5	152.1
2	164.2
3	147.0
5	145.6
10	124.6

The non-linear plot shows measurable TOC uptake on GAC (non-zero S) while C_{eq} remains high (C_{eq}roughly within 120-170 mg/L). This indicates partial partitioning of a multi-component TOC mixture: organics accumulate on the adsorbent while a large residual fraction remains dissolved, sustaining solution-phase competition for PFAS over the entire dose range.

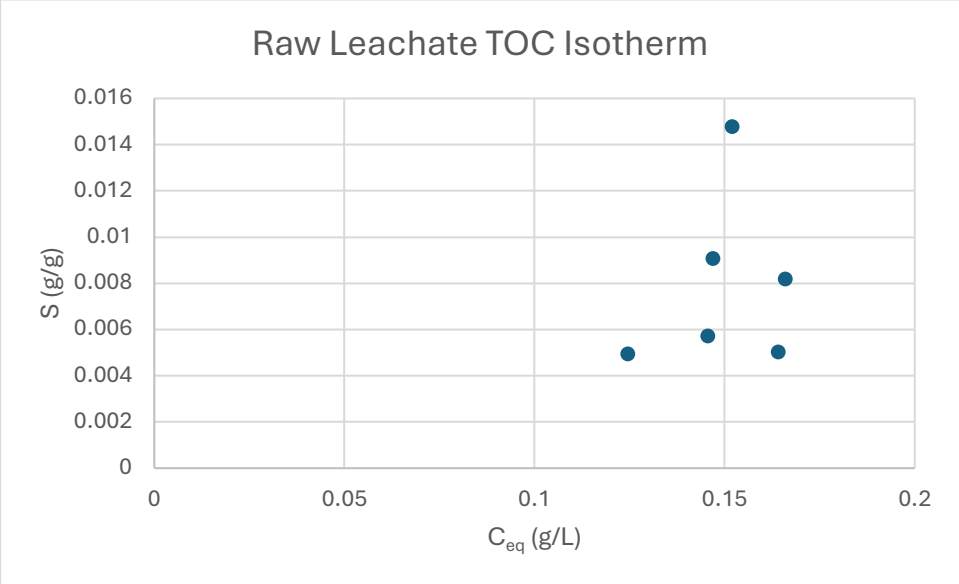

Figure 27. Raw leachate TOC adsorption isotherm (141 h, Carbopur 1240 GAC), illustrating limited reduction in C_{eq} despite increasing GAC dose, consistent with multi-component TOC competition.

Freundlich Isotherm log-log linearization

The fitted relationship was:

$$Log\ S = 1.1524 Log\ C_{eq} - 1.1811 \qquad R^2 = 0.08$$

Where n = 0.868 and $K_f = 6.6 \times 10^{-2}$

The very low R^2 indicates that, in this low-dose configuration, TOC does not behave as a single solute that follows power-law partitioning relationship across the measured window. Accordingly, K_f and n are not treated as physically meaningful constants here; instead, the log-log result supports the conclusion that the observed response reflects multi-fraction TOC behavior plus a narrow equilibrium concentration range. The most defensible competition descriptors for this matrix are therefore the persistence of high C_{eq} and the presence of S.

Oxidized Leachate: TOC adsorption regime and competition behavior

The oxidized leachate test shows comparatively small changes in equilibrium TOC across 0-10 g/L of GAC, with TOC remaining consistently in the high 10^2 mg/L range. This near constant C_{eq} indicates that oxidation shifts the TOC composition toward fractions that are less responsive to GAC at low doses, so that increasing GAC primarily removes only a limited adsorbable fraction while the bulk TOC remains in solution. As a result, the solution-phase competitor background experienced by PFAS remains relatively constant across the series.

Table 21. Oxidized Leachate batch test results for TOC (141 h)

Oxidized Leachate	
141h	
GAC	**TOC**
Conc GAC (g/L)	**Conc C_{eq} ppm**
0	188.8
0.5	181.9
1	178.7
1.5	172.5
2	170.9
3	165.9
5	170.9
10	165.5

The $S - C_{eq}$ plot clusters at higher equilibrium concentrations (approximately 0.166-0.183 g/L) while still showing measurable TOC uptake on GAC. This again could contribute to partial partitioning, there are organics load on the adsorbent, but a large, dissolved fraction persists. Relative to the Raw Leachate, the oxidized series visually emphasizes higher residual C_{eq} (a more persistent solution-phase TOC background) over the low-dose range.

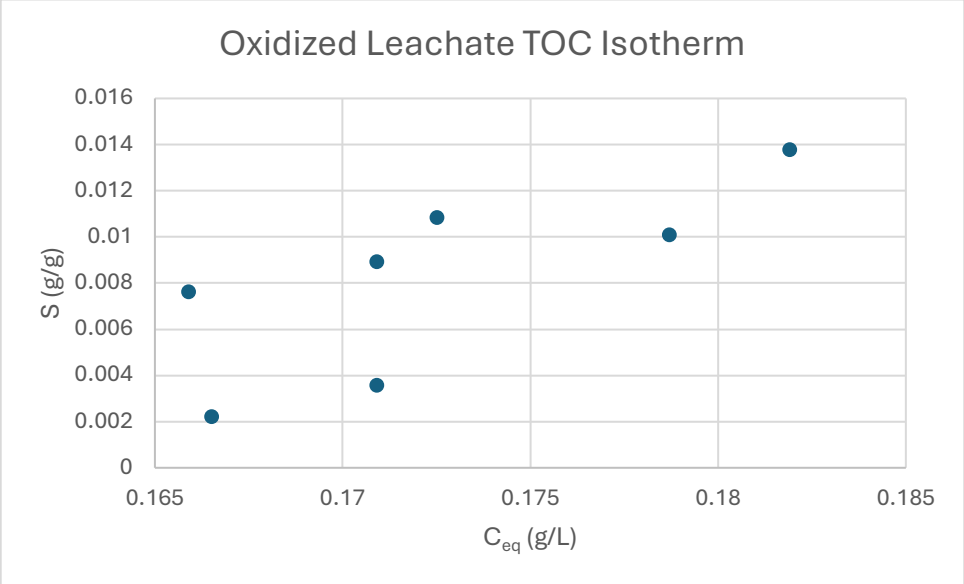

Figure 28. Oxidized leachate TOC isotherm (141 h, Carbopur 1240 GAC) highlighting high residual C_{eq} and partial partitioning of a refractory organic fraction.

Freundlich Isotherm log-log linearization

The log-log regression for oxidized leachate was:

$Log\ S = 12.848 Log\ C_{eq} + 7.6548 \qquad R^2 = 0.4424$

Where n $= 0.0778$ and $K_f = 4.5 \times 10^7$

Although R^2 is higher than in the Raw Lechate matrix, it remains too low to justify interpreting these parameters as intrinsic adsorption constants for TOC. The extreme fitted values further indicate that the regression is dominated by the narrow equilibrium window and mixture behavior rather than a stable Freundlich regime.

As for the raw matrix, the competition-relevant explanation relies on the observed persistence of high C_{eq} together with measurable TOC loading S, rather than on the numerical magnitude of K_f and n.

Matrix Comparison on TOC Adsorption Competition

Across both matrices, equilibrium TOC remains high in the 0-10 g/L GAC range, indicating that PFAS adsorption occurred under sustained TOC competition

rather than in a low-TOC regime. The $S - C_{eq}$ plots confirm concurrent organic loading on GAC while a substantial dissolved fraction persists, so PFAS uptake is influenced by both solution-phase competition (high TOC C_{eq}) and adsorbent occupancy (non-zero TOC of S). The oxidized matrix maintains a higher and flatter C_{eq} across dose changes, implying a more persistent dissolved competitor pool, whereas the raw matrix shows a clearer dose-dependent reduction in C_{eq} while still retaining substantial residual TOC. A constant solvent-derived TOC contribution from PFAS spiking may shift absolute TOC levels but is expected to be dose-independent and therefore does not affect the comparative interpretation between matrices.

5.5.2 PFAS adsorption results under competitive conditions (Final Experiment)

5.5.2.1 PFBA adsorption test under TOC competition

Table 22. PFBA Adsorption in final configuration

PFBA				
	Raw Leachate		Oxidized Leachate	
Conc GAC (g/L)	Conc C_{eq} (ppb)		Conc C_{eq} (ppb)	
	70h	141h	70h	141h
0	90.3239	85.3255	88.6494	88.2245
0.5	50.8615	39.3652	64.5571	59.3338
1	17.3198	11.8666	32.9423	29.3934
1.5	10.0347	6.6108	17.2049	14.4382
2	5.9735	3.6242	8.9525	7.3530
3	2.3808	1.5259	4.5064	2.9691
5	0.7964	0.4895	1.0956	0.7330
10	0.2631	0.1199	0.2741	0.2410

PFBA remained quantifiable across the full low-dose GAC range (0-10 g/L) at both contact times (70 h and 141 h) and in both matrices (Raw Leachate and Oxidized Leachate), and therefore provides a suitable concentration range to compare matrix effects (Raw vs Oxidized) under TOC competition and evaluate time effects (70 h and 141 h) as the system progresses toward equilibrium.

Across both matrices, PFBA C_{eq} decreased systematically as GAC dose increased, confirming a clear dose-response under competitive conditions. Extending contact time from 70 h to 141 h generally shifted C_{eq} downward at the same GAC dose, consistent with continued uptake and/or approach to equilibrium, with the time effect being more evident in the raw leachate series than in the oxidized series at the highest dose.

A consistent matrix effect was also apparent, for the same GAC dose and contact time, the oxidized leachate typically retained higher PFBA C_{eq} than the diluted raw leachate. This indicates weaker apparent PFBA removal in the oxidized matrix within this low-dose GAC range, consistent with a competition regime in which the oxidized condition maintained a more persistent dissolved organic background (as established in the TOC section).

Freundlich isotherm results

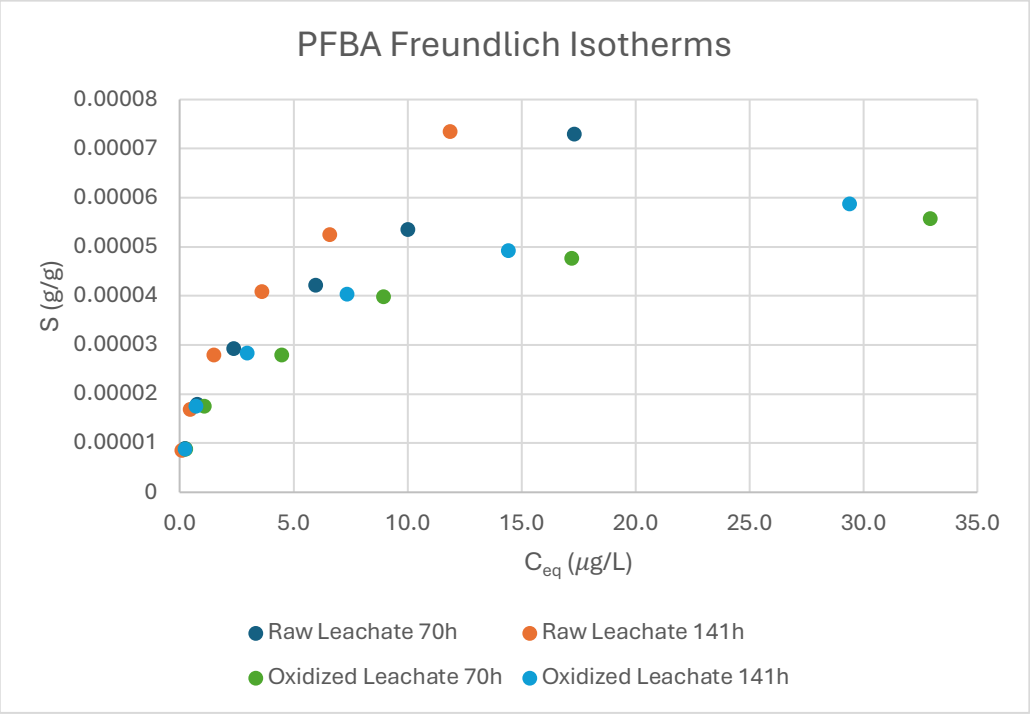

Figure 29. PFBA adsorption isotherms (Raw vs. Oxidized leachate, 70 h and 141 h) showing time-dependent uptake and matrix-induced suppression in the oxidized series.

The non-linear PFBA isotherm plot (S - C_{eq}) shows monotonic partitioning across all four conditions (raw/oxidized and 70/141 h) in which increasing C_{eq} corresponds to increasing S. Two qualitative features are important for competition interpretation:

Time effect: the 141 h points generally correspond to lower C_{eq} at comparable sorbed loadings than the 70 h points, indicating continued uptake with time.

Matrix effect: oxidized-leachate points tend to occupy the higher C_{eq}region at comparable sorbed loadings, consistent with suppressed uptake relative to the raw matrix under the same GAC dosing range.

Moreover, In the low C_{eq} region (sub-µg/L to a few µg/L), the Oxidized Leachate points are generally right-shifted relative to the Raw Leachate points which explains for comparable sorbed loading S, the oxidized matrix tends to retain higher C_{eq}. This is consistent with the Table.22 as well (e.g., at 10 g/L GAC, the Oxidized Leachate series keeps PFBA higher than Raw Leachate, especially at 141 h: 0.241 µg/L Oxidized and 0.120 µg/L Raw). This right-shift means weaker effective removal because more PFBA remains in solution for the same amount sorbed onto adsorbent. As the Oxidized matrix maintains a more persistent dissolved TOC background (as shown in the TOC section 5.4.1.3 where C_{eq} stays high and nearly constant across 0-10 g/L), A persistent solution phase competitor pool increases the probability that PFBA encounters a surface already occupied by organics and reduces access to the microporous domains where PFBA uptake is most efficient. In contrast, the raw matrix shows a clearer dose-response in TOC and reaches lower TOC C_{eq}, which is consistent with a slightly less suppressive competition environment for PFBA at the same GAC dose.

In these PFBA non-linear plots, the “plateau” is not a classic saturation plateau of a single solute isotherm; it is the regime where increasing dose yields small additional reductions in C_{eq} because the system approaches a near-depletion range for PFBA under the tested conditions.

Raw leachate reaches the near-depletion regime earlier and more strongly: by the highest dose (10 g/L) PFBA is already down to 0.26 µg/L at 70 h and 0.12 µg/L at 141 h, meaning the curve is pushed toward the low-C_{eq} end. Once C_{eq} is this low, further improvements become limited by the remaining measurable range and by competitive site availability.

Oxidized leachate approaches the same regime more slowly: at 10 g/L of GAC, PFBA remains 0.27 µg/L at 70 h and 0.24 µg/L at 141 h, i.e., the curve stays shifted

to higher C_{eq}. And even at the highest GAC dose in this range, Oxidized Leachate sustains a stronger effective competition background, preventing PFBA from entering as deep a near-depletion regime as in the Raw Leachate case.

Linearized PFBA Freundlich isotherm results

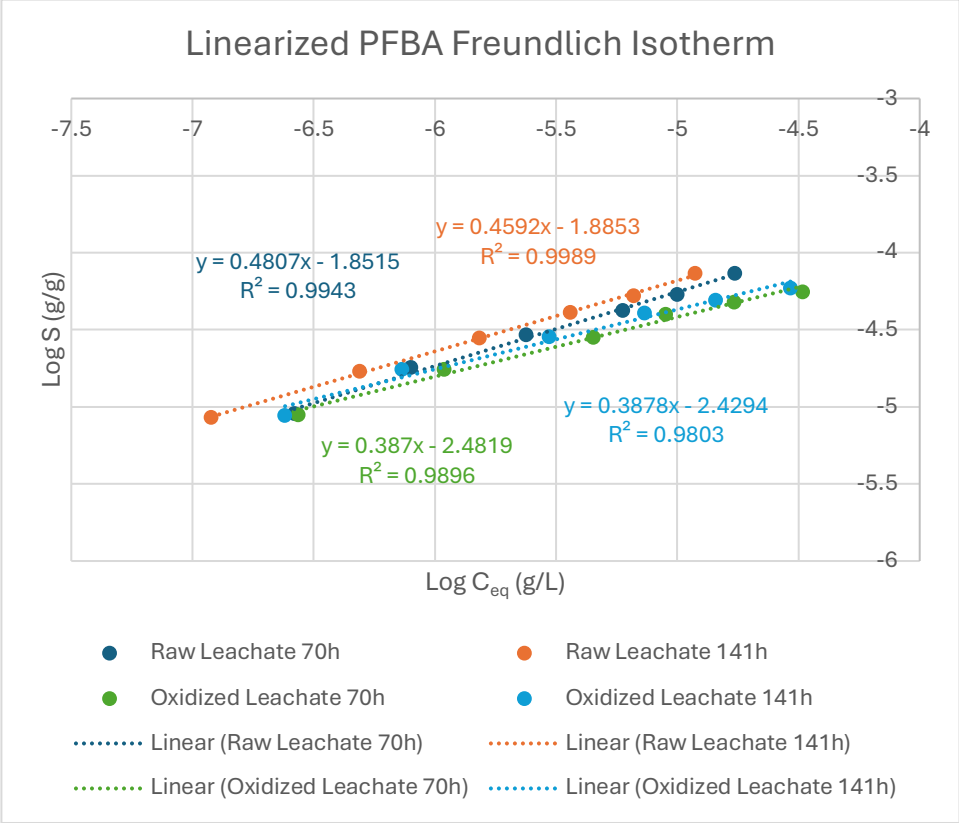

Figure 30. Linearized Freundlich plots for PFBA (Raw vs. Oxidized leachate, 70 h and 141 h) showing higher K_f in raw leachate.

Freundlich fits were evaluated in log-log form:

Raw leachate

70 h: $Log\ S = 0.4807 Log\ C_{eq} - 1.8515$ $R^2 = 0.9943$

n = 2.08 and $K_f = 1.41 \times 10^{-2}$

141 h: $Log\ S = 0.4592 Log\ C_{eq} - 1.8853$ $R^2 = 0.9989$

n = 2.18 and $K_f = 1.30 \times 10^{-2}$

Oxidized leachate

70 h: $Log\ S = 0.3870 Log\ C_{eq} - 2.4819$ $R^2 = 0.9896$
n $= 2.58$ and $K_f = 3.30 \times 10^{-3}$
141 h: $Log\ S = 0.3878 Log\ C_{eq} - 2.4294$ $R^2 = 0.9803$
n $= 2.58$ and $K_f = 3.72 \times 10^{-3}$

1- K_f controls the vertical position of the log-log isotherm (how high S is at a given C_{eq}). Oxidized Leachate has K_f about $\times 3 - 4$ lower than Raw Leachate ($3.3 - 3.7 \times 10^{-3}$ vs $1.3 - 1.4 \times 10^{-2}$). This is exactly the quantitative expression of the right-shift seen in the non-linear plot where for a given equilibrium concentration, less PFBA is effectively sorbed per gram of GAC.

Oxidation typically increases the fraction of TOC as smaller, more polar and mobile components, which can access and occupy the same pore domains that PFBA relies on (i.e., micropores), thereby reducing effective adsorption capacity for PFBA. In contrast, Raw Leachate TOC includes a larger fraction of high molecular weight material that may preferentially adsorb on external surfaces or block entrances without penetrating as deeply; this can still suppress adsorption, but it may leave relatively more micropore capacity available for PFBA compared with an oxidized TOC pool dominated by smaller fragments.

The TOC results support this interpretation because oxidized leachate maintains a high, relatively constant TOC C_{eq}, i.e., a persistent dissolved competitor pool.

2- The Oxidized Leachate slopes are consistently lower (0.387) than the raw slopes (0.46-0.48). A lower 1/n means that $Log\ S$ increases less per unit increase in $Log\ C_{eq}$, i.e., PFBA partitioning becomes less responsive to changes in C_{eq} under the Oxidized matrix.

A more uniform and persistent competition environment (steady high TOC C_{eq}, greater access of competitor organics to pore space) tends to "flatten" the effective adsorption response because incremental changes in PFBA concentration do not translate into proportional increases in sorbed PFBA meaning many adsorption environments are already occupied. In the Raw matrix, where the TOC background decreases more with dose, PFBA experiences relatively more variation in effective site availability across the GAC range, which is consistent with a somewhat steeper apparent 1/n.

3- Raw leachate shows a clearer time-driven shift toward lower C_{eq} of PFBA at high GAC dose (e.g., 10 g/L: 0.263 µg/L at 70 h vs 0.120 µg/L at 141 h), whereas

oxidized leachate shows a smaller shift (0.274 µg/L vs 0.241 µg/L). This indicates that, in the Oxidized matrix, extending contact time yields less additional PFBA removal within the tested range which is consistent with a stronger persistent competition regime that limits the "available capacity gain" over time.

Clean-matrix reference (PFBA standard): baseline for competition

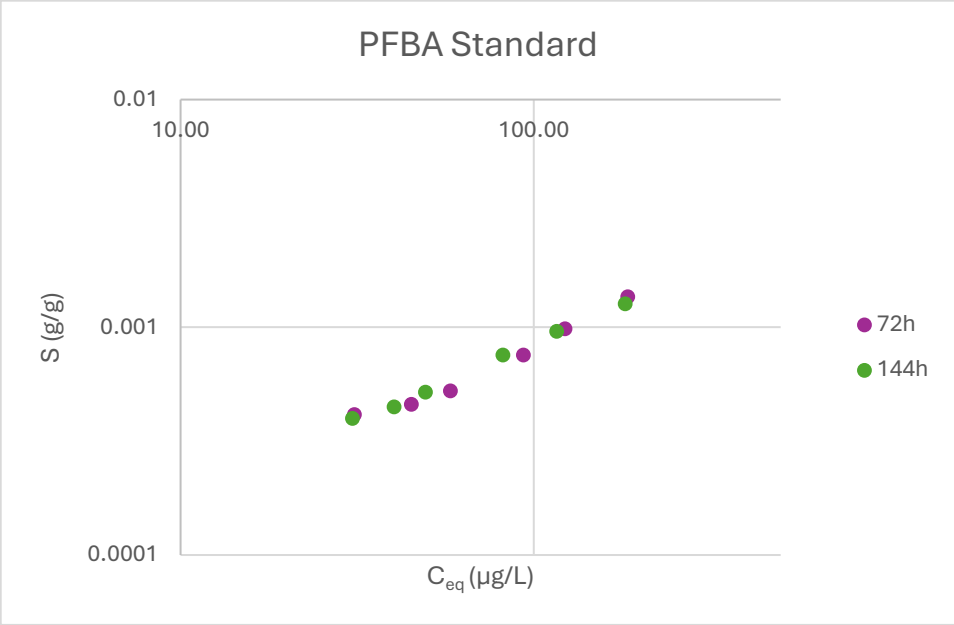

Figure 30. PFBA Standard Freundlich Isotherm at 72 h and 144 h

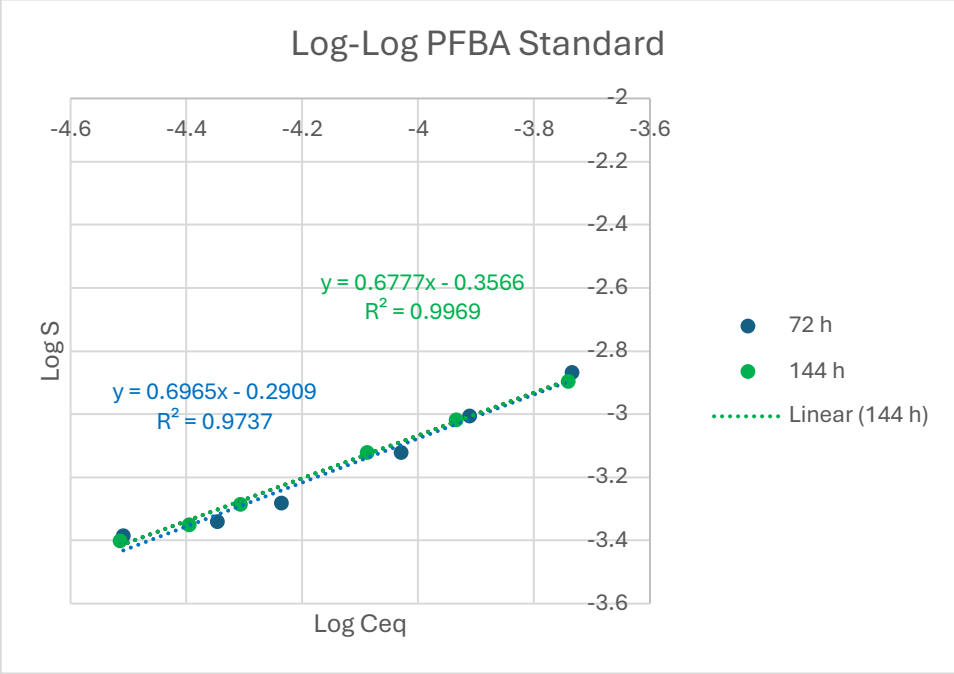

Figure 31. Linearized PFBA Standard Freundlich Isotherm at 72 h and 144 h

The standard PFBA fits provide the clean reference behavior:

72 h: $Log\ S = 0.6965 Log\ C_{eq} - 0.2909$ $R^2 = 0.9737$

n = 1.44 and $K_f = 5.12 \times 10^{-1}$

144 h: $Log\ S = 0.6777 og\ C_{eq} - 0.3566$ $R^2 = 0.9969$

n = 1.48 and $K_f = 4.40 \times 10^{-1}$

The standard PFBA isotherm was constructed at very low GAC dosages (0.1-0.7 g/L) to deliberately populate a broad equilibrium range and capture the intrinsic PFBA-GAC partitioning shape under a simple, single-solute matrix. In contrast, the leachate experiments require a much higher GAC range (0-10 g/L) because the system is not single-solute, a large pool of co-solutes (dominantly TOC, plus other constituents) competes for adsorption domains and conditions the carbon surface.

Using higher GAC dosages in leachate is therefore justified to ensure measurable PFBA adsorption under realistic competition and site-availability constraints. Graphically, this shift in operating regime explains why the standard test remains well spread in C_{eq}, whereas the leachate datasets compress toward low C_{eq} as dose increases, higher site supply combined with matrix competition drives PFBA into a near-depletion region more quickly, limiting resolution of the mid-range isotherm while still providing the effective adsorption response relevant for leachate treatment.

Also relative to the Standard PFBA linearization plot, both leachate matrices are strongly suppressed in apparent capacity, K_f decreases from $4.4 \sim 5.12 \times 10^{-1}$ (Standard) to $1.3 \sim 1.4 \times 10^{-2}$ (Raw Leachate) and $3.3 \sim 3.7 \times 10^{-3}$ (Oxidized Leachate). This corresponds to an approximate suppression factor of $\times 30$ (Raw Leachate vs Standard) and $\times 120 \sim 130$ (Oxidized Leachate vs Standard), within the fitted range. The slope reduction from 0.68 (Standard) to $0.46 \sim 0.48$ (Raw Leachate) and 0.39 (Oxidized Leachate) indicates a flatter adsorption response under competitive matrices, consistent with reduced access to high affinity adsorption environments in leachate relative to the clean reference.

5.5.2.2 PFBS adsorption test under TOC competition

Table 23. PFBS Adsorption in final configuration

PFBS				
	Raw Leachate		Oxidized Leachate	
Conc GAC (g/L)	Conc C_{eq} (ppb)		Conc C_{eq} (ppb)	
	70h	141h	70h	141h
0	71.5594	79.2163	69.7127	72.2800
0.5	17.9830	10.4792	19.6541	13.5780
1	1.5554	0.7554	2.9538	2.0745
1.5	0.7723	0.4230	1.0098	0.6594
2	0.4209	0.2236	0.4002	0.2369
3	0.1170	0.0841	0.1474	0.1009
5	0.0342	0.0111	0.0495	0.0204
10	0.0039	-0.0039	0.0018	0.0059

PFBS remained quantifiable over most of the 0-10 g/L window, but the highest-dose points approach the analytical limit. In particular, the negative value at 10 g/L (Raw Leachate, 141 h) is not physical and indicates <LOQ; it is treated as censored data and excluded from fitting.

Across both matrices and contact times, PFBS C_{eq} decreases steeply with increasing GAC dose, confirming a strong dose-response within 0-10 g/L. The matrix contrast is clearest in the low-dose region (0.5-2 g/L), where the oxidized leachate generally retains higher PFBS C_{eq} than the raw leachate at the same time, indicating stronger matrix suppression of PFBS removal in the Oxidized Leachate. At the high-dose end (5-10 g/L), both matrices approach a near-depletion regime

(sub-0.1 µg/L), where small absolute differences become difficult to interpret because results are close to LOQ.

Time effects are evident primarily at intermediate doses, extending contact time from 70 h to 141 h tends to further reduce C_{eq}, with the strongest improvement typically occurring before the near-depletion region is reached.

Freundlich isotherm results

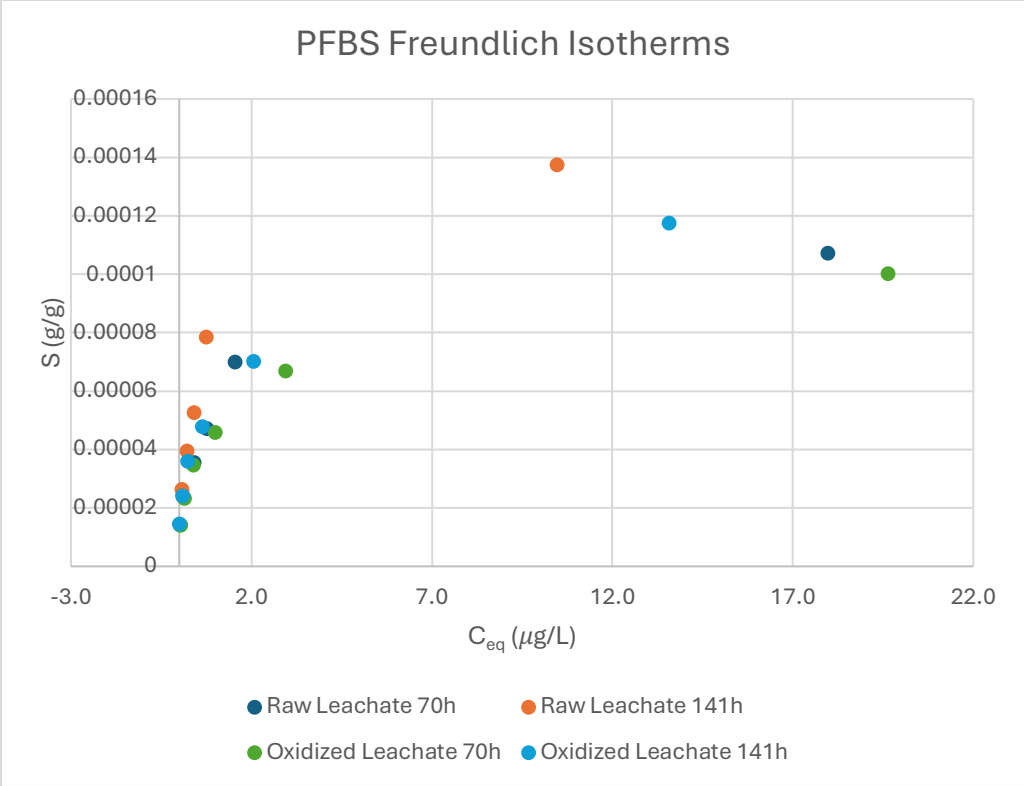

Figure 32. PFBS non-linear Freundlich isotherms (Carbopur 1240, 0-10 g L^{-1}; 70 h and 141 h) showing right-shifted oxidized leachate data at low C_{eq}, indicating stronger matrix competition, and near-depletion behavior at higher GAC doses.

In the non-linear $S - C_{eq}$ Freundlich Isotherm plot, the Oxidized Leachate points are again generally right-shifted relative to the raw-leachate points in the low-C_{eq} region (for similar S, higher C_{eq} remains). This visually encodes the same message as the Table 23 in which at comparable GAC dose and time, especially at 0.5-2 g/L, the Oxidized matrix leaves more PFBS in solution, consistent with a stronger competing background.

A plausible competition-consistent explanation is that oxidation produces a TOC pool that remains highly persistent in solution and is more pore-accessible, maintaining surface conditioning and site competition that suppresses PFBS uptake more strongly than in the diluted raw matrix.

At higher doses (5-10 g/L), C_{eq} approaches the low end of the measurable domain (down to 0.01 μg/L and below). In this region the isotherm appears to flatten, evidently not because adsorption saturates in the classic sense, but because the system enters a near-depletion regime, additional dose or time produces only small absolute changes in an already very low C_{eq}, and analytical uncertainty becomes relatively more important. This is also the region where censored values (<LOQ) begin to appear (e.g., raw 141 h at 10 g/L).

Moreover, PFBS reaches this near-depletion behavior at lower doses than PFBA under the same matrices and times, which is consistent with a stronger adsorption propensity of PFBS. This difference could be attributed not to chain length (PFBS and PFBA are both C4), but to functional-group effects, PFBS is a sulfonate, and the PFBS curves compress toward low C_{eq} much earlier than PFBA, providing direct experimental evidence (within this dataset) of higher GAC affinity for PFBS than for PFBA under competitive leachate conditions.

Linearized PFBS Freundlich isotherm results

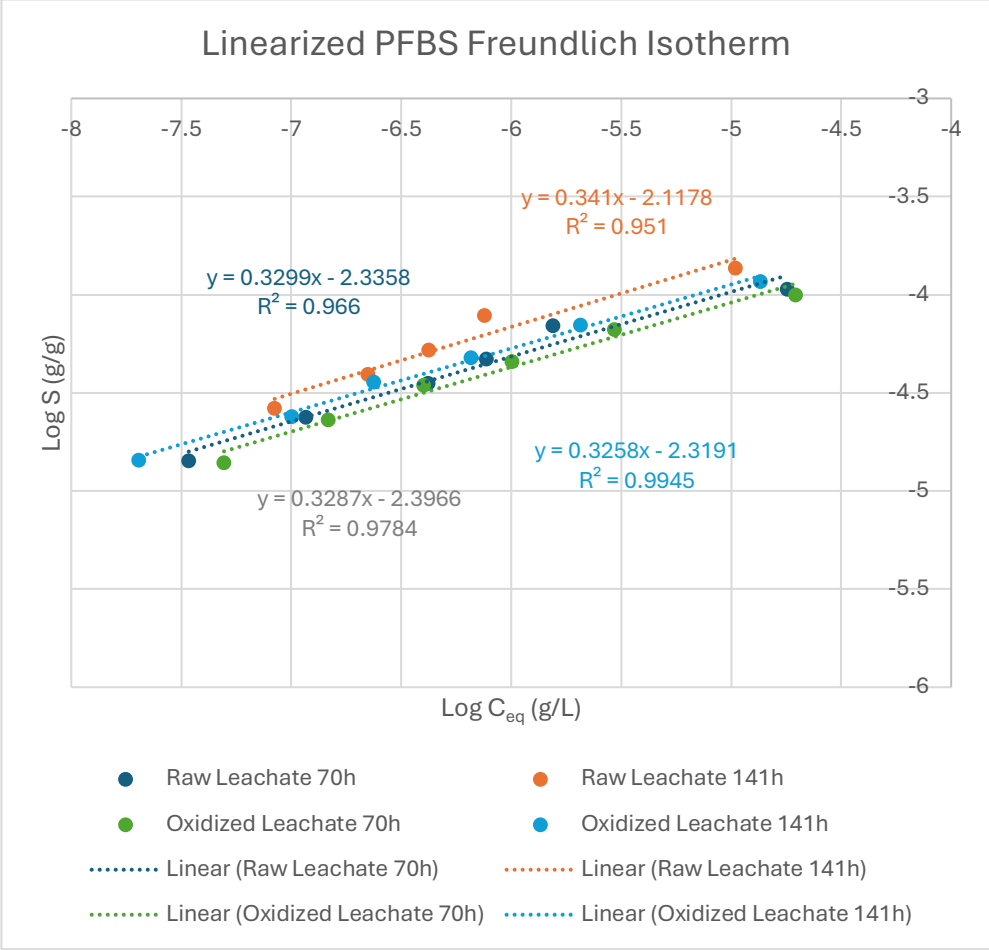

Figure 33. Log-log Freundlich isotherms for PFBS (Carbopur 1240, 0–10 g L^{-1}; 70 h and 141 h) showing comparable slopes (1/n) across matrices and times, with slightly higher K_f in raw leachate.

All regressions show good linearity in the log-log space (high R^2), so the comparison focuses on Log K_f (vertical shift/apparent adsorption capacity) and 1/n (adsorption intensity/concentration dependence).

Raw leachate

70 h: $Log\ S = 0.3299 Log\ C_{eq} - 2.3358$ $R^2 = 0.966$

n = 3.03 and $K_f = 4.6 \times 10^{-3}$

141 h: $Log\ S = 0.3410 Log\ C_{eq} - 2.1178$ $R^2 = 0.951$

n = 2.93 and $K_f = 7.6 \times 10^{-3}$

Oxidized leachate

70 h: $Log\ S = 0.3287 Log\ C_{eq} - 2.3966$ $R^2 = 0.9784$
n = 3.04 and $K_f = 4.0 \times 10^{-3}$

141 h: $Log\ S = 0.3258 Log\ C_{eq} - 2.3191$ $R^2 = 0.9945$
n = 3.07 and $K_f = 4.8 \times 10^{-3}$

1- At both times, Oxidized Leachate has a more negative Log K_f (lower K_f) than Raw Leachate:

70 h: Oxidized Leachate K_f is 4.0×10^{-3} and Raw Leachate 4.6×10^{-3} (slightly lower)

141 h: Oxidized Leachate K_f 4.8×10^{-3} and Raw Leachate 7.6×10^{-3} (meaningfully lower)

This is the cleanest matrix distinction in the fitted parameters, the Oxidized matrix exhibits a downward shift of the PFBS isotherm relative to Raw matrix, particularly after long contact time. So, for a given equilibrium concentration C_{eq}, the Oxidized matrix corresponds to less PFBS on the carbon (lower S).

2- The slopes $(1/n)$ are very similar across the two matrices (0.326-0.341). This indicates that the shape (concentration dependence) of PFBS partitioning is broadly conserved; the dominant matrix effect is therefore not a change in adsorption intensity, but a capacity/availability shift (captured by K_f).

The small slope differences that exist are interpretable as secondary effects, Raw Leachate at 141 h is slightly steeper (0.341) than oxidized at 141 h (0.326), implying PFBS uptake in raw becomes marginally more responsive to changes in C_{eq} across the sampled window. Oxidized slopes remain nearly unchanged with time, suggesting the competitive environment is more stable (or more uniformly suppressive) across the GAC range.

3- A lower Log K_f in oxidized leachate means that the effective PFBS uptake per unit adsorbent is reduced at a given C_{eq}.The most consistent interpretation (supported by TOC results) is:

Oxidation produces a TOC pool that is more persistent in solution and more pore-accessible, keeping the GAC surface conditioned and adsorption domains partially occupied even at low doses.

In the TOC section, oxidized leachate displayed a flatter C_{eq} response across 0-10 g/L (persistent solution-phase TOC), which is the signature of a stable competitor background.

That persistent competitor background reduces the number of effective high-affinity sites available to PFBS, primarily shifting the isotherm downward (lower K_f) rather than changing its shape dramatically (similar $1/n$).

In other words, the oxidized matrix appears to impose a stronger "site availability penalty" rather than fundamentally changing how PFBS responds to concentration.

4- The raw matrix shows a clearer increase in apparent K_f with time (from 4.6×10^{-3} to 7.6×10^{-3}), whereas the oxidized matrix increases only modestly (from 4.0×10^{-3} to 4.8×10^{-3}).

This pattern is consistent with the idea that, in Raw Leachate, continued contact time allows PFBS to access additional adsorption domains (e.g., slower diffusion into micropores or gradual displacement/redistribution among sorbed species), producing a stronger upward shift in the effective isotherm. In Oxidized Leachate, where the competitor pool remains more persistent and more uniformly present, additional time brings less new capacity, so the isotherm shift is smaller.

5- When PFBS is compared to PFBA under the same experimental framework, there is clear evidence of functional-group driven affinity differences at the same chain length:

PFBS (C4 sulfonate) reaches near-depletion at lower doses and exhibits lower C_{eq} than PFBA at comparable doses/times, consistent with stronger adsorption. This is not a chain-length effect (both are C4); it is a headgroup effect (sulfonate vs carboxylate) that manifests as stronger uptake and earlier approach to the low-C_{eq} regime.

So, within the C4 class, PFBS showed stronger adsorption than PFBA (earlier approach to near-depletion), indicating a functional-group effect (sulfonate > carboxylate) under competitive leachate conditions.

Clean-matrix reference (PFBS standard): baseline for competition

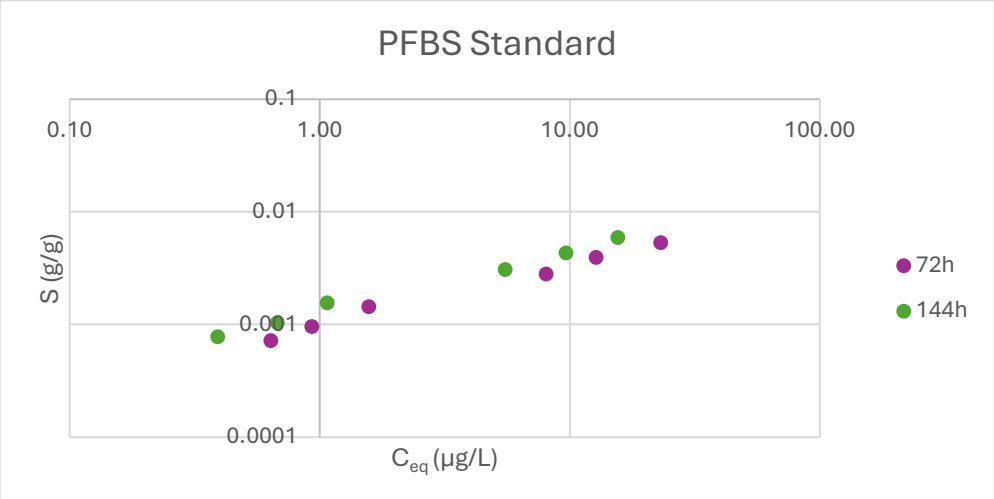

Figure 34. PFBS Standard Freundlich Isotherm at 72 h and 144 h

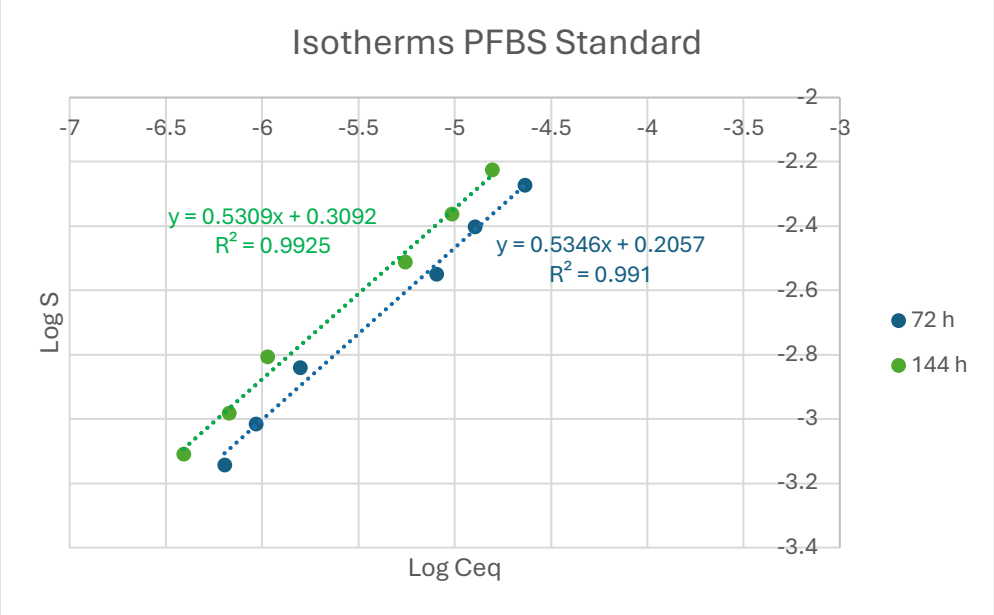

Figure 35. Linearized PFBS Standard Freundlich Isotherm at 72 h and 144 h

The standard PFBS log-log fits provide the clean reference:

72 h: $Log\ S = 0.5346 Log\ C_{eq} + 0.2057$ $R^2 = 0.991$

n = 1.87 and $K_f = 1.61$

144 h: $Log\ S = 0.5309 Log\ C_{eq} + 0.3092$ $R^2 = 0.9925$

n = 1.88 and $K_f = 2.04$

The same logic as PFBA could apply also to PFBS, with an even stronger contrast because PFBS usually adsorbs more strongly than PFBA. The standard PFBS isotherm used 0.05-0.4 g/L GAC to avoid rapid depletion and to map the intrinsic isotherm under clean conditions; if Leachate-level complexity were present, that low-dose window would be insufficient to overcome competition and to achieve a measurable adsorption signal across the range.

However, in the Leachate matrices, the higher dosing window (0-10 g/L) is therefore methodologically appropriate to compensate for TOC-driven site competition and pore conditioning, but it also means that PFBS approaches the low-C_{eq} (near LOQ) regime rapidly, visually compressing the non-linear curve. Consequently, differences between the standard and leachate non-linear plots reflect a true matrix effect (competition and conditioning reducing effective site

availability) and an intentional change in operating regime (low-dose shape-definition standard vs higher-dose competitive leachate tests).

The reference is also essential for competition analysis, the Leachate matrices can be interpreted as suppressed isotherms relative to the Standard, in fact in both Raw and Oxidized Leachate, Log K_f shifts downward by several orders of magnitude and $1/n$ decreases which is consistent with reduced effective site availability and altered partitioning under matrix competition and GAC surface conditioning.

5.5.2.3 PFOA adsorption test under TOC competition

Table 24. PFOA Adsorption in final configuration

PFOA				
	Raw Leachate		Oxidized Leachate	
Conc GAC (g/L)	Conc C_{eq} (ppb)		Conc C_{eq} (ppb)	
	70h	141h	70h	141h
0	58.8634	47.7279	57.2093	48.7912
0.5	14.7259	6.3787	10.8182	4.2172
1	0.5694	0.1145	0.8549	0.2060
1.5	0.2098	0.0317	0.1432	0.0409
2	0.0976	0.0218	0.0482	0.0101
3	0.0173	-0.0050	0.0117	-0.0007
5	0.0016	-0.0091	0.0043	-0.0046
10	0.0037	-0.0098	0.0202	0.0039

PFOA shows a much stronger affinity than the C4 compounds (PFBA/PFBS), so the dataset enters a near-depletion regime already at moderate doses. This is visible in the table as several negative values at 141 h (and at some higher doses), which are treated as <LOQ rather than true concentrations. Interpretation of matrix effects is therefore emphasizing the low-to-intermediate dose range (0-2 g/L) where C_{eq} remains clearly quantifiable and differences are meaningful.

Across both matrices, C_{eq} decreases steeply with increasing GAC dose, and extending contact time from 70 h to 141 h consistently shifts C_{eq} downward, especially in the 0.5-2 g/L window. A matrix effect is also apparent, at the same dose and time, Oxidized Leachate generally retains lower C_{eq} than Raw Leachate in the quantifiable window (e.g., 0.5-2 g/L), indicating less suppression and more

effective uptake for PFOA under oxidized conditions in this dataset. At GAC ≥3 g/L, both matrices rapidly approach the LOQ domain.

PFOA Freundlich isotherm results

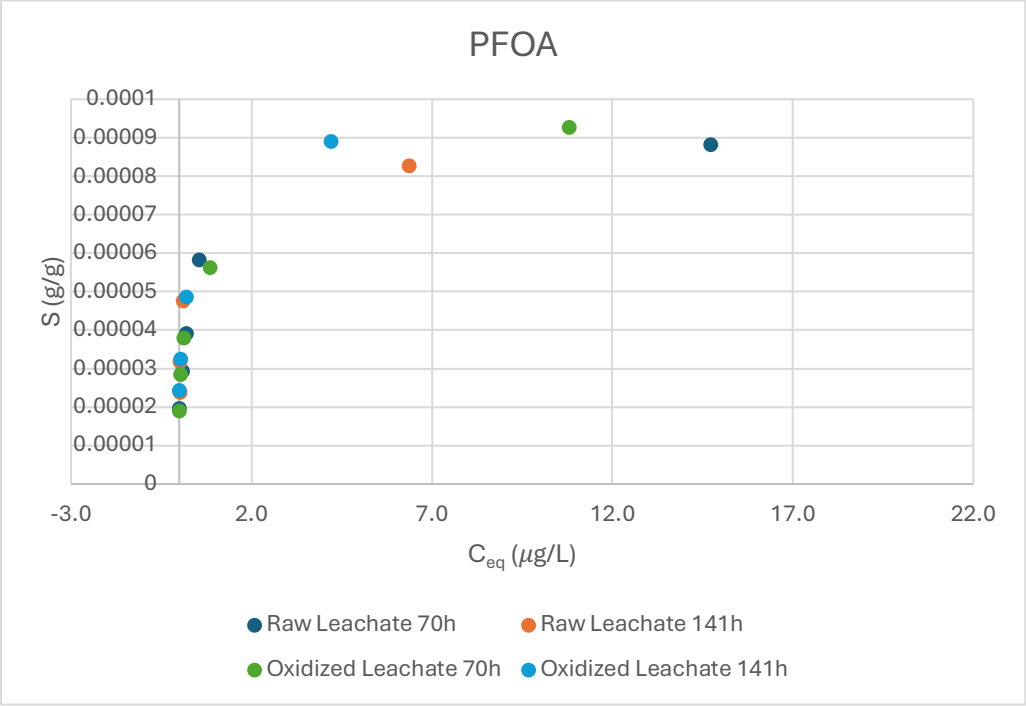

Figure 36. PFOA non-linear Freundlich isotherms under competitive conditions (Carbopur 1240, 0-10 g L^{-1}; 70 h and 141 h) showing rapid shift toward very low equilibrium concentrations, near-depletion behavior at higher doses with relatively stronger adsorption to shorter-chain PFAS.

In the non-linear $S - C\_eq$ Freundlich Isotherm plot, most points cluster near the y-axis (very low C_{eq}), confirming that the tested GAC dose even in generally low ranges pushes PFOA rapidly into low equilibrium concentrations. Relative separation between matrices is primarily visible in the few points at higher C_{eq} at relatively low GAC doses. There, the Oxidized series tends to occupy the lower-C_{eq} side at comparable S, consistent with the Table 24 observation that Oxidized Leachate gives lower residual PFOA in the measurable region.

The apparent flattening at higher doses is best interpreted as a near-depletion plateau rather than site saturation, once C_{eq} falls to 0.01 µg/L (and below),

additional dose/time cannot be resolved reliably because the system is close to the quantification limit and the remaining measurable mass in solution is extremely small. This is the expected behavior for a stronger-adsorbing PFAS and is direct evidence that PFOA adsorption is substantially stronger than PFBA/PFBS under the same competitive matrices as a chain-length effect within the PFCA class where (C8 > C4).

Linearized PFOA Freundlich isotherm results

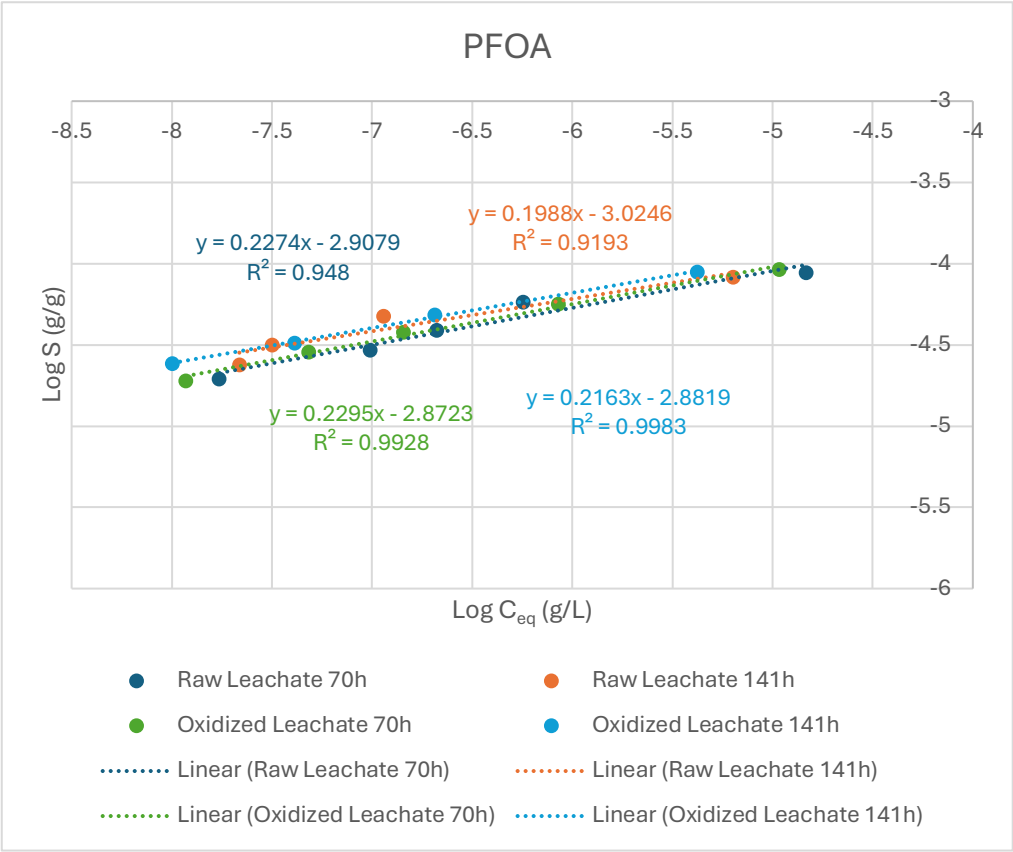

Figure 37. Log-log Freundlich isotherms for PFOA (Carbopur 1240, 0-10 g L^{-1}; 70 h and 141 h) showing high linearity and similar slopes across matrices, with minor differences in K_f, indicating strong adsorption and limited matrix-induced suppression compared to shorter-chain PFAS.

All regressions show good linearity and the plotted linearizations give:

Raw leachate

70 h: $Log\ S = 0.2274 Log\ C_{eq} - 2.9079$ $\quad R^2 = 0.948$

n = 4.40 and $K_f = 1.24 \times 10^{-3}$

141 h: $Log\ S = 0.1988 Log\ C_{eq} - 3.0246$ $R^2 = 0.919$

n = 5.03 and $K_f = 9.45 \times 10^{-4}$

Oxidized leachate

70 h: $Log\ S = 0.2295 Log\ C_{eq} - 2.8723$ $R^2 = 0.9928$

n = 4.36 and $K_f = 1.34 \times 10^{-3}$

141 h: $Log\ S = 0.2163 Log\ C_{eq} - 2.8819$ $R^2 = 0.9983$

n = 4.62 and $K_f = 1.31 \times 10^{-3}$

1- In contrast to PFBA and PFBS, the Oxidized matrix does not show a lower K_f; instead, Oxidized Leachate exhibits a slightly higher K_f than Raw Leachate at both contact times (particularly clear at 141 h: 1.31×10^{-3} Oxidized Leachate vs 9.45×10^{-4} Raw Leachate). In practical terms, this corresponds to a modest upward shift of the oxidized-leachate PFOA isotherm (higher S at a given C_{eq}, or lower C_{eq} for a given uptake), suggesting weaker matrix suppression for PFOA in the Oxidized condition in the test.

This direction of oxidation effect is notable when compared with the earlier molecules. For PFBA and PFBS, oxidation produced the opposite pattern where lower $Log\ K_f$ (downward shift) and, in the non-linear plots, a consistent right-shift at low C_{eq} , indicating stronger suppression in Oxidized Leachate.

The PFOA behavior therefore suggests that Oxidation does not impose a uniform "more suppressive" competition regime for all PFASs; rather, the net effect depends on which adsorption domains control uptake for the specific molecule. In this test the similarity in $1/n$ implies that the competitive environment did not strongly alter the adsorption intensity of PFOA, while the higher K_f under Oxidation indicates a small increase in effective availability/accessibility of the adsorption capacity relevant to PFOA.

A competition-consistent interpretation is that PFOA which is a C8 PFCA, adsorbs more strongly and relies more on high-affinity microporous domains; under such conditions, the dominant limitation can shift from site competition to domain accessibility. Oxidation alters TOC composition, and the observed upward shift for PFOA is consistent with a scenario in which Oxidation reduces the fraction of organics that most effectively restrict access to the domains controlling PFOA uptake (even if bulk TOC remains high), whereas for weaker PFAS (PFBA/PFBS) the dominant effect remains overall capacity suppression by persistent competition. This could be also aligned with the time behavior: Oxidized Leachate PFOA parameters change little from 70 h to 141 h, suggesting a quickly established

effective partitioning regime, while raw leachate shows greater tendency to enter near-depletion/censored behavior at longer time, which can distort intercepts.

The test supports a PFCA chain-length effect when PFOA is compared with PFBA under the same experimental framework: PFOA approaches the near-depletion/LOQ regime at substantially lower GAC doses (and with more censored high-dose points), indicating stronger adsorption for the longer-chain PFCA (C8 > C4) under competitive leachate conditions.

2- The slopes are very similar across matrices and times (0.20-0.23), indicating that the concentration dependence of PFOA partitioning is comparable; the principal difference is a modest vertical shift (intercept) rather than a major change in intensity. This aligns with the non-linear plots where both matrices enter near-depletion rapidly, so the available window mainly captures the low-C_{eq} regime where isotherm shapes are similar.

3- A clear time trend is not strongly expressed in K_f for Oxidized Leachate (almost unchanged from 70 to 141 h), whereas Raw Leachate shows a small downward shift at 141 h. Given that many high-dose points are censored at 141 h, this difference is plausibly influenced by the narrowing of the quantifiable range rather than a true reduction in adsorption.

Clean-matrix reference (PFOA standard): baseline for competition

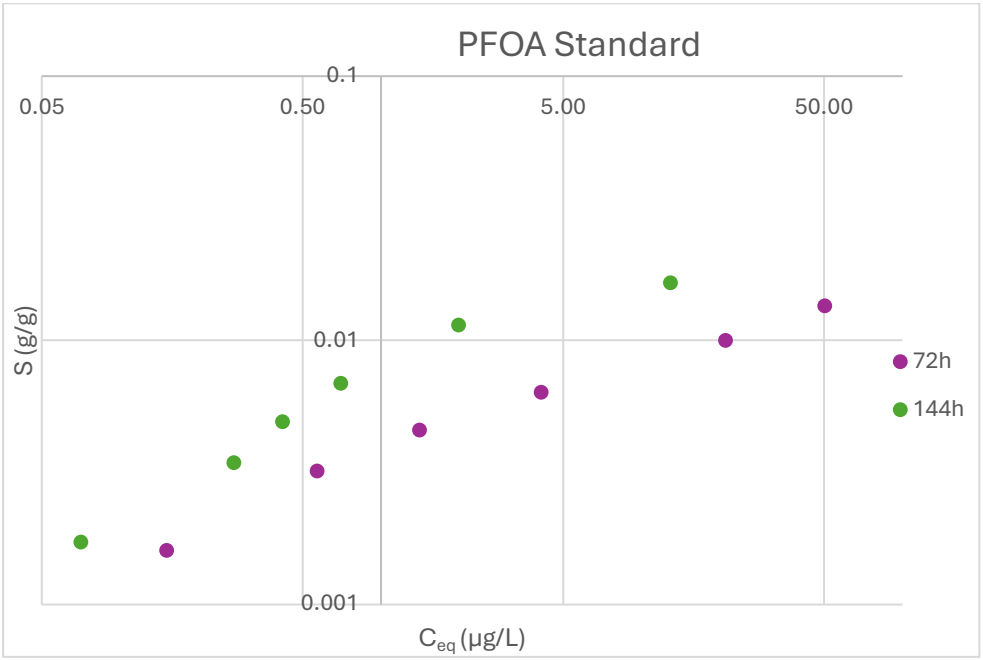

Figure 38. PFOA Standard Freundlich Isotherm at 72 h and 144 h

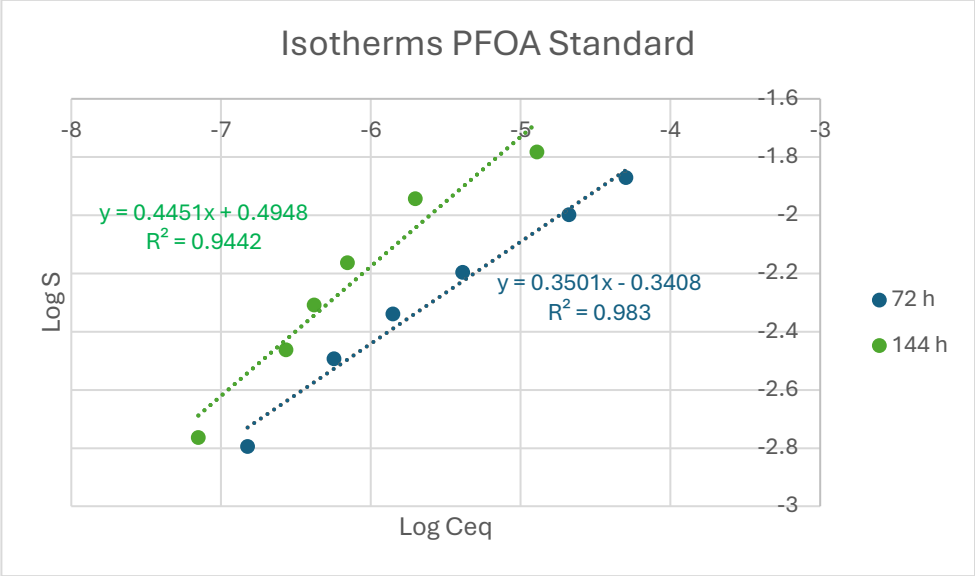

Figure 39. Linearized PFOA Standard Freundlich Isotherm at 72 h and 144 h

The PFOA standard isotherms provide the adsorption baseline of a long-chain PFCA on GAC in the absence of Leachate-derived competitors (TOC and co-solutes). In log-log form, the standard fits are:

72 h: $Log\ S = 0.3501 Log\ C_{eq} - 0.3408$ $R^2 = 0.983$

n = 2.86 and $K_f = 4.56 \times 10^{-1}$

144 h: $Log\ S = 0.4451 Log\ C_{eq} + 0.4948$ $R^2 = 0.944$

n = 2.25 and $K_f = 3.13$

Across the Standard PFOA test, both time series define a coherent reference relationship between S and C_{eq}. The increase in $Log\ K_f$ at 144 h indicates an upward shift of the standard isotherm with longer contact time (higher sorbed loading at a given C_{eq}, consistent with continued approach toward equilibrium and/or improved utilization of adsorption domains. The change in slope (higher $1/n$ at 144 h) indicates a modest change in the concentration dependence across the measured window, but the overall behavior remains well-structured and reproducible.

In the non-linear $S - C_{eq}$ comparison, the key contextual difference is that the standard PFOA isotherm was generated using very low GAC dosages (0.02-0.2 g/L), whereas the leachate isotherms are generated with substantially higher

dosages (0-10 g/L). This dosing contrast explains the graphical behavior in which the standard system intentionally samples a wide equilibrium window because low adsorbent loading leaves PFOA partially in solution (higher C_{eq}), producing a well-populated curve, while the leachate tests, run at much higher GAC loading, drive PFOA rapidly toward very low C_{eq} (often near the quantification limit), compressing the non-linear isotherm into a near-depletion regime.

Consequently, the non-linear plots could be interpreted as showing two different operating regimes: the standard curve represents the intrinsic partitioning relationship under low-carbon loading, whereas the Leachate curves reflect effective adsorption under competitive matrix conditions at relatively higher carbon loading, where competition plus high site supply collapses C_{eq} and limits resolution of the mid-range isotherm.

This clean-matrix reference is very helpful for competition interpretation, relative to the standard, both Leachate matrices exhibit much lower apparent capacities (substantially more negative $Log\ K_f$), demonstrating strong suppression of PFOA uptake under TOC competition.

In addition, comparison within the PFCA family (PFBA vs PFOA) highlights a chain-length effect, the long-chain PFCA reaches near-depletion at lower adsorbent loadings and exhibits stronger uptake behavior than the short-chain PFCA under comparable conditions, even before matrix competition is considered.

5.5.2.4 PFOS adsorption test under TOC competition

Table 25. PFOS Adsorption in final configuration

PFOS				
	Raw Leachate		**Oxidized Leachate**	
Conc GAC (g/L)	**Conc C_{eq} (ppb)**		**Conc C_{eq} (ppb)**	
	70h	141h	70h	141h
0	82.5001	73.5817	74.5787	70.6912
0.5	12.5340	4.8184	5.8584	0.2924
1	0.1962	0.1110	0.2377	0.1614
1.5	0.1803	0.0888	0.1273	0.1021
2	0.1770	0.0851	0.1436	0.2269
3	0.2030	0.0710	0.1943	0.2313
5	0.2417	0.0753	0.2768	0.2001

10	0.3415	0.0547	0.6865	0.7962

PFOS is the strongest-adsorbing target in the set (C8 sulfonate), and the results quickly enter an ultra-low C_{eq} regime (0.05-0.3 µg/L) already around 1-1.5 g/L. In this regime, two issues become central:

Sensitivity to low-signal effects: When true C_{eq} is very small, minor analytical or handling biases can appear as real trends.

Non-monotonicity at higher GAC doses: Several series show C_{eq} increasing again with higher GAC dose, which is not expected for a simple equilibrium adsorption curve and therefore requires careful discussion as an anomaly, not as intrinsic adsorption behavior.

Diluted raw leachate

Main adsorption regime (0 to 1-1.5 g/L). The Raw Leachate series shows the expected behavior, a very steep decrease from the 0 g/L control to 0.5 g/L and then into the sub-µg/L domain by 1-1.5 g/L. This is the robust range where adsorption dominates and conclusions are most defensible.

Strange indication (70 h), rebound at high dose. At 70 h, C_{eq} increases again from 0.18-0.24 µg/L (1-5 g/L) up to 0.34 µg/L at 10 g/L. This trend raises a direct key point: A higher adsorbent dose corresponds to higher dissolved PFOS. A conventional equilibrium interpretation cannot explain that it suggests a non-ideal effect that becomes visible in the ultra-low range.

In 141 h contact time Leachate behaves more regularly, but still not perfectly monotonic. At 141 h, the Raw Leachate series continues toward lower values overall (down to 0.055 µg/L at 10 g/L), which is more consistent with continued equilibration and stronger net uptake. A minor increase at 5 g/L (slightly higher than 3 g/L) still raises the question of whether high-dose points are affected by near-LOQ sensitivity.

Key finding for Raw Leachate adsorption pattern could be that the high dose rebound is clear at 70 h but not at 141 h. This pattern could suggest a time-dependent stabilization (approach to equilibrium or settling/conditioning effects), rather than a true equilibrium trend.

Oxidized leachate

Main adsorption regime (0 to 1-1.5 g/L). The oxidized series also shows the expected steep initial drop and reaches low C_{eq} values quickly. In this low-dose region, interpretation is robust and comparable to the raw matrix.

Strange indication (both times, strongest at 141 h). Strong rebound at high dose. Oxidized leachate exhibits the most pronounced non-monotonicity, after reaching 0.10-0.16 µg/L for around GAC 1-1.5 g/L, C_{eq} rises again at higher doses. The increase becomes dramatic at 10 g/L at 141 h (0.80 µg/L), which is qualitatively inconsistent with a simple adsorption equilibrium curve.

This raises the central key point especially for Oxidized Leachate, the process in which at high carbon loading, the measured aqueous PFOS signal could elevate. Because the trend strengthens with oxidation and long time, it points toward matrix-dependent effects (not random noise) that are amplified in the ultra-low concentration domain.

PFOS Freundlich isotherm results

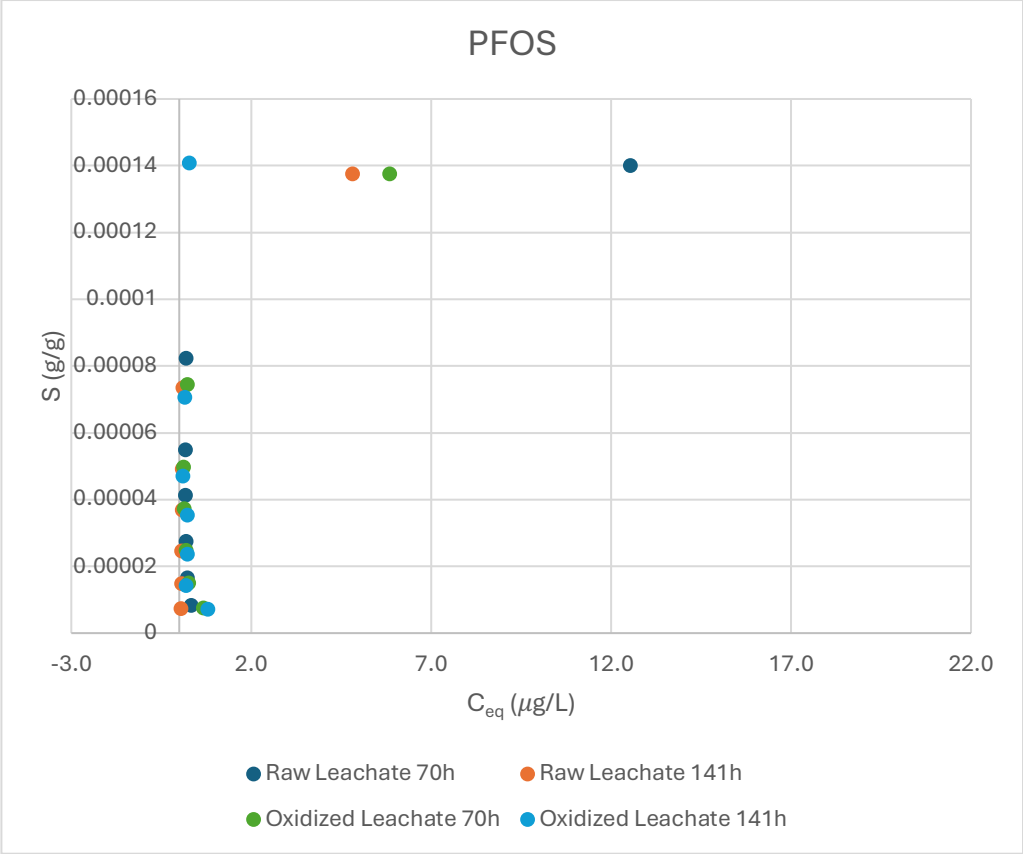

Figure 40. PFOS non-linear Freundlich isotherms under competitive conditions (Carbopur 1240, 0-10 g L^{-1}; 70 h and 141 h) showing rapid collapse toward very low equilibrium concentrations (sub-µg L^{-1}) at low GAC doses, consistent with near-depletion behavior and markedly stronger adsorption relative to PFBA and PFBS.

The PFOS non-linear isotherms are strongly compressed toward the low-C_{eq} axis, once the system reaches 1-1.5 g/L GAC, most points fall into the sub-µg/L domain. This early collapse is itself meaningful, PFOS behaves as a very strong adsorbate, entering a near-depletion regime at much lower doses than PFBA and PFBS under the same Leachate conditions.

This is consistent with a chemically sound strength hierarchy visible in the test results (sulfonate headgroup + longer perfluoroalkyl chain has stronger adsorption), i.e. PFOS (C8 sulfonate) reaches near-depletion faster than PFBS (C4 sulfonate) and much faster than PFBA (C4 carboxylate). In that sense, the non-linear shape provides direct experimental evidence of a chain-length effect within sulfonates (PFOS vs PFBS) and a functional-group effect (sulfonate vs carboxylate) when considered across the full set.

Because PFOS collapses so quickly, the isotherm is not well populated in the mid-C_{eq} region; most of the curve that would normally define a smooth adsorption relationship is effectively skipped. As a result, the non-linear plot becomes dominated by the ultra-low concentration regime, where small absolute differences in measured C_{eq} correspond to large relative changes and where sensitivity to handling/measurement conditions is higher. This is a PFOS-specific interpretive constraint, the stronger the adsorption, the easier it is for the experiment to move into a region where the isotherm becomes difficult to resolve and where deviations from monotonicity become more visible.

For all matrices, adsorption capacity was calculated as:

$$S = \frac{(C_0 - C_{eq}) \times V}{m_{GAC}}$$

where:

C_0 = initial PFOS concentration

C_{eq} = equilibrium concentration

V = solution volume

m_{GAC} = adsorbent mass

When $C_{eq} \ll C_0$, the expression simplifies to:

$$S \approx \frac{C_0 \times V}{m_{GAC}}$$

Thus, once the system approaches near-depletion, S becomes governed primarily by the initial solute mass and adsorbent loading rather than the exact residual C_{eq}.

This principle is essential for interpreting the oxidized 141 h dataset.
At 141 h, more contact time allows more PFOS to access internal pores and residual C_{eq} becomes very small. Because:

$$S = \frac{(C_0 - C_{eq}) \times V}{m_{GAC}}$$

and C_{eq} is already minimum so the numerator is nearly constant and at low GAC doses (e.g., 0.5-1 g/L), m_{GAC} is small, so:

$$S \sim \frac{1}{m_{GAC}}$$

Therefore, even when C_{eq} is extremely low, S remains relatively high at low adsorbent loading.

The Oxidized 141 h test simply reaches this regime earlier and more clearly than the others.

Comparing Oxidized Leachate 70 h and 141 h reveals that 141 h produces systematically lower C_{eq} at the same GAC dose. This indicates that equilibrium was not fully achieved at 70 h. Additional contact time allows PFOS redistribution into micropores.

Importantly, the increase in adsorption extent with time is more pronounced for PFOS than for PFBA or PFBS. This could be due to the PFOS's stronger hydrophobicity and higher affinity for high-energy sites.

Thus, Oxidized Leachate 141 h reflects that it reduces competitive interference (relative to Raw Leachate) and earlier entry into near-depletion regime.

A subset of high-dose points demonstrates an apparent rebound (higher C_{eq} at higher GAC), most pronounced for Oxidized Leachate at 141 h. In a single-solute equilibrium, that trend is not expected, and in the non-linear plot it appears as isolated points separated from the near-depletion cluster. One observation is that, once PFOS is driven close to the low end of the quantifiable range, the measured aqueous concentration is disproportionately influenced by probably some non-ideal effects (e.g., carbon-associated sampling effects at high solids loading, matrix-dependent recovery/response effects in the ultra-low range, or evolving conditioning of the carbon surface in a strongly competitive matrix). Importantly, these anomalies occur exactly where PFOS adsorption is expected to be strongest, which supports treating them as near-depletion sensitivity artifacts or secondary processes, rather than as evidence of a true equilibrium isotherm shape reversal.

In fact, the standard PFOS experiment (which will be evaluated later) was deliberately performed at very low GAC doses (0.02-0.2 g/L), which is consistent with PFOS's strong adsorption, low loading is required to avoid immediate depletion and to populate the isotherm across a measurable C_{eq} range. The need for such low doses in the standard system is itself corroborating evidence that PFOS has a uniquely strong adsorption propensity compared with the other analytes, and it explains why, in leachate experiments run at 0-10 g/L, PFOS rapidly enters a compressed near-depletion regime where the non-linear isotherm is difficult to resolve and where anomalous high-dose points become more apparent.

Linearized PFOS Freundlich isotherm results

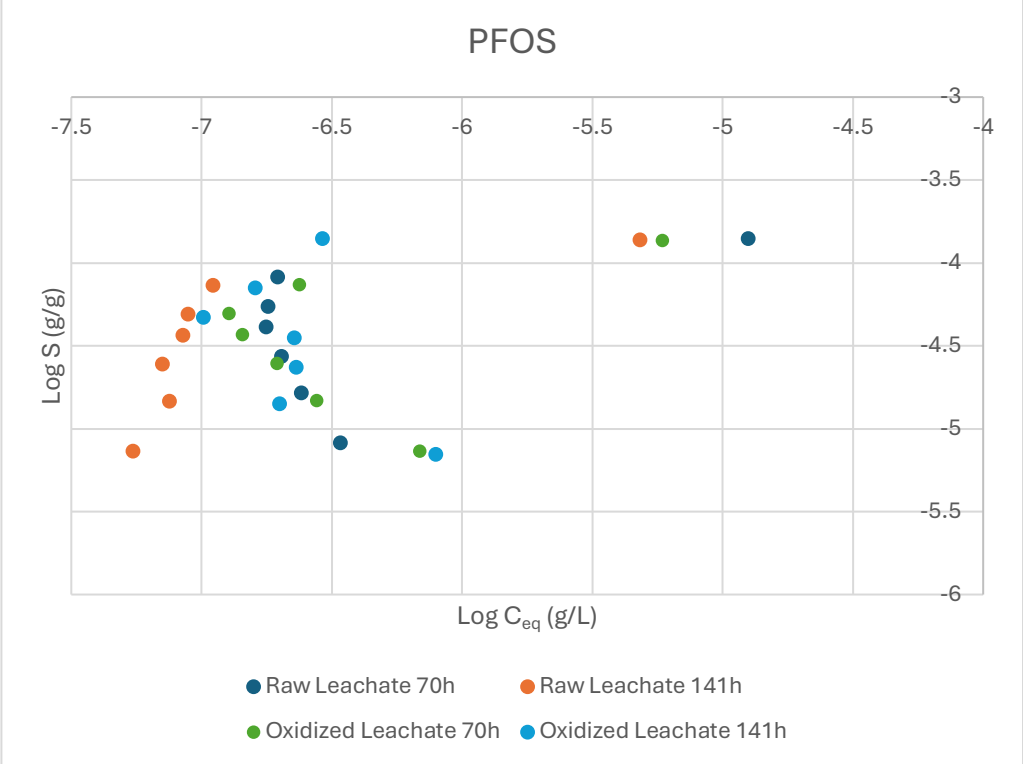

Figure 41. Log-Log PFOS adsorption plot under competitive conditions (Carbopur 1240, 0-10 g L^{-1}; 70 h and 141 h) showing tight clustering in the ultra-low C_{eq} region and deviation from a single linear trend, indicating rapid near-depletion and the limited suitability of a single global Freundlich model for PFOS in leachate matrices.

1- For PFOS in leachate, a single global Freundlich model is not the most appropriate primary descriptor because the graphical evidence shows that the test does not represent a single monotonic adsorption regime across the full 0-10 g/L

GAC range. This limitation is fundamentally different from what was observed for PFBA, PFBS and PFOA.

In none-linear space (S vs C_{eq}), PFOS rapidly collapses into the ultra-low C_{eq} domain (0.05-0.2 µg/L) already by 1-1.5 g/L. In log-log space, this appears as a tight clustering of most points within a narrow low-C_{eq} band, and a small number of high-dose outliers that deviate upward.

2- Unlike PFBA, PFBS and PFOA, where the log-log plots show clean, nearly parallel linear trends across matrices, PFOS log-log plots display a compressed usable range and visible scatter or separation at high dose. This is direct graphical evidence that the dataset is dominated by a near-depletion regime, not by a broad equilibrium partitioning regime.

While a single Freundlich fit assumes monotonic behavior, consistent partitioning physics across the fitted range and sufficient dynamic range in C_{eq}, for PFOS in Leachate, those conditions are only satisfied in the low-dose monotonic subset of GAC (≤1-1.5 g/L). Beyond that, the log-log representation becomes dominated by ultra-low concentration sensitivity and non-idealities.

3- The unique behavior of PFOS is supported directly by the test when compared to previous molecules:

PFBA (C4 PFCA) exhibits a broad measurable equilibrium window, well-structured and stable log-log fits, and no early transition into near-depletion, indicating comparatively weaker adsorption.

PFBS (C4 PFSA) adsorbs more strongly than PFBA, consistent with a sulfonate headgroup effect, yet still maintains a sufficiently wide log-log domain before approaching near-depletion.

PFOA (C8 PFCA) shows a clear chain-length effect within the carboxylate class: equilibrium concentrations collapse at lower GAC doses than for PFBA, and the system enters a near-depletion regime more rapidly.

PFOS (C8 PFSA) The combination of both longer perfluoroalkyl chain and sulfonate headgroup, entering near-depletion at the lowest doses of all four compounds, compressing the measurable isotherm range and amplifying low-concentration sensitivity.

This study therefore supports a consistent adsorption strength hierarchy under competitive conditions:

C8 PFSA (PFOS) > C8 PFCA (PFOA) > C4 PFSA (PFBS) > C4 PFCA (PFBA), reflecting the combined influence of chain length and functional group on GAC affinity.

It is evident that due to very strong PFOS adsorption, it effectively skips the mid-isotherm region and jumps directly into a near-depletion regime, where Freundlich linearization loses resolution power.

4- In other 3 PFASs, Oxidation primarily shifted the intercept (K_f) while preserving a clean power-law structure. For PFOS, Oxidation produces more pronounced rebound in the ultra-low C_{eq} range (especially at 141 h).

This suggests that for very strong adsorbates, oxidation-driven changes in TOC character affect not just overall capacity but also the stability of the near-depletion regime. Once PFOS is pushed to extremely low concentrations, small matrix-dependent effects become visible in log-log space as curvature or deviations.

Therefore, the oxidation effect for PFOS is expressed less as a simple vertical shift (as with PFBA/PFBS) and more as instability in the ultra-low domain, which further reduces the suitability of a single Freundlich model across the full dataset.

Clean-matrix reference (PFOS standard): baseline for competition

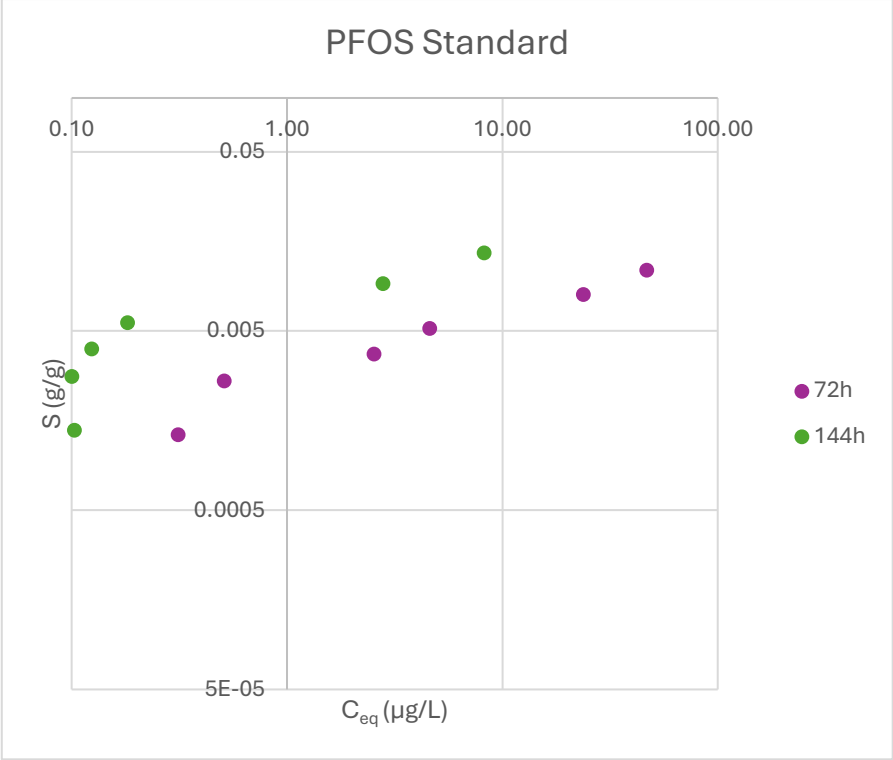

Figure 42. PFOS Standard Freundlich Isotherm at 72 h and 144 h

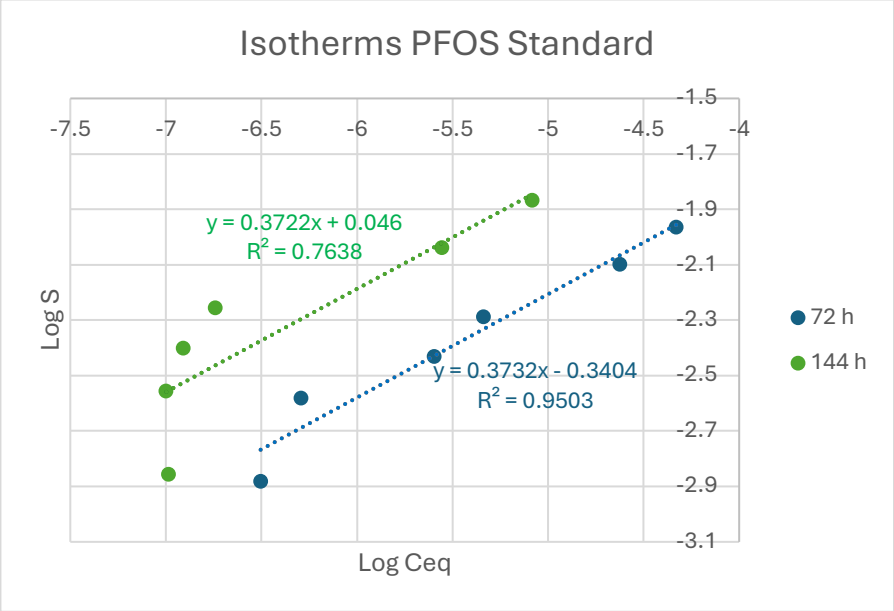

Figure 43. Linearized PFOS Standard Freundlich Isotherm at 72 h and 144 h

The PFOS standard system (0-0.2 g/L GAC) represents single-solute adsorption in the absence of dissolved organic matter and therefore defines the intrinsic adsorption behavior of PFOS on the selected GAC.

Non-linear isotherm (S vs C_{eq})

In the clean system, S increases smoothly and monotonically as C_{eq} increases across the investigated range. No early near-depletion plateau is observed within 0.02-0.2 g/L. Instead, the adsorption range remains broad, measurable C_{eq} persists across all doses and the curve exhibits a stable power-type shape without rebound or flattening.

This behavior contrasts sharply with the Leachate matrices, where PFOS enters near-depletion at ≥1 g/L and deviations appear at higher doses. The absence of any non-monotonic behavior in the standard confirms that the irregularities observed in leachate are matrix-driven, not intrinsic to PFOS adsorption characteristics.

Time effect is evident but controlled where at 144 h, S values are systematically higher than at 72 h for similar C_{eq}. This indicates continued approach to equilibrium without distortion of curve shape. The adsorption mechanism remains stable over time.

Thus, in clean water, PFOS behaves as a classical strongly adsorbing solute with predictable monotonic uptake.

Log-log Freundlich representation

From the linearized plot:

72 h: $Log\ S = 0.3732 Log\ C_{eq} - 0.3404$ $R^2 = 0.9503$

$1/n = 0.3732$, n = 2.68 and $K_f = 0.456$

144 h: $Log\ S = 0.3722\ Log\ C_{eq} + 0.046$ $R^2 = 0.7638$

$1/n = 0.3722$, n = 2.69 and $K_f = 1.11$

1- The slopes are nearly identical at both contact times (0.37). This indicates that adsorption intensity remains unchanged with time, the adsorption mechanism is consistent and PFOS adsorption exhibits moderate nonlinearity, typical of strong hydrophobic interactions with heterogeneous carbon sites.

Compared with shorter-chain PFAS (PFBA, PFBS), this lower slope reflects stronger affinity and less sensitivity to concentration changes which is consistent with the longer C8 perfluoroalkyl chain and sulfonate headgroup.

2- The intercept increases from $-0.3404\ (72\ h)\ to\ +0.046\ (144\ h)$.

This indicates that apparent adsorption capacity increases with longer contact time, no change is observed in mechanism (only progression toward equilibrium) and absence of matrix interference.

Importantly, there is no distortion of slope, no collapse of the concentration window, and no artificial near-depletion compression.

The PFOS standard system (0-0.2 g/L GAC) defines the intrinsic adsorption behavior of PFOS in the absence of dissolved organic matter or complex matrix. It therefore represents the baseline against which competitive Leachate systems must be interpreted.

Establishing the baseline for competition

The clean PFOS isotherm demonstrates:

1- Broad, stable equilibrium range.

2- Monotonic concentration decreases with increasing adsorbent.

3- Consistent Freundlich slope over time.

4- No high-dose deviations:

When compared to Raw and Oxidized Leachate matrices:

1- The compression of the measurable concentration range arises from competition and capacity dominance.

2- Apparent deviations at high GAC in leachate do not reflect a change in PFOS characteristics but rather operation in a low-concentration, competition-influenced regime. In fact, PFOS longer fluorinated chain enhances hydrophobic interactions with carbon micropores, while the sulfonate group provides strong electrostatic interaction potential. This may explain why, in Leachate matrices, PFOS reaches ultra-low C_{eq} at relatively modest GAC doses and why small measurement deviations become visible once the system approaches the analytical limit.

Thus, the PFOS standard defines the intrinsic adsorption envelope, while the leachate matrices represent constrained subsets of that envelope under competitive organic loading.

5.6 Experimental Evaluation of Three Commercial GAC Products for PFAS Adsorption in Raw Leachate

5.6.1 Characterization of the Selected Granular Activated Carbons

Three high-strength, steam-activated, coal-based granular carbons were compared: Carbopur 1240, Organosorb 10-AA, and Organosorb 10-AM. A summary of their technical specifications is given in the table below. All are granular activated carbons intended for water treatment, but they differ in surface area, pore structure, and particle size, which can influence PFAS adsorption.

Table 26. GAC Products Characterization

Property	Carbopur 1240	Organosorb 10-AA	Organosorb 10-AM
Carbon Type	Granular activated (coal)	Agglomerated GAC (coal blend)	Agglomerated GAC (coal blend)
Iodine Number (min.)	950 mg/g	900 mg/g	1100 mg/g
Particle Size	$12 \times 40\ mesh$ $(0.425 - 1.70\ mm)$	$0.425 - 1.70\ mm$	$0.60 - 2.36\ mm$
Particle Size (min)	93% $(> 0.425\ mm)$	90% $(> 0.425\ mm)$	90% $(< 2.36, > 0.60\ mm)$

Apparent Density	$490 \pm 10\ kg/m^3$	$430\ kg/m^3$	$470\ kg/m^3$
BET Surface Area	$1009\ m^2/g$	$940\ m^2/g$	$1150\ m^2/g$
Hardness (min.)	95%	93%	93%
Ash Content (max.)	15%	-	-
pH (water)	9.4	-	-

Microporosity, a key structural feature governing adsorption behavior, is commonly assessed through the iodine number and the BET specific surface area, which together provide complementary information on pore development and accessible internal surface. The three investigated carbons all exhibit high iodine numbers (>900 mg/g). Carbopur 1240 presents an iodine number of 950 mg/g and a BET surface area of 1009 m²/g, indicating a balanced and extensively developed pore network. Organosorb 10-AA shows a minimum iodine number of 900 mg/g and a BET surface area of 940 m²/g, reflecting a slightly lower but still substantial degree of microporosity. Organosorb 10-AM exhibits the highest values among the three materials, with an iodine number ≥1100 mg/g and a BET surface area of 1150 m²/g, suggesting a more intensively developed internal surface.

Particle size: Carbopur 1240 and Organosorb 10-AA have similar fine-grade sizes (0.42-1.70 mm), whereas Organosorb 10-AM's specification (0.60-2.36 mm) indicates coarser granules. Finer particles (smaller diameter) generally enhance mass transfer rates by shortening diffusion paths, while coarser particles reduce pressure drop in flow-through systems.

Density and hardness: Carbopur 1240 is denser (490 kg/m³) and slightly harder (≥95%) than the Organosorb products (430-470 kg/m³, 93% hardness). Higher density can be advantageous for fixed-bed capacity (mass per volume) but may reduce pore accessibility if correlated with micropore content.

In summary, Organosorb 10-AM exhibits the highest reported microporosity, reflected by both its iodine number (≥1100 mg/g) and BET surface area (1150 m²/g), indicating the most extensively developed internal surface among the three materials. Carbopur 1240 presents an intermediate level of porosity, with an iodine number of 950 mg/g and a BET surface area of 1009 m²/g, combined with comparatively high apparent density and mechanical hardness. Organosorb 10-AA shows slightly lower iodine number (≥900 mg/g) and BET surface area (940 m²/g),

while remaining within the range of highly microporous water-treatment carbons. Overall, the three materials differ quantitatively in internal surface development and bulk physical properties, establishing a structural basis for comparative adsorption evaluation without implying specific performance outcomes.

5.6.2 PFBA adsorption on different GAC materials under competitive Raw Leachate conditions (72 h)

The objective of this experiment was to compare the relative adsorption parameters of three different granular activated carbons (GACs) under realistic competitive conditions, where PFBA adsorption occurs in the presence of dissolved organic matter (TOC) and other matrix constituents.

Carbopur 1240 data under Raw Leachate conditions was previously presented in 70 h dataset from the Final experiment, the same values are used for comparison.

Table 27. PFBA adsorption on different GAC products

PFBA			
	72h		70 h
Conc GAC (g/L)	Concentration (ppb)		
	10-AA	10-AM	1240
0	88.9743	88.9743	90.3239
0.5	51.0115	40.7898	50.8615
1	17.4048	14.0159	17.3198
1.5	6.2159	6.3333	10.0347
2	4.2090	3.7467	5.9735
3	1.2206	1.5967	2.3808
5	0.5225	0.4922	0.7964
10	0.1624	0.1660	0.2631

At almost the same contact times, PFBA adsorption on Organosorb 10-AA, Organosorb 10-AM, and Carbopur 1240 was evaluated under identical Raw Leachate conditions, starting from comparable initial concentrations (89-90 ppb). All three carbons exhibited a consistent and monotonic decrease in PFBA concentration with increasing GAC dose, confirming effective removal under TOC competition.

Differences between materials are most evident in the low-to-intermediate dose range (0.5-3 g/L). At 0.5 g/L, Organosorb 10-AM achieved the lowest residual concentration (40.8 ppb), while 10-AA and Carbopur 1240 remained around 51

ppb. At 1 g/L, all materials converged to approximately 14-17 ppb, indicating similar adsorption behavior at this loading. Between 2 and 3 g/L, residual concentrations further decreased to the low single-digit ppb range, with slight variations among materials but no consistent large separation. At higher doses (5-10 g/L), PFBA approached near-depletion for all carbons (0.16-0.80 ppb), and differences became negligible.

Overall, the dataset shows that while TOC competition governs the adsorption regime, measurable but moderate performance differences exist among the three GAC products, particularly in the low-dose operational range where adsorption sites are limited and competitive effects are strongest.

Freundlich Isotherm representation

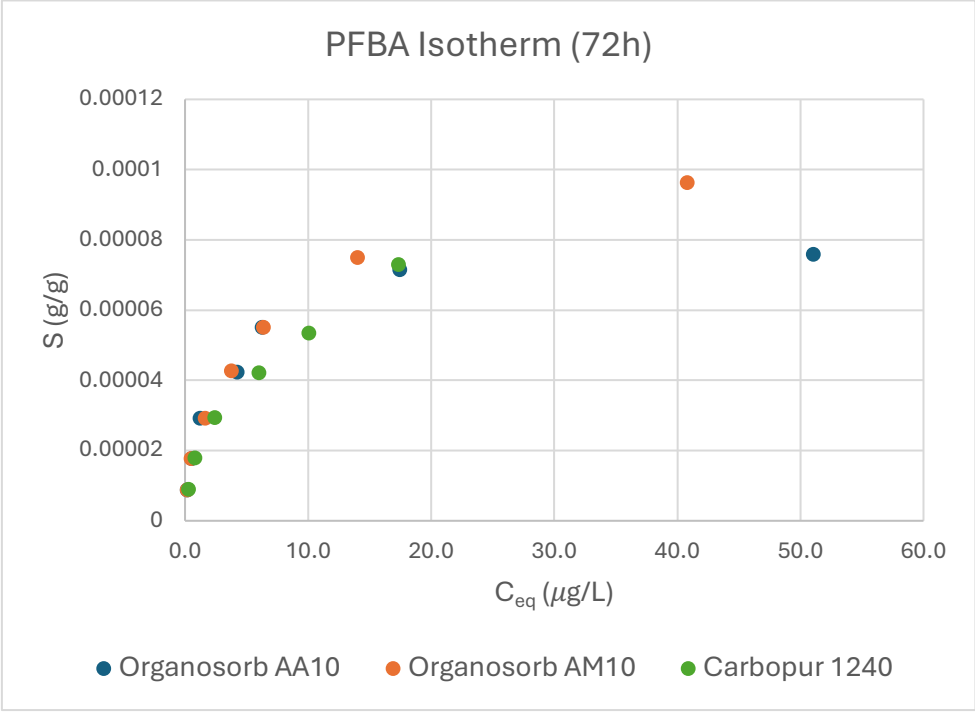

Figure 44. PFBA non-linear isotherms (72 h, raw leachate) comparing Organosorb 10-AA, Organosorb 10-AM, and Carbopur 1240 (0-10 g L^{-1}). Organosorb 10-AM shows the highest sorbed loadings across the equilibrium range, followed by 10-AA, while Carbopur 1240 exhibits comparatively lower uptake.

Under competitive Raw Leachate conditions, the non-linear PFBA isotherms demonstrate clear performance differentiation among the tested GAC materials. Organosorb 10-AM consistently exhibits the highest sorbed amounts (*S*) across the

equilibrium range, indicating the strongest adsorption activity under TOC competition. Organosorb 10-AA shows slightly lower but comparable uptake, while Carbopur 1240 generally presents reduced loading, particularly in the intermediate concentration region. The overall isotherm shapes confirm that adsorption efficiency follows the order Organosorb 10-AM > Organosorb 10-AA > Carbopur 1240, reflecting intrinsic material differences in PFBA affinity within a complex matrix.

Log-log Freundlich representation and parameter comparison

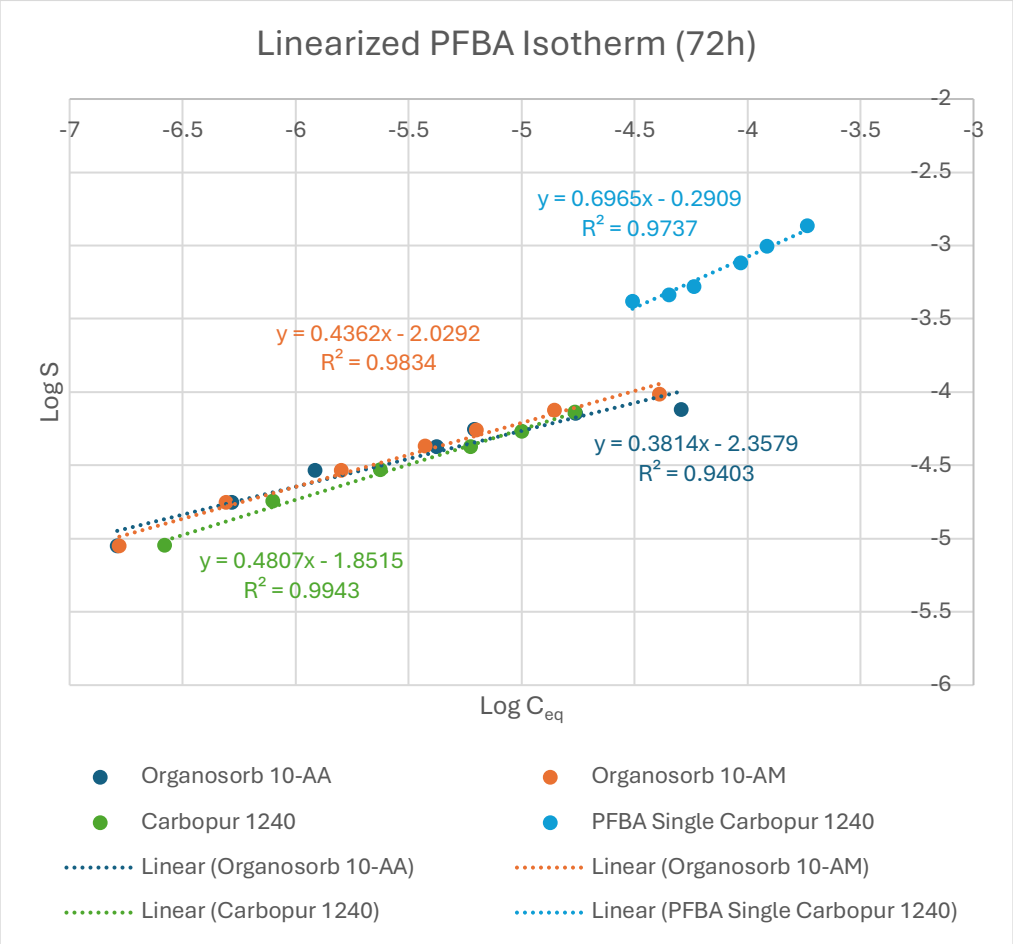

Figure 45. Log-Log (linearized) PFBA Freundlich isotherms (72 h, raw leachate) comparing Organosorb 10-AA, Organosorb 10-AM, Carbopur 1240, and the PFBA standard. Differences in intercept (K_f) highlight material-dependent adsorption capacity under competitive conditions across GAC products.

The linearized Freundlich fits provide a quantitative framework for comparing competitive adsorption performance.

Table 28. PFBA Linearized Freundlich isotherm parameters

	$1/n$	n	$Log\ K_f$	K_f
Organosorb 10-AA	0.3814	2.62	−2.3579	0.0044
Oragnosorb 10-AM	0.4362	2.29	−2.0292	0.0094
Carbopur 1240	0.4807	2.08	−1.8515	0.0141
Single PFBA Carbopur 1240	0.6965	1.44	−0.2909	0.51

The dominant observation is the drastic reduction of K_f from approximately 0.51 in the reference system to values between 0.004 and 0.014 in Raw Leachate, corresponding to roughly two orders of magnitude lower apparent affinity/capacity under competition. This quantitatively demonstrates that TOC strongly suppresses PFBA adsorption across all carbons.

However, within this competitive regime, the GACs remain distinguishable. Carbopur 1240 exhibits the highest apparent K_f among the three materials in leachate, indicating the greatest effective PFBA uptake under TOC competition. Organosorb 10-AM performs intermediately, while Organosorb 10-AA shows the lowest KF. The ranking in terms of competitive adsorption efficiency at 72 h is therefore: Carbopur 1240 > Organosorb 10-AM > Organosorb 10-AA

The slope parameter ($1/n$) also increases progressively from 10-AA (0.3814) to 1240 (0.4807), suggesting that Carbopur 1240 exhibits slightly stronger concentration sensitivity and a more favorable adsorption intensity in the competitive domain. Nevertheless, all competitive slopes remain significantly lower than that of the clean reference (0.6965), indicating that adsorption heterogeneity and site blocking effects are enhanced in the presence of dissolved organic matter.

One important takeaway could be that under competitive Raw leachate conditions (72 h), the non-linear PFBA isotherms show only moderate separation among the three GAC materials, with Organosorb 10-AM displaying slightly higher sorbed amounts in parts of the intermediate equilibrium range. However, evaluation

through the linearized Freundlich parameters provides a more integrated comparison over the entire fitted domain. The calculated capacity constants follow the order Carbopur 1240 (K_f = 1.41 × 10^{-2}) > Organosorb 10-AM (K_f = 9.36 × 10^{-3}) > Organosorb 10-AA (K_f = 4.39 × 10^{-3}), indicating that Carbopur 1240 exhibits the highest overall apparent adsorption affinity for PFBA under TOC competition when considering the complete concentration range. The apparent discrepancy between local non-linear trends and global Freundlich parameters reflects the difference between pointwise visual comparison and model-based integration of the adsorption domain.

In the end, when assessed quantitatively, competitive adsorption efficiency follows the order Carbopur 1240 > Organosorb 10-AM > Organosorb 10-AA at 72 h.

5.6.3 PFBS adsorption on different GAC materials under competitive Raw Leachate conditions (72 h)

The performance of Organosorb 10-AA, Organosorb 10-AM, and Carbopur 1240 was evaluated for PFBS removal in Raw Leachate at 72 h in order to directly compare their adsorption efficiency under competitive TOC conditions.

Table 29. PFBS adsorption on different GAC products

PFBS			
	72h		70h
Conc GAC (g/L)	Concentration (ppb)		
	AA10	AM10	1240
0	81.8287	81.8287	71.5594
0.5	7.1101	16.9336	17.9830
1	1.0192	1.9028	1.5554
1.5	0.2336	0.5575	0.7723
2	0.1290	0.1907	0.4209
3	0.0392	0.0977	0.1170
5	0.0178	0.0267	0.0342
10	0.0101	0.0066	0.0039

Freundlich Isotherm representation

All three carbons achieved substantial PFBS reduction; however, differences in adsorption behavior became evident when equilibrium concentrations and sorbed amounts were examined. Organosorb 10-AA consistently reached lower equilibrium concentrations at comparable sorbed loadings, indicating superior removal efficiency in the presence of dissolved organic matter. Organosorb 10-AM exhibited intermediate behavior, while Carbopur 1240 generally maintained slightly higher residual PFBS concentrations within the same adsorption regime.

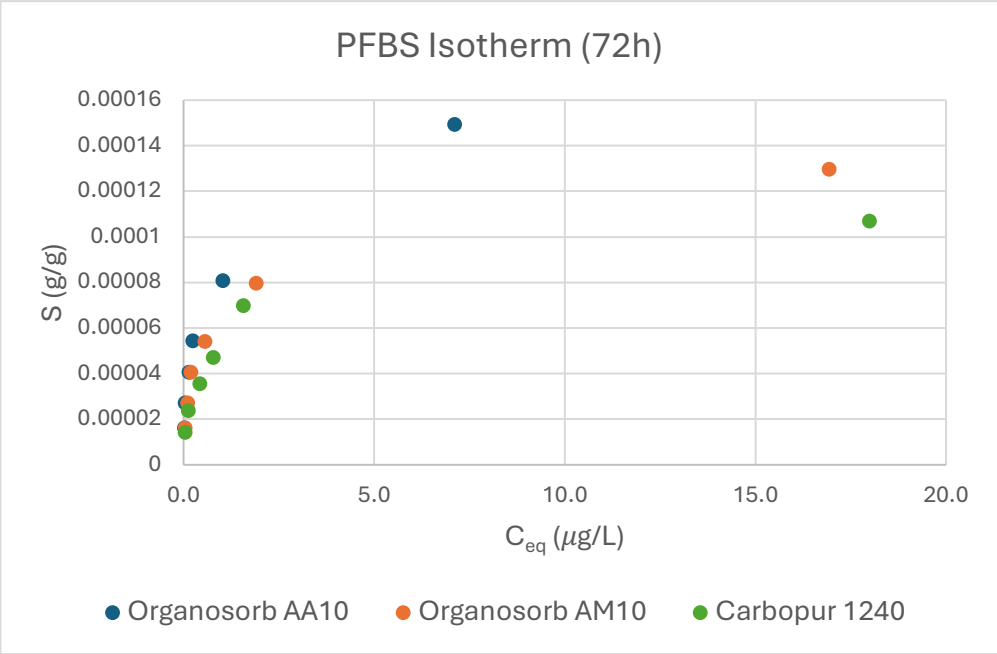

Figure 46. PFBS non-linear adsorption isotherms (72 h, raw leachate) comparing Organosorb 10-AA, Organosorb 10-AM, and Carbopur 1240 (0-10 g L^{-1}). Organosorb 10-AA shows the most favorable positioning (higher S at lower C_{eq}), followed by 10-AM, while Carbopur 1240 exhibits comparatively lower uptake.

The non-linear S versus C_{eq} isotherms reveal clear but moderate separation between the GACs. Organosorb 10-AA displays the most favorable isotherm position, achieving greater sorbed mass at lower equilibrium concentrations across most of the measurable range. Organosorb 10-AM follows a similar trend but remains slightly shifted toward higher C_{eq} values, while Carbopur 1240 shows the least favorable positioning among the three, particularly in the intermediate concentration region.

Log-log Freundlich representation and parameter comparison

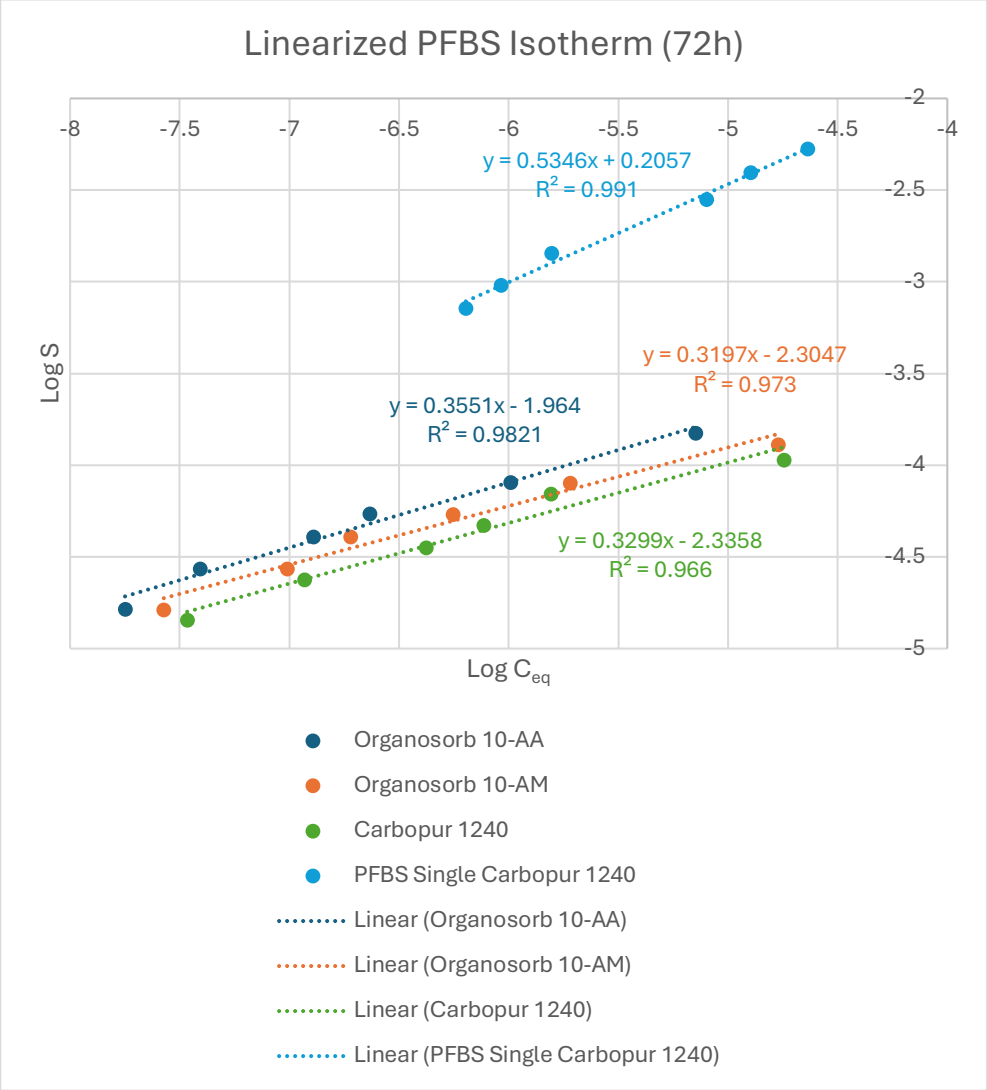

Figure 47. Log–log (linearized) PFBS Freundlich isotherms (72 h, raw leachate) comparing Organosorb 10-AA, Organosorb 10-AM, Carbopur 1240, and the PFBS single-solute reference. Organosorb 10-AA exhibits the highest K_f under competitive conditions, followed by Carbopur 1240 and Organosorb 10-AM.

The linearized Freundlich fits provide a quantitative framework for comparing competitive adsorption performance.

Table.30 PFBS Linearized Freundlich isotherm parameters

	$1/n$	n	$Log\ K_f$	K_f
Organosorb 10-AA	0.3551	2.82	-1.964	1.09×10^{-2}

Oragnosorb 10-AM	0.3197	3.13	-2.3047	4.95×10^{-3}
Carbopur 1240	0.3299	3.03	-2.3358	4.61×10^{-3}
Single PFBS Carbopur 1240	0.5346	1.87	0.2057	1.61

The slope values ($1/n$ = 0.32-0.36) are relatively similar, indicating comparable adsorption intensity and surface heterogeneity across materials. The main differentiation arises from the capacity constant (K_f), where Organosorb 10-AA shows approximately twice the apparent affinity of the other two carbons under competitive conditions. Organosorb 10-AM and Carbopur 1240 exhibit nearly identical K_f values, suggesting similar effective performance in this matrix.

Within the Raw Leachate matrix, where PFBS adsorption occurs under strong dissolved organic matter (DOM) competition, differences in performance among the carbons can be interpreted considering both adsorbent structure and PFBS molecular properties. PFBS (C4 perfluorobutane sulfonate) is a short-chain perfluorosulfonic acid characterized by a relatively small hydrophobic tail and a strongly acidic sulfonate headgroup. Compared with long-chain PFAS, its adsorption relies more critically on accessible microporosity and surface chemistry rather than purely on hydrophobic interactions.

Organosorb 10-AA, despite having a slightly lower iodine number (900 mg/g) and BET surface area (940 m²/g) than 10-AM (1100 mg/g; 1150 m²/g), demonstrates the highest competitive adsorption efficiency. This suggests that its pore size distribution (0.425-1.70 mm particle class with controlled lower size fraction) and potentially more favorable micropore accessibility provide effective confinement for short-chain PFBS molecules under TOC competition.

In contrast, Organosorb 10-AM, although exhibiting the highest theoretical surface area, may possess a pore structure with a greater contribution of larger pores that are more susceptible to TOC co-adsorption and competitive blocking.

Carbopur 1240, with intermediate BET (1009 m²/g) but higher apparent density (490 kg/m³) and coal-based granular structure, shows comparable but slightly lower effective affinity, possibly reflecting differences in internal pore accessibility and surface heterogeneity. Because the Freundlich slopes remain similar across materials, the governing mechanism appears consistent, and the observed separation is primarily capacity related.

Overall, the results indicate that for short-chain sulfonated PFAS such as PFBS, competitive adsorption efficiency in complex leachate systems is controlled less by total surface area alone and more by the effective accessibility and stability of microporous domains under organic matrix competition.

5.6.4 PFOA adsorption on different GAC materials under competitive Raw Leachate conditions (72 h)

The equilibrium concentration trends for Organosorb 10-AA, Organosorb 10-AM, and Carbopur 1240 indicate a consistent reduction in aqueous PFOA across all materials under competitive raw leachate conditions. However, the rate and pattern of this reduction differ among the carbons.

Table 31. PFOA adsorption on different GAC products

PFOA			
	72h		70h
Conc GAC (g/L)	Concentration (ppb)		
	AA10	AM10	1240
0	49.2047	49.2047	58.8634
0.5	2.4122	9.7253	14.7259
1	0.1218	0.7730	0.5694
1.5	0.0318	0.1456	0.2098
2	0.0242	0.0511	0.0976
3	0.0062	0.0289	0.0173
5	0.0129	0.0083	0.0016
10	0.0327	0.0062	0.0037

Organosorb 10-AA exhibits a more pronounced early decrease in equilibrium concentration, suggesting stronger initial uptake in the low-to-intermediate region. Organosorb 10-AM follows a more gradual trajectory, with equilibrium concentrations declining steadily but remaining comparatively higher over part of the concentration range. Carbopur 1240 shows a similar progressive decrease but with a tendency toward higher residual concentrations at comparable stages of the adsorption sequence.

The divergence between the three materials becomes most evident in the mid-region of the dataset, where adsorption proceeds under active TOC competition and surface sites are not yet fully saturated.

Freundlich Isotherm representation

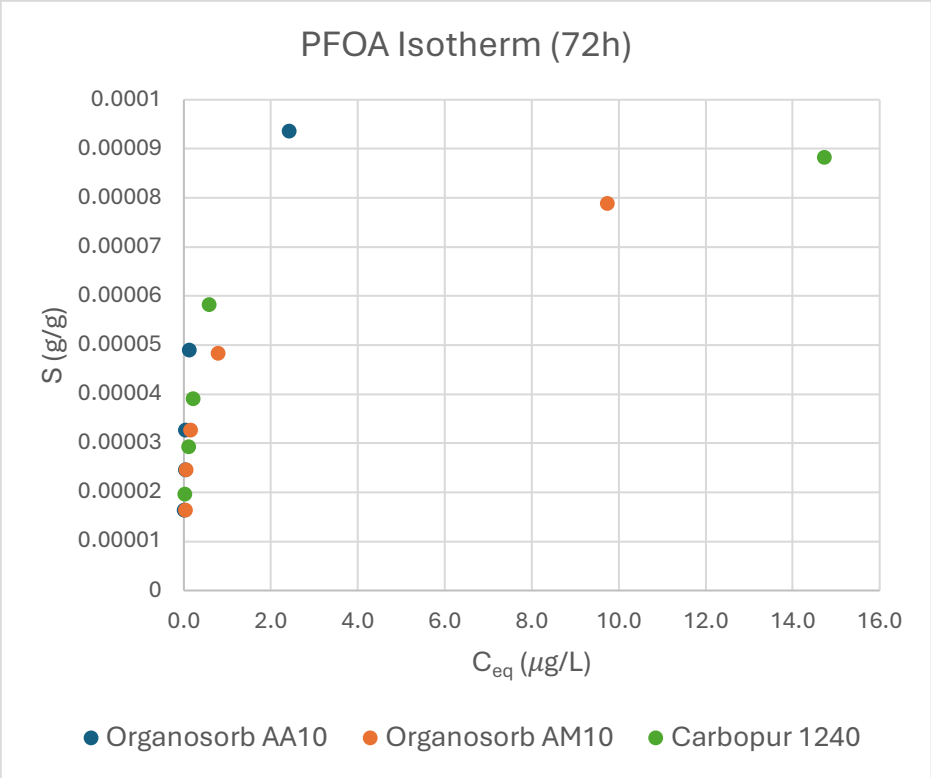

Figure 48. PFOA non-linear adsorption isotherms (72 h, raw leachate) comparing Organosorb 10-AA, Organosorb 10-AM, and Carbopur 1240 (0-10 g L^{-1}). Organosorb 10-AA shows the most favorable low-C_{eq} positioning and steep initial uptake, while 10-AM and Carbopur 1240 exhibit slightly higher residual concentrations.

The non-linear S vs C_{eq} representation confirms that PFOA adsorption remains favorable across all materials, but with distinct curvature and position shifts. Organosorb 10-AA demonstrates the steepest initial uptake and the lowest equilibrium concentrations in the low-C_{eq} region, indicating high accessible microporosity effective for long-chain PFCA uptake.

Organosorb 10-AM, despite having the highest BET surface area (1150 m^2/g) and iodine number (1100 mg/g), does not outperform 10-AA under competitive leachate conditions. This suggests that total surface area alone does not dictate performance, and that pore accessibility and effective micropore distribution under TOC competition are critical.

Carbopur 1240, although possessing a relatively high BET surface area (1009 m^2/g) and iodine number (950 mg/g), displays slightly higher residual concentrations at comparable S values. This may reflect differences in pore architecture and accessibility under complex matrix conditions.

Log-log Freundlich representation and parameter comparison

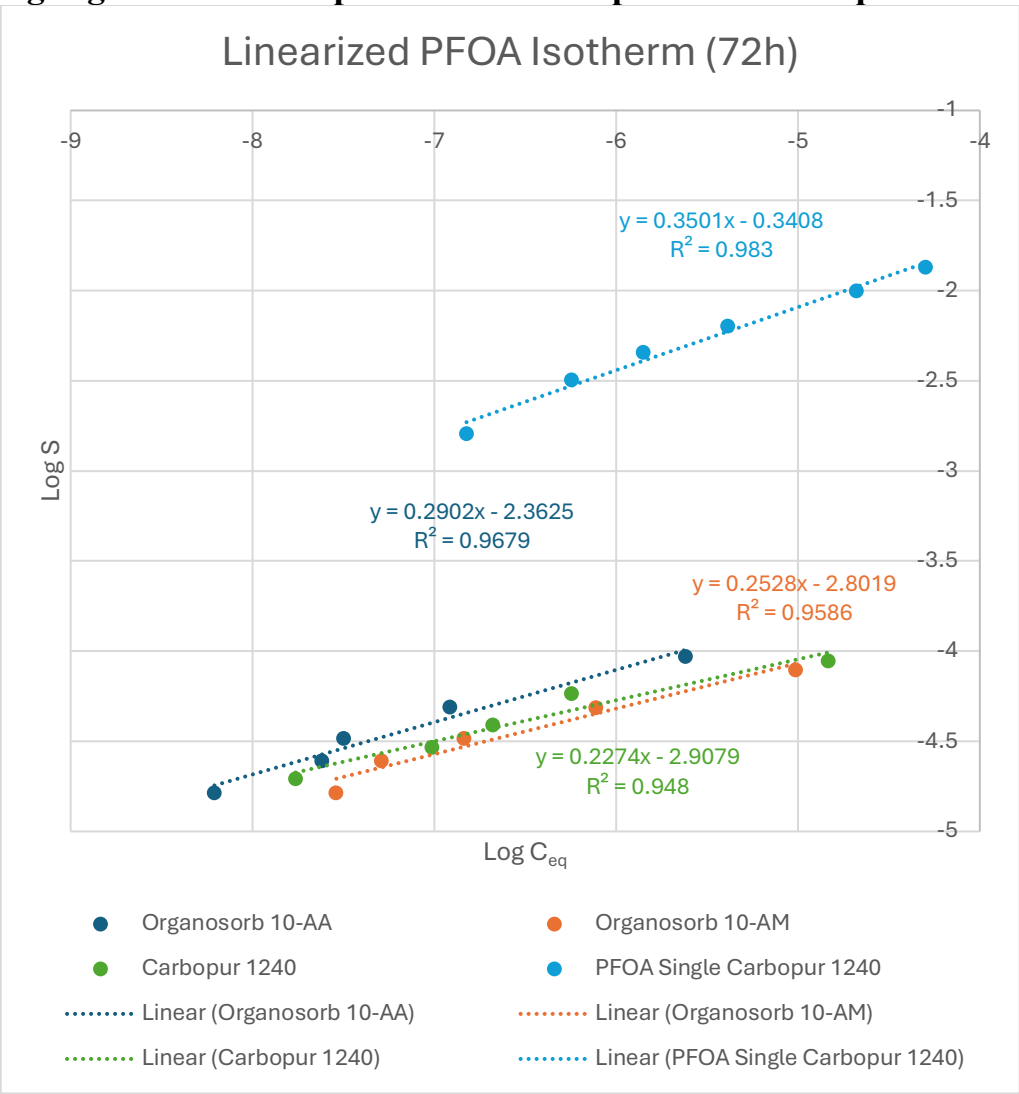

Figure 49. Log–log (linearized) PFOA Freundlich isotherms (72 h, raw leachate) comparing Organosorb 10-AA, Organosorb 10-AM, Carbopur 1240, and the PFOA single-solute reference. Organosorb 10-AA exhibits the highest K_f under competitive conditions, followed by 10-AM and Carbopur 1240.

The linearized Freundlich fits provide a quantitative framework for comparing competitive adsorption performance.

Table 32. PFBS Linearized Freundlich isotherm parameters

	$1/n$	n	$Log\ K_f$	K_f
Organosorb 10-AA	0.2902	3.45	-2.3625	4.34×10^{-3}
Oragnosorb 10-AM	0.2528	3.96	-2.8019	1.58×10^{-3}
Carbopur 1240	0.2274	4.40	-2.9079	1.24×10^{-3}
Single PFBS Carbopur 1240	0.5346	1.87	0.2057	1.61

The slopes $(1/n)$ are of similar magnitude, indicating that the adsorption mechanism and surface heterogeneity remain comparable across materials. The primary difference lies in the intercept K_f, which ranks:

Organosorb 10-AA > Organosorb 10-AM > Carbopur 1240

Thus, performance differences are governed predominantly by effective adsorption capacity under competitive conditions rather than mechanistic differences.

PFOA (C8 PFCA) possesses a longer hydrophobic perfluoroalkyl chain than PFBA and PFBS, increasing its hydrophobic interaction with carbon surfaces. Under Raw Leachate conditions, where TOC competes for adsorption sites, carbon-specific structural properties determine competitive efficiency.

Despite Organosorb 10-AM having the highest nominal BET surface area and iodine number, Organosorb 10-AA demonstrates the highest effective Freundlich capacity (K_f) under matrix conditions. This indicates that accessible micropore structure and pore size distribution, rather than total surface area alone, govern competitive PFOA uptake. Carbopur 1240, while structurally robust and possessing substantial surface area, shows comparatively lower effective affinity in the competitive matrix.

Overall, under realistic leachate conditions at 72 h, Organosorb 10-AA exhibits the most favorable adsorption efficiency for PFOA, followed by Organosorb 10-AM and Carbopur 1240. The separation between materials is driven primarily by effective capacity and resistance to TOC suppression rather than differences in adsorption mechanism.

5.6.5 PFOS adsorption on different GAC materials under competitive Raw Leachate conditions (72 h)

The equilibrium concentration trends for Organosorb 10-AA, Organosorb 10-AM, and Carbopur 1240 show a markedly different adsorption pattern compared with the shorter-chain PFAS. While all three materials demonstrate substantial PFOS removal at low equilibrium concentrations, the dataset reveals non-monotonic behavior at higher sorbent levels, particularly for Organosorb 10-AA and Carbopur 1240.

Table 33. PFOS adsorption on different GAC products

PFOS			
	72h		70h
Conc GAC (g/L)	Concentration (ppb)		
	AA10	AM10	1240
0	90.5129	90.5129	82.5001
0.5	-0.4805	8.9758	12.5340
1	0.3159	0.5127	0.1962
1.5	0.3568	0.3255	0.1803
2	0.4283	0.3509	0.1770
3	0.3912	0.4583	0.2030
5	0.3986	0.4509	0.2417
10	0.9725	0.3818	0.3415

Organosorb 10-AM exhibits a relatively consistent suppression of equilibrium concentration across the range, whereas Organosorb 10-AA shows stronger reduction at low levels but greater variability at higher conditions. Carbopur 1240 demonstrates effective initial removal but displays a more pronounced increase in equilibrium concentration in the upper region of the dataset.

These patterns suggest that, for PFOS, adsorption is extremely strong in the initial uptake phase but becomes sensitive to matrix effects and possible measurement limitations once near-depletion conditions are approached. The divergence between materials is therefore less linear and more influenced by high-affinity site saturation and competitive interactions with dissolved organic matter.

Freundlich Isotherm representation

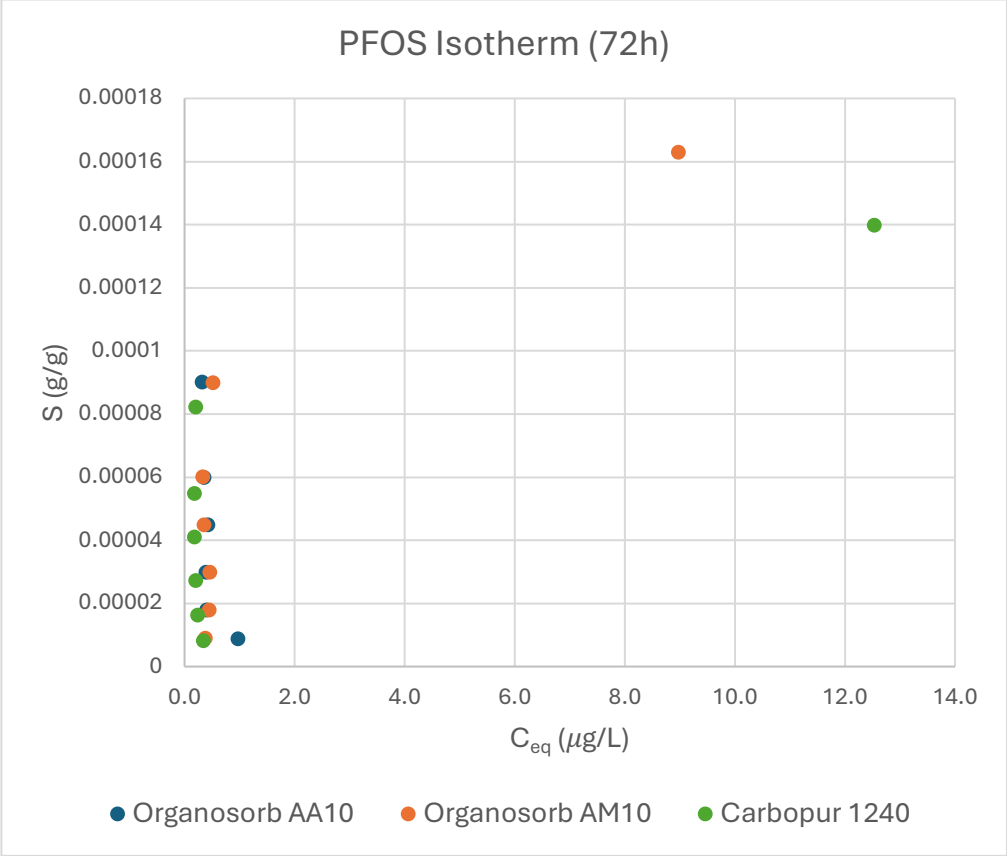

Figure 50. PFOS non-linear adsorption isotherms (72 h, raw leachate) comparing Organosorb 10-AA, Organosorb 10-AM, and Carbopur 1240 (0-10 g L^{-1}). All materials exhibit very steep initial uptake and rapid transition to near-depletion, reflecting the strong affinity of long-chain PFOS (C8 PFSA); differences between carbons become more visible only at higher C_{eq}.

The non-linear S vs C_{eq} plots show very steep initial uptakes for all three carbons, consistent with the long-chain structure of PFOS (C8 PFSA) and its strong hydrophobic interaction with activated carbon surfaces. Compared with PFBA and PFBS, PFOS enters the near-depletion regime at much lower equilibrium concentrations.

Organosorb 10-AM maintains relatively stable adsorption progression, whereas Organosorb 10-AA and Carbopur 1240 display visible dispersion at higher equilibrium values. This behavior indicates that once PFOS concentrations approach the lower analytical limit, small variations in measured C_{eq} can produce amplified differences in calculated S, especially under competitive leachate conditions.

Unlike shorter-chain compounds, PFOS adsorption appears to approach high-affinity saturation rapidly, and the isotherm shape reflects strong initial sorption followed by increased sensitivity to matrix interference.

Log-log Freundlich representation and parameter comparison

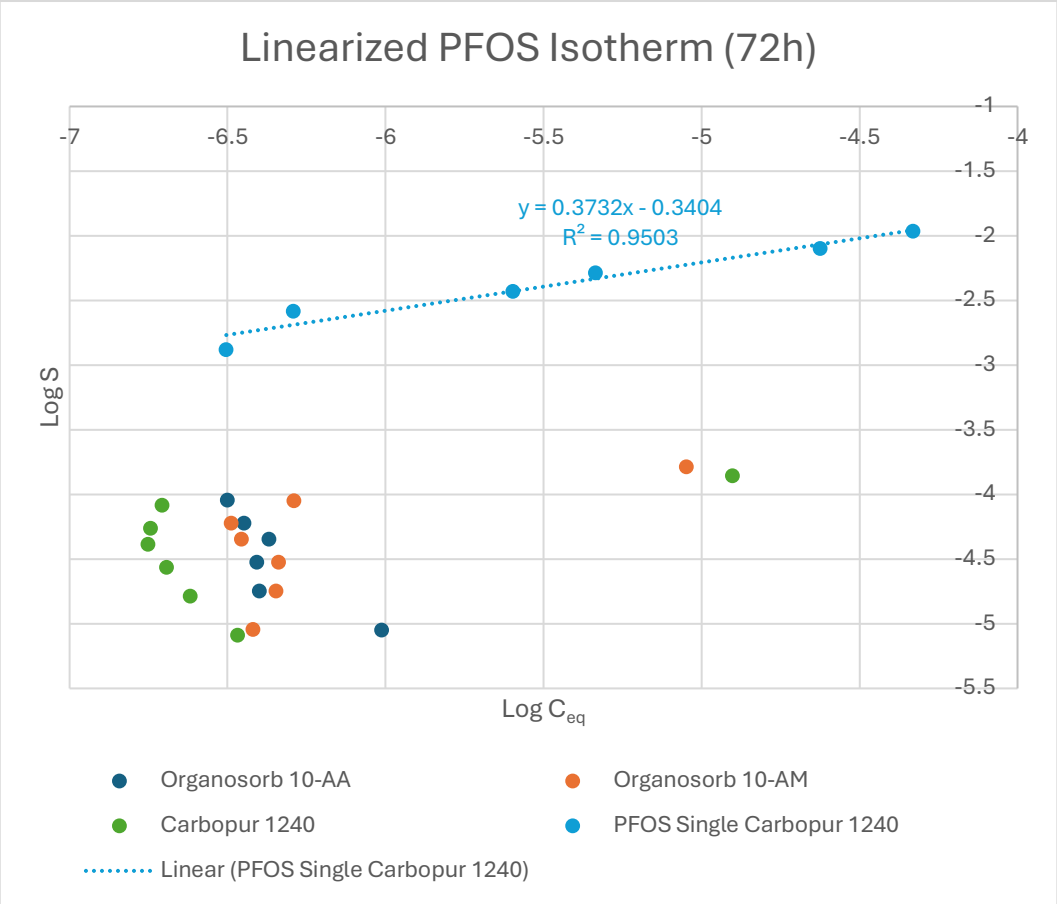

Figure 51. Log-Log (linearized) PFOS adsorption plots (72 h, raw leachate) comparing Organosorb 10-AA, Organosorb 10-AM, Carbopur 1240, and the PFOS single-solute reference. The strong clustering of leachate data within a narrow low-C_{eq} range and the absence of a well-defined linear domain.

The linearized representation shows considerably greater dispersion compared with PFBA, PFBS, and PFOA. The clustering of most points within a narrow low-C_{eq} range reduces the effective dynamic range for reliable regression fitting. In contrast to shorter-chain PFAS, the PFOS log-log plots do not form a clearly

distributed linear domains for all materials. Therefore, while a Freundlich fit can be mathematically produced, it does not serve as the primary descriptor for PFOS behavior under these matrix conditions.

PFOS (C8 PFSA) possesses both a long perfluoroalkyl chain and a sulfonate functional group, resulting in stronger hydrophobic and electrostatic interactions with activated carbon compared with PFBA and PFBS. This structural characteristic explains the very steep initial adsorption and rapid entry into the near-depletion regime for all three carbons.

Under Raw Leachate conditions, differences between Organosorb 10-AA, Organosorb 10-AM, and Carbopur 1240 become less governed by classical Freundlich behavior and more influenced by high-affinity site accessibility and resistance to competitive suppression. Organosorb 10-AM exhibits comparatively stable performance across the tested range, suggesting favorable pore accessibility under matrix competition. Organosorb 10-AA demonstrates strong initial uptake but increased variability at higher levels, while Carbopur 1240 shows effective early removal but greater sensitivity in the upper region of the dataset.

Overall, PFOS adsorption in complex leachate conditions is dominated by very high affinity and rapid saturation behavior. Material-specific structural differences influence stability and consistency of removal, but the dominant controlling factor is the inherent strong adsorption tendency of PFOS itself, which reduces the discriminative power between carbons once near-depletion conditions are reached.

Chapter 6

General Conclusions and Future Research Directions

6.1. Integrated Synthesis of Research Objectives and Scientific Context

This thesis has investigated the occurrence, transport behavior, and adsorption removal of selected per- and polyfluoroalkyl substances (PFAS): PFBA, PFBS, PFOA, and PFOS, in a landfill leachate system and associated groundwater environment. The research was structured to progress from environmental characterization to controlled adsorption experiments under increasingly realistic competitive conditions. By integrating hydrochemical assessment, PFAS distribution analysis, TOC competition evaluation, solvent mass-balance verification, isotherm modeling, and comparative granular activated carbon (GAC) performance testing, the work provides a mechanistically coherent and environmentally relevant understanding of PFAS behavior in complex matrices.

The central scientific premise guiding this research is that adsorption performance cannot be meaningfully interpreted without reference to source dynamics, hydrochemical boundary conditions, and competitive organic background. Accordingly, this final chapter synthesizes site characterization and treatment investigation into a unified interpretation framework.

6.2. Hydrochemical Characterization and PFAS Occurrence

6.2.1. Source-Pathway Context

The characterization campaigns conducted in April 2025 and January 2026 establish the environmental baseline for the study. The landfill leachate, collected from tanks C1+C2+C3, represents the primary PFAS source. Groundwater was monitored upstream (PZ38) and downstream (PZ3TER), allowing evaluation of spatial gradients along the flow path.

Across both campaigns, PFAS concentrations in groundwater remained orders of magnitude lower than those measured in leachate, confirming significant attenuation between source and monitoring wells. Nevertheless, consistent detection of short-chain PFAS and replacement compounds demonstrates incomplete natural attenuation and sustained subsurface transport.

6.2.2. Temporal Variability and Leachate Production

A pronounced temporal contrast was observed between April and January. April corresponded to a high leachate generation period (2,171.6 t), whereas January represented a low-production regime (257.5 t), an approximately 8.4-fold reduction in throughput.

This operational shift was reflected in groundwater chemistry. In April 2025, detected ΣPFAS values were approximately 30.3 ng L^{-1} (PZ38) and 37.9 ng L^{-1} (PZ3TER). In January 2026, concentrations decreased to approximately 12.6 and 13.1 ng L^{-1}, respectively. The 2 to 3-fold reduction in ΣPFAS, although smaller than the production change, is directionally consistent with decreased source forcing. This non-proportional response indicates aquifer buffering effects, including storage, retardation, and mixing.

Chloride and sulfate concentrations exhibited substantial decreases from 2025 to 2026. As conservative tracers, their parallel evolution supports the interpretation that PFAS transport is coupled to leachate loading intensity and hydrodynamic forcing.

6.2.3. Spatial Gradients

A conditional downstream enrichment pattern was observed. In April 2025, ΣPFAS increased by approximately 25% from upstream to downstream, driven largely by highly mobile short-chain PFAS (e.g., PFBA). In January 2026, the gradient largely collapsed (4% difference), indicating that under low-loading conditions dilution and dispersion dominate overactive source-driven amplification.

6.2.4. Chain-Length Distribution

Across both leachate and groundwater, short-chain PFAS (C4-C6) and replacement compounds (e.g., C6O4) dominated the detected profile. Their persistent detection downstream confirms higher mobility and lower retardation relative to long-chain homologues.

Long-chain PFAS (e.g., PFOS) were detected at lower relative groundwater contributions compared with leachate, consistent with stronger sorption and attenuation.

Collectively, the characterization results define the environmental boundary conditions within which adsorption treatment must operate sustained TOC presence, dynamic source forcing, and dominance of mobile short-chain PFAS fractions.

6.3. Role of TOC and Competitive Boundary Conditions

A central outcome of this study is the explicit demonstration that PFAS adsorption in landfill leachate cannot be interpreted independently of the prevailing TOC regime. Across screening and final experiments, equilibrium TOC concentrations remained in the order of 10^2 mg L^{-1} within the applied GAC dose window, confirming that adsorption occurred under continuous TOC competition rather than in a low-organic or clean-water regime.

The non-linear TOC isotherms did not conform to classical single-solute Freundlich behavior. This observation is consistent with established adsorption theory: Freundlich modeling assumes a single adsorbate interacting with a heterogeneous distribution of surface energies, whereas TOC in landfill leachate represents a complex mixture of humic substances, fulvic fractions, low-molecular-weight acids, and hydrophilic compounds. Consequently, the observed $S - C_{eq}$ relationships reflect superimposed adsorption behaviors rather than a single thermodynamic partitioning process.

Furthermore, the oxidized leachate exhibited a flatter C_{eq} response across increasing GAC doses compared with raw leachate. This indicates that the Oxidized TOC was less dose-responsive within the tested range, suggesting altered molecular size distribution or increased hydrophilicity following oxidative treatment. The implication is that adsorption boundary conditions differ between raw and oxidized matrices, and PFAS removal must be interpreted relative to these matrix-specific competitive baselines.

These findings reinforce a concept in adsorption science: TOC can suppress micropore accessibility and compete for high-energy adsorption sites, thereby reducing apparent PFAS capacity. The present work experimentally confirms this phenomenon within a real leachate system and quantifies its influence across multiple PFAS.

6.4. Quantification and Verification of Solvent-Derived TOC Contribution

An important methodological clarification emerged during the investigation of unexpectedly elevated TOC concentrations in PFAS-spiked systems. The mixed PFAS working stock contained 10% (v/v) methanol, and its constant 0.4% (v/v) addition resulted in a final methanol fraction of 0.04% (v/v) in all reactors. Stoichiometric calculation demonstrated that this methanol addition corresponds to approximately 118 mg C L^{-1} TOC.

Experimental verification controls confirmed this theoretical value. DIW + methanol and DIW + PFAS working stock yielded TOC concentrations of 140 and 146 mg L^{-1}, respectively. The negligible difference between these controls demonstrates that the dominant TOC contribution originated from methanol, not PFAS carbon. When combined with the intrinsic diluted leachate TOC (~40 mg L^{-1}), the resulting TOC levels align with the experimentally observed 10^2 mg L^{-1} range.

This validation was essential for preserving internal quantitative coherence. It ensures that adsorption results are interpreted as PFAS removal occurring under a controlled and quantified competitive TOC background. The study therefore demonstrates rigorous mass balance consistency and eliminates ambiguity regarding TOC anomalies.

6.5. Influence of PFAS Molecular Structure on Adsorption Behavior

A systematic molecular hierarchy emerged across all experimental conditions:
PFBA (C4 PFCA): weakest adsorption
PFBS (C4 PFSA): stronger than PFBA
PFOA (C8 PFCA): significantly stronger
PFOS (C8 PFSA): strongest adsorption

Chain Length Effect

Increasing perfluoroalkyl chain length markedly enhanced adsorption affinity. This trend is consistent with established hydrophobic partitioning theory: longer fluorinated chains increase van der Waals interactions and hydrophobic driving forces for micropore adsorption. The present data demonstrate that C8 compounds (PFOA, PFOS) entered near-depletion regimes at lower GAC doses relative to C4 compounds (PFBA, PFBS).

Functional Group Effect

For equivalent chain length, sulfonates exhibited stronger adsorption than carboxylates (PFBS > PFBA; PFOS > PFOA). This is consistent with literature demonstrating stronger electrostatic and specific interactions of sulfonate groups with carbon surfaces, as well as reduced desorption tendencies relative to carboxylates.

Importantly, these structural effects remained evident even under competitive DOM conditions, confirming that molecular-level interactions remain operative despite multi-solute interference.

6.6. Interpretation of Freundlich Modeling Across PFAS

For PFBA, PFBS, and PFOA, log-log Freundlich linearization produced coherent slopes ($1/n$) and interpretable intercepts (K_f). Differences between carbons were primarily reflected in capacity constants rather than in slope variations, indicating that adsorption mechanisms remained consistent while effective capacity varied under competition.

PFOS displayed distinct behavior. Due to its extremely strong adsorption, equilibrium concentrations were compressed into a narrow low-concentration window. Under such near-depletion conditions, Freundlich linearization becomes less descriptive, as small analytical deviations in C_{eq} generate disproportionate effects in log-log space. This deviation does not indicate mechanistic inconsistency but rather reflects high-affinity saturation dynamics.

Thus, the Freundlich model remains appropriate for short- and mid-chain PFAS within measurable equilibrium domains but becomes limited for very strongly adsorbing compounds approaching analytical detection limits.

6.7. Comparative Evaluation of GAC Materials

Three GAC materials were evaluated: Organosorb 10-AA, Organosorb 10-AM, and Carbopur 1240. Although Organosorb 10-AM exhibited the highest nominal BET surface area and iodine number, superior theoretical porosity did not uniformly translate into highest competitive adsorption performance.

Organosorb 10-AA frequently demonstrated higher effective K_f values under raw leachate conditions, suggesting more favorable micropore accessibility under TOC competition. Carbopur 1240 exhibited robust performance but slightly lower competitive affinity in several systems.

These findings reinforce a critical principle: total surface area alone is insufficient to predict adsorption efficiency under competitive environmental conditions. Rather, accessible micropore structure, pore size distribution, and resistance to DOM-induced blockage govern effective performance.

6.8. Integrated Mechanistic Understanding

Across all experiments, adsorption behavior was governed by three interacting mechanisms:

1- Hydrophobic partitioning (chain-length dependent)

2- Functional group-surface interaction (sulfonate > carboxylate)

3- Competitive site occupation by Leachate TOC and solvent-derived TOC

The integrated dataset demonstrates that adsorption in real leachate systems represents a dynamic equilibrium between high-affinity PFAS uptake and sustained organic competition. Carbon-specific structural properties influence how effectively high-energy micropores remain accessible under this competition.

The study therefore advances understanding from simple capacity comparison toward mechanistic interpretation under realistic treatment conditions.

6.9. Future Research Directions

While the present work provides a mechanistic framework for PFAS adsorption under competitive leachate conditions, several research avenues remain open for further refinement.

Kinetic Modeling Under Competitive Conditions

This thesis primarily addressed equilibrium behavior at defined contact times. Further research should incorporate time-resolved kinetic modeling under TOC competition to evaluate intraparticle diffusion limitations and rate-controlled site occupation.

Competitive Multi-PFAS Systems

Although multi-PFAS spiking was applied, future studies should isolate inter-PFAS competition effects separate from TOC competition to evaluate displacement phenomena and preferential adsorption within mixed PFAS systems.

Column-Scale and Dynamic Testing

Batch isotherms provide mechanistic insight but do not fully replicate fixed-bed operational conditions. Future research should validate findings under continuous-flow column systems to evaluate breakthrough behavior under realistic loading rates.

Regeneration and Long-Term Stability

Long-term carbon performance under repeated loading and regeneration cycles in leachate matrices remains insufficiently characterized. Investigation of pore structure evolution under fouling conditions would enhance treatment sustainability assessment.

6.10 Final Statement

In conclusion, this thesis demonstrates that PFAS adsorption in landfill leachate systems is a multi-factorial process governed by molecular structure, carbon pore accessibility, and persistent organic competition. The work provides experimentally validated, internally consistent evidence that adsorption efficiency under realistic conditions cannot be predicted solely from clean-water isotherms or nominal surface area metrics.

By integrating quantitative TOC mass balance verification, structural PFAS comparison, Freundlich modeling, and multi-carbon evaluation, this research establishes a comprehensive mechanistic framework for interpreting PFAS adsorption under complex environmental conditions.

The findings contribute directly to improving predictive understanding of carbon-based PFAS treatment and provide a scientifically robust foundation for future technological optimization.

References

Appleman, T. D., Higgins, C. P., Quinones, O., Vanderford, B. J., Kolstad, C., Zeigler-Holady, J. C., & Dickenson, E. R. V. (2014). Treatment of poly- and perfluoroalkyl substances in U.S. full-scale water treatment systems. *Water Research, 51*, 246-255. https://doi.org/10.1016/j.watres.2013.10.067

Chen, Y., Zhang, H., Liu, Y., Bowden, J. A., Tolaymat, T. M., Townsend, T. G., & Solo-Gabriele, H. M. (2023). Evaluation of per- and polyfluoroalkyl substances (PFAS) in leachate, gas condensate, stormwater and groundwater at landfills. *Chemosphere, 318*, 137903. https://doi.org/10.1016/j.chemosphere.2023.137903

Fernandez, N. A., Rodriguez-Freire, L., Keswani, M., & Sierra-Alvarez, R. (2016). Effect of chemical structure on the sonochemical degradation of perfluoroalkyl and polyfluoroalkyl substances (PFASs). *Environmental Science: Water Research & Technology, 2*, 975-983. https://doi.org/10.1039/c6ew00150e

Gilak Hakimabadi, S., Taylor, A., & Pham, A. L.-T. (2023). Factors affecting the adsorption of per- and polyfluoroalkyl substances (PFAS) by colloidal activated carbon. *Water Research, 242*, 120212. https://doi.org/10.1016/j.watres.2023.120212

Higgins, C. P., & Luthy, R. G. (2006). Sorption of perfluorinated surfactants on sediments. *Environmental Science & Technology, 40*(23), 7251-7256. https://doi.org/10.1021/es061000n

Hui, K., Li, H., Xing, C., Xi, B., Yuan, Y., & Tan, W. (2026). Adsorption and fate of per- and polyfluoroalkyl substances from landfill leachate onto aquifer media under the influence of dissolved organic matter. *Environmental Chemistry and Ecotoxicology, 8*, 13-28. https://doi.org/10.1016/j.enceco.2025.11.008

Kjeldsen, P., Barlaz, M. A., Rooker, A. P., Baun, A., Ledin, A., & Christensen, T. H. (2002). Present and long-term composition of MSW landfill leachate: A review. *Critical Reviews in Environmental Science and Technology, 32*(4), 297-336. https://doi.org/10.1080/10643380290813462

McCleaf, P., Englund, S., Östlund, A., Lindegren, K., Wiberg, K., & Ahrens, L. (2017). Removal efficiency of multiple perfluoroalkyl substances (PFAS) in drinking water using granular activated carbon and anion exchange column tests. *Water Research, 120*, 77-87. https://doi.org/10.1016/j.watres.2017.04.057

Rahman, M. F., Peldszus, S., & Anderson, W. B. (2014). Behaviour and fate of perfluoroalkyl and polyfluoroalkyl substances in drinking water treatment: A review. *Chemosphere, 104*, 1-11. https://doi.org/10.1016/j.watres.2013.10.045

Röhler, K., Susset, B., & Grathwohl, P. (2023). Production of perfluoroalkyl acids (PFAAs) from precursors in contaminated agricultural soils: Batch and leaching experiments. *Science of the Total Environment, 902*, 166555. https://doi.org/10.1016/j.scitotenv.2023.166555

Schumacher, B. A., Zimmerman, J. H., Williams, A. C., Lutes, C. C., Holton, C. W., Escobar, E., Hayes, H., & Warrier, R. (2024). Distribution of select per- and polyfluoroalkyl substances at a chemical manufacturing plant. *Journal of Hazardous Materials, 464*, 133025. https://doi.org/10.1016/j.jhazmat.2023.133025

Wang, X., Liu, K., Tao, J., Tang, Z., Fu, R., Zeng, J., Liu, N., & Qiu, J. (2025). *Study on groundwater PFAS pollution near large livestock farms in Guangdong–Hong Kong–Macao Greater Bay Area*. Environmental Chemistry and Ecotoxicology, 7, 2569–2579. https://doi.org/10.1016/j.enceco.2025.10.022

Yu, Q., Hu, J., & Deng, S. (2009). Sorption of perfluorinated compounds on activated carbon and resin: Kinetics and isotherms. *Water Research, 43*(4), 1150-1158. https://doi.org/10.1016/j.watres.2008.12.001

Zhang, D., He, Q., Wang, M., Zhang, W., & Liang, Y. (2021). Sorption of perfluoroalkylated substances (PFASs) onto granular activated carbon and biochar. *Environmental Technology, 42*(12), 1798-1809. https://doi.org/10.1080/09593330.2019.1680744

Regulation (EU) 2019/1021 of the European Parliament and of the Council on persistent organic pollutants (recast) (consolidated version 1 January 2026). (2019, June 20). Official Journal of the European Union, L 169, 45-77. http://data.europa.eu/eli/reg/2019/1021/oj

Determinazione del dirigente n. 899 del 01/04/2025: D.Lgs. 152/2006 e ss.mm.ii. Installazione IPPC denominata "Discarica per rifiuti non pericolosi ubicata in loc. Cascina Boschetto nel Comune di Cerro Tanaro" - Rettifica D.D. n. 279 del 30/01/2025. (2025, April 1). Provincia di Asti, Area Direzione Operativa, Servizio Programmazione e Gestione del Territorio, Ufficio Autorizzazioni Ambientali.

Piano di sorveglianza e controllo della discarica per rifiuti non pericolosi di Cerro Tanaro (Revisione 2). (2025, February 14). GAIA S.p.A.

Legge regionale 19 ottobre 2021, n. 25. Legge annuale di riordino dell'ordinamento regionale anno 2021. (2021, October 19). Regione Piemonte.

Deliberazione della Giunta Regionale 14 giugno 2022, n. 60-5220. Indicazioni esplicative ed elementi interpretativi di supporto alla prima applicazione dei disposti di cui all'articolo 74 (Scarico di sostanze perfluoroalchiliche) della legge regionale 25/2021 e del relativo allegato tabellare (Allegato A). (2022, June 14). Regione Piemonte.

Standard test method for determination of per- and polyfluoroalkyl substances in water, sludge, influent, effluent, and wastewater by liquid chromatography tandem mass spectrometry (LC/MS/MS) (ASTM D7979–20). (2020). ASTM International.

Relazione semestrale di esercizio e monitoraggio ambientale - II semestre 2024. (2024). GAIA S.p.A., Discarica per rifiuti non pericolosi di Cerro Tanaro.